Technische Universität München

TUM School of Life Sciences

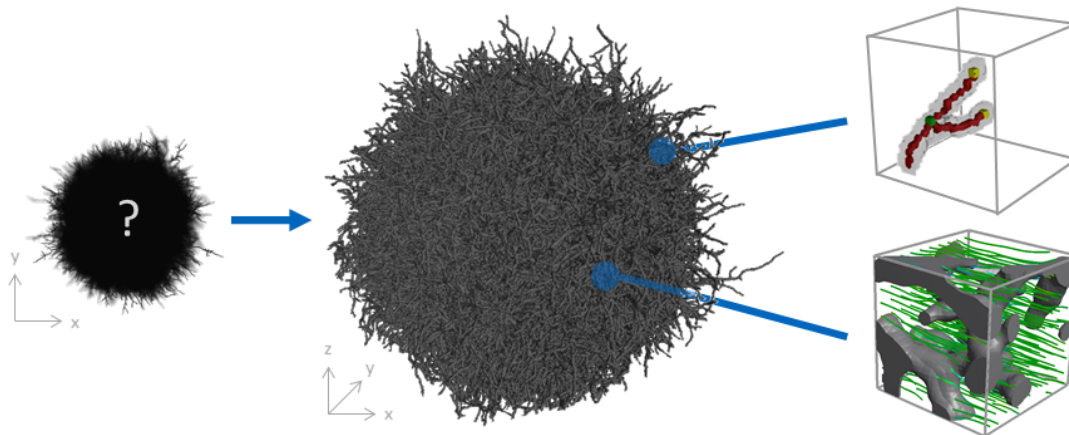Lehrstuhl für Systemverfahrenstechnik

Following fungal features – Micromorphology and diffusivity of filamentous fungal pellets revealed by three-dimensional imaging and simulation

Stefan Schmideder

Technische Universität München

TUM School of Life Sciences

Following fungal features – Micromorphology and diffusivity of filamentous fungal pellets revealed by three-dimensional imaging and simulation

Stefan Schmideder

Vollständiger Abdruck der von der TUM School of Life Sciences der Technischen Universität München zur Erlangung des akademischen Grades eines Doktors der Ingenieurwissenschaften (Dr.-Ing.) genehmigten Dissertation.

Vorsitzender: Prof. Dr.rer.nat. Philipp Benz

Prüfer der Dissertation: 1. Prof. Dr.-Ing. Heiko Briesen
2. Prof. Dr.-Ing. Andreas Kremling
3. Prof. Dr. Peter J. Punt

Die Dissertation wurde am 01.04.2021 bei der Technischen Universität München eingereicht und durch die TUM School of Life Sciences am 11.10.2021 angenommen.

Abstract

Filamentous fungal biotechnology started in 1919 with the industrial production of citric acid in *Aspergillus niger*. Today, more than 100 years later, it has emerged as a promising key technology for the transition from a petroleum-based economy into a bio-based circular economy. Filamentous fungi in industrial applications are usually cultivated under submerged conditions where their morphology strongly correlates with the productivity. In many processes, dense hyphal agglomerates known as pellets are formed. Due to their size of up to several millimeter and their dense hyphal network, the transport of nutrients and oxygen to the center of pellets is diffusion-limited. This alters product formation. Although the inner structure and the resulting diffusivity of pellets have a high impact on their productivity, they remained largely unexplored. For example, there is no method to analyze the hyphal network, i.e., the micromorphology, of whole pellets. In addition, correlations between the morphology and the diffusive transport of nutrients through pellets are lacking in literature.

In this publication-based dissertation, three papers are embedded showing methods to analyze the morphology and diffusivity of filamentous fungal pellets . The first paper describes techniques enabling the visualization and analysis of hyphal networks of whole pellets for the first time. Based on X-ray microcomputed tomography (µCT) measurements and three-dimensional (3D) image analysis, various morphological properties including the location of tips, branches, and hyphal material can be investigated. In the second paper, the first approach of correlating 3D hyphal networks to diffusivity known until today is introduced. For this purpose, diffusion computations were conducted through the structure of pellets gained from µCT measurements. The third paper reveals a universal law for the diffusivity through mycelial networks. This law is based on correlation analysis between diffusivities and structures of 66 µCT measured pellets originating from four filamentous fungi as well as 3125 Monte Carlo simulated pellets. Therein, the simulated pellets cover the broad morphological range of filamentous fungi. Regardless of the detailed morphology gained from experiments and simulations, the data showed that diffusivity follows a scaling law with respect to the solid hyphal fraction.

The methods and findings of this thesis enable the analysis of the micromorphology and the prediction of the diffusive mass transport of nutrients, oxygen, and secreted metabolites within any filamentous fungal pellet. These achievements will open new paths towards targeted morphological engineering of pellets to enhance productivities in fungal biotechnology.

Zusammenfassung

Die Biotechnologie filamentöser Pilze begann 1919 mit der industriellen Produktion von Zitronensäure in *Aspergillus niger*. Heute, mehr als 100 Jahre später, ist sie ein Hoffnungsträger für den Übergang von einer erdölbasierten Wirtschaft in eine biobasierte Kreislaufwirtschaft. Filamentöse Pilze werden industriell normalerweise submers kultiviert, wobei ihre Morphologie stark mit der Produktivität korreliert. In vielen Anwendungen bilden sich Hyphen-Agglomerate, sogenannte Pellets. Aufgrund ihrer Größe von bis zu einigen Millimetern und ihres dichten Hyphen-Netzwerks ist der Transport von Nährstoffen und Sauerstoff in Pellets diffusionslimitiert, was sich auf die Produktivität auswirkt. Obwohl bekannt ist, dass das Innere der Pellets ihre Produktivität beeinflusst, blieb es bisher weitgehend unerforscht. Beispielsweise gibt es keine Methode, um das Hyphen-Netzwerk von ganzen Pellets zu analysieren. Darüber hinaus fehlen Korrelationen zwischen der Pellet-Struktur und dem diffusiven Stofftransport.

Im Zentrum dieser publikationsbasierten Dissertation befinden sich drei Paper, die zeigen, wie die Morphologie und Diffusivität von filamentösen Pilz-Pellets bestimmt werden können. Im ersten Paper wird basierend auf Röntgen-Mikrocomputertomographie (μCT) und dreidimensionaler (3D) Bildanalyse die erste Methode zur Visualisierung und Analyse des Hyphen-Netzwerks ganzer Pellets vorgestellt. Dadurch können einige morphologische Eigenschaften einschließlich der Lage von Spitzen, Verzweigungen und Hyphen erstmals untersucht werden. Das zweite Paper beschreibt den ersten Ansatz zur Korrelation der 3D-Struktur mit der Diffusivität. Dafür wurden zahlreiche Diffusions-Berechnungen durch die Strukturen von Pellets durchgeführt, welche aus μCT-Messungen gewonnen wurden. Im dritten Paper liefern die Korrelationen zwischen den Diffusivitäten und Strukturen von 66 μCT gemessenen sowie 3125 Monte Carlo simulierten Pellets ein universelles Gesetz für die Diffusivität durch filamentöse Netzwerke. Dabei decken die simulierten Pellets den breiten morphologischen Bereich filamentöser Pilze ab. Unsere Daten zeigen, dass die Diffusivität einem einfachen Skalierungsgesetz in Bezug auf den Feststoffvolumenanteil folgt.

Die Methoden und Erkenntnisse dieser Arbeit ermöglichen die Analyse der Mikromorphologie und die Vorhersage des diffusiven Stofftransports von Nährstoffen, Sauerstoff und sekretierten Metaboliten in beliebigen filamentösen Pilz-Pellets. Diese Ergebnisse eröffnen neue Möglichkeiten zum gezielten morphologischen Design von Pellets, um die Produktivität in der Pilzbiotechnologie zu erhöhen.

Danksagung

Contents

1 Introduction

In 1917, the food chemist James Currie described the filamentous fungus *Aspergillus niger* as an efficient producer of citric acid. Only two years later, mass production of citric acid started and industrial biotechnology was born (Cairns et al., 2018). Further, the discovery of penicillin as a filamentous fungal metabolite in *Penicillium chrysogenum* (Fleming, 1929) and the industrialization thereof during World War II was probably the most important breakthrough of fungal biotechnology and started the antibiotic era. Today, filamentous fungi are still indispensable for the mass production of citric acid (Cairns et al., 2018; Meyer et al., 2020) and antibiotics (Keller, 2019; Zacchetti et al., 2018), opening multibillion dollar markets and being a lifesaver for millions of people (Demain, 2014). While large-scale manufacturing processes have been developed for several products (Meyer et al., 2016), filamentous fungal biotechnology has emerged as a hope for a sustainable future (Meyer et al., 2020). According to a thinktank consisting of researchers and companies, filamentous fungal biotechnology can be key for the transition from a petroleum-based economy into a bio-based circular economy (Meyer et al., 2020). Thus, this biotech sector will make significant contributions to climate change mitigation and will meet several United Nations's sustainable development goals.

Filamentous fungi are favorable hosts for many biotechnological applications (Wösten, 2019) including the production of acids, enzymes, and secondary metabolites (Hoffmeister and Keller, 2007; Meyer, 2008; Punt et al., 2002). Compared to bacteria, filamentous fungi benefit from their ability to perform complex post-translational modifications (Wang et al., 2020), their greatly expanded protein secretion apparatus (Ward, 2012), and their potential to produce various bioactive molecules (Brakhage, 2013; Keller, 2019; Nielsen et al., 2017). Further, filamentous fungi are the only microorganisms with the ability to fully degrade lignocellulosic biomass sustainably to a rich and diverse set of useful products (Meyer et al., 2020).

In industrial biotechnology, filamentous fungi are usually cultivated under submerged conditions. In such processes, fungal morphology affects productivity (Böl et al., 2021; Krull et al., 2013; Veiter et al., 2018). Generally, filamentous fungi consist of branched tubes called hyphae and the macromorphology ranges from loose dispersed hyphae to dense hyphal agglomerates called pellets (Papagianni, 2004; Veiter et al., 2018). Both macromorphologies, dispersed hyphae and pellets, come with some advantages and limitations. Dispersed hyphae result in a high viscosity of the cultivation broth, and thus, reduce the nutrient supply due to insufficient mixing (Krull et al., 2010, 2013). Contrary, cultivation broths with pellets as predominant macromorphology show low viscosities (Cairns et al., 2019b; Krull et al., 2013). Compared to dispersed hyphae, pellets display enhanced resistance to shear stress (Cairns et al., 2019b). However, the transport of nutrients and oxygen into pellets is diffusion-limited

by the dense structure (Hille et al., 2005, 2009), which alters growth, metabolic activity, and finally product formation (Cairns et al., 2019b; Krull et al., 2013; Veiter et al., 2018).

The inner structure of pellets, e.g., the spatial distribution of tips and hyphal material, is known to affect their productivity. However, the micromorphology within whole intact pellets has not yet been determined. Similarly, there are no correlations between the three-dimensional (3D) structure and the diffusive mass transport of nutrients, oxygen, and secreted metabolites within pellets. Both knowledge gaps are caused by the absence of techniques to measure and analyze the microscopic structure of whole pellets.

In this publication-based dissertation, methods based on X-ray microcomputed tomography (µCT) measurements and 3D image analysis were developed to determine the micromorphology of whole pellets (Paper I). Further, a method for diffusion computations through 3D images of pellets was developed (Paper II). As counterpart to the measured pellets, a 3D Monte Carlo growth approach was extended to enable the formation of pellets with the broad morphological range of filamentous microorganisms (Paper III). Diffusion computations through 66 measured pellets originating from four filamentous fungi and 3125 simulated pellets revealed a universal correlation between the structure and diffusivity of hyphal networks (Paper III).

Based on the described methods and findings, micromorphologies of whole intact pellets can be determined and the diffusion of nutrients, oxygen, and secreted metabolites through dense hyphal networks can be predicted. Applying 3D morphological analysis of pellets, the outcome of morphological engineering approaches can be investigated in utmost detail. In addition, existing approaches to model the morphological development of pellets can be validated and improved through the use of 3D morphological data and the universal diffusion law. Thus, this thesis will contribute to the targeted design of pellet morphologies, i.e., morphological engineering, and to enhanced productivities in fungal biotechnology.

2 Theoretical background

Cultivated under submerged conditions, the macromorphology of filamentous fungi ranges from dispersed hyphae to dense hyphal agglomerates called pellets (Krull et al., 2013; Veiter et al., 2018). Due to limitations in characterizing the structure and mass transport processes inside pellets, the focus of this dissertation is on pelletized fungi. Because filamentous bacteria and filamentous fungi in sumberged cultures are similar from a morphological perspective (Böl et al., 2021; Olmos et al., 2013; Zacchetti et al., 2018), the methods to characterize and model their morphology are often identical. Furthermore, the mass transport of nutrients and oxygen through both fungal and bacterial pellets is limited by the dense hyphal network and the inner part of pellets can be starved (Böl et al., 2021; Zacchetti et al., 2018). Due to these similarities between filamentous fungi and filamentous bacteria, a selection of findings and methods for filamentous bacteria are also mentioned in this dissertation. In Section 2.1, the morphology is elaborated. The interplay between morphology and metabolic activity and resulting morphological engineering approaches for pellets are described in Sections 2.2 and 2.3, respectively.

2.1 Morphology of pellets

This section describes the development of pellets in submerged cultures, morphological properties, and morphological measurement techniques.

2.1.1 Morphological development: from spore to pellet

Spores play a crucial role for the formation of pellets (Krull et al., 2013; Zhang and Zhang, 2016). Thus, the development of pellets starting from spores is described here.

Filamentous fungal spores are produced under stressful environmental conditions to ensure the survival of the organism and can be assumed as metabolically inactive cells (Riquelme et al., 2018). When bioprocesses are inoculated with spores, favorable conditions activate their metabolism, initiate swelling, and ultimately, result in germ tube formation (Bizukojc and Ledakowicz, 2006; Paul et al., 1993). Germ tubes represent first hyphal elements and grow, like all fungal hyphae, based on tip extension. Both germination and the growth of hyphae are polarized processes, i.e., the formation of new cell composites is directed. Thus, tubular structures are created (Cairns et al., 2019b; Riquelme et al., 2018). The simultaneous extension of tips and the development of new tips by branching of hyphae result in filamentous networks. This process leads to an exponential increase of the biomass under unlimited growth conditions (Krull et al., 2010).

Traditionally, it is distinguished between coagulative and non-coagulative pellet formation types (Metz and Kossen, 1977), which are illustrated in Figure 1. During non-coagulative pellet formation, spores and germinated spores remain dispersed. For example, Žnidaršič et al. (1998) showed that *Rhizipus stolonifer* (synonym *R. nigricans*) pellets can develop from single spores. Contrary, coagulative pellets can form from hundreds or thousands of agglomerated spores (Fontaine et al., 2010; Metz and Kossen, 1977). A classical representative of the coagulative type is *Aspergillus niger* (Cairns et al., 2018). However, different cultivation conditions cause different morphological behaviors and a final classification of an organism into coagulative or non-coagulative type is difficult (Veiter et al., 2018; Zhang and Zhang, 2016). For instance, Nielsen et al. (1995) showed that *Penicillium chrysogenum* exhibit characteristics of both types. In their study, spores remained dispersed whereas branched hyphae agglomerated and subsequently developed to pellets. Thus, Veiter et al. (2018) assigned *P. chrysogenum* to a third group, the hyphal element agglomerating type.
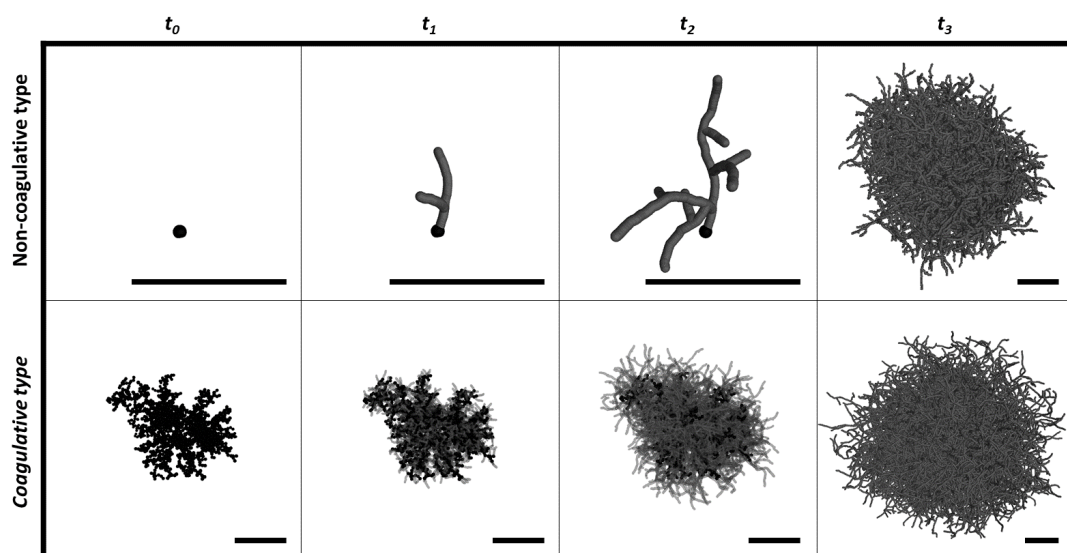
Figure 1: Development of non-coagulative and coagulative pellets. Spores are marked black, whereas hyphae are grey. Three-dimensional morphologies were simulated with an own stochastic growth-model that is based on Celler et al. (2012). Scale bar: 100 μm.

2.1.2 Morphological properties

According to Krull et al. (2013), "pellets can be described as stable spherical agglomerates composed of a branched network of hyphae. Their shape can vary from smooth and spherical to elongated and hairy" (p. 113). Further, the micromorphology describes the details of the hyphal network (Krull et al., 2013; Veiter et al., 2018). In this subsection, quantitative morphological properties of filamentous microorganisms are described together with their measurement techniques. The advantages and limitations of the mentioned techniques are elaborated in Section 2.1.3. To group morphological properties of pellets, they are assigned to the following classes: size, shape, compactness, morphology number, and spatial distribution of hyphal material. In addition, micromorphological descriptors for dispersed hyphae

exist. However, due to a lack of suitable methods, these descriptors have not yet been studied for pellets. Table 1 gives an overview of morphological properties and their corresponding measurement techniques, which are elaborated in the following.

Size The size of individual pellets is specified by the projected area, various diameters, perimeter, chord length, and signal length. Additionally, size distributions of pellet populations can be investigated.

The projected area is the two-dimensional area of the projection of a three-dimensional object on a plane and often applied to pellets (Cairns et al., 2019a; Walisko et al., 2017; Wucherpfennig et al., 2011). To determine the projected area, two-dimensional images are acquired and analyzed. Based on the projected area, different diameters can be calculated. The Feret diameter is defined as the distance between two parallel lines touching the edge of the projected area (Cairns et al., 2019a; Walisko et al., 2017; Wucherpfennig et al., 2011). Additionally, the surface equivalent spherical diameter of the projected area can be determined (Schrinner et al., 2020). Some studies investigated the perimeter, defined as the total length of the object boundary. A distinction is made between the perimeter of the convex area (Cairns et al., 2019a; Wucherpfennig et al., 2011) and the perimeter of the projected area (Schrinner et al., 2020; Walisko et al., 2017).

With focused beam reflectance measurement (FBRM) (Grimm et al., 2004; Kelly et al., 2006; Lin et al., 2008; Pearson et al., 2003, 2004) and novel flow cytometry systems (Ehgartner et al., 2017; Schrinner et al., 2020; Veiter and Herwig, 2019), the chord length and signal length of pellets can be investigated, respectively. While the previously mentioned techniques enable the investigation of numerous pellets individually, the application of laser diffraction ultimately results in a size distribution of pellets (Lin et al., 2010; Petersen et al., 2008; Quintanilla et al., 2018; Rønnest et al., 2012; Wucherpfennig et al., 2011).

Shape Based on image analyses of the projected area, the shape parameters circularity and aspect ratio can be investigated. Schrinner et al. (2020) and Wucherpfennig et al. (2011) applied the circularity, which is a function of the projected area and the perimeter:

$$Circularity = 4\pi \, \frac{Projected \, area}{Perimeter^2}. \tag{2.1}$$

While the projection of a perfect sphere would have a circularity of 1, values closer to 0 indicate elongated and/or non-convex objects. The aspect ratio is defined as the ratio between the maximum and minimum Feret diameter (Cairns et al., 2019a; Wucherpfennig et al., 2011). Symmetrical objects in all axis such as circles or squares would have an aspect ratio of 1, whereas elongated objects result in higher aspect ratios. Thus, the aspect ratio is applied to describe the elongation of pellets (Cairns et al., 2019a; Wucherpfennig et al., 2011).

Compactness The solidity is described as a surface property, measured on base of image analysis, and defined as the ratio between the projected area and the convex area (Cairns et al., 2019a; Wucherpfennig et al., 2011). A convex shape would result in a solidity of 1,

Table 1: Morphological properties determined for pellets and dispersed hyphae

	Class	Property	Technique	References
Pellet	Size	Projected area	Microscopy	Barry et al. (2015); Cairns et al. (2019a); Schrinner et al. (2020); Walisko et al. (2017); Wucherpfennig et al. (2011)
		Diameter	Microscopy	Cairns et al. (2018); Cairns et al. (2019a); Schrinner et al. (2020); Walisko et al. (2017); Willemse et al. (2018); Schrinner et al. (2020); Walisko et al. (2017); Wucherpfennig et al. (2011)
		Perimeter	Microscopy	Cairns et al. (2019a); Schrinner et al. (2020); Walisko et al. (2017); Wucherpfennig et al. (2011)
		Chord length	FBRM	Grimm et al. (2004); Kelly et al. (2006); Pearson et al. (2003, 2004)
		Signal length	Flow cytometry	Ehgartner et al. (2017); Schrinner et al. (2020); Veiter and Herwig (2019)
		Size distribution	Laser diffraction	Lin et al. (2010); Petersen et al. (2008); Quintanilla et al. (2018); Rønnest et al. (2012); Wucherpfennig et al. (2011)
	Shape	Circularity	Microscopy	Barry et al. (2015); Schrinner et al. (2020); Walisko et al. (2017); Wucherpfennig et al. (2011)
		Aspect ratio	Microscopy	Cairns et al. (2019a); Wucherpfennig et al. (2011)
	Compactness	Solidity of periphery	Microscopy	Cairns et al. (2019a); Wucherpfennig et al. (2011)
		Relative annular diameter	Flow cytometry	Ehgartner et al. (2017)
		Compactness of core	Flow cytometry	Ehgartner et al. (2017); Schrinner et al. (2020); Veiter and Herwig (2019)
	Combination of size, shape, and compactness	Morphology number	Microscopy	Cairns et al. (2019a); Wucherpfennig et al. (2011)
	Spatial distribution of hyphal material	Hyphal fraction	Microscopy of slices	Hille et al. (2005, 2009)
Dispersed hyphae	Micromorphology of dispersed hyphae	Total hyphal length	Microscopy	Barry et al. (2015); Bocking et al. (1999); Cardini et al. (2020); Kwon et al. (2013); Lecault et al. (2007); Sachs et al. (2019); Schmideder et al. (2018); Vidal-Diez de Ulzurrun et al. (2019)
		Number of tips	Microscopy	Barry et al. (2015); Lecault et al. (2007); Sachs et al. (2019); Schmideder et al. (2018); Vidal-Diez de Ulzurrun et al. (2019)
		Number of branches	Microscopy	Barry et al. (2015); Lecault et al. (2007); Sachs et al. (2019); Schmideder et al. (2018)
		Hyphal growth unit	Microscopy	Barry et al. (2015); Bocking et al. (1999); Choy et al. (2011); Colin et al. (2013); Kwon et al. (2013); Sachs et al. (2019)
		Branch angle	Microscopy	Du et al. (2016); Lehmann et al. (2019); Yang et al. (1992b)
		Internodal length	Microscopy	Du et al. (2016); Lehmann et al. (2019); Sachs et al. (2019)
		Hyphal diameter	Microscopy	Choy et al. (2011); Colin et al. (2013); Lehmann et al. (2019)

whereas non-convex shapes would result in lower values. Based on forward scatter signals of flow cytometry, the properties relative annular diameter (RAD) and compactness can be determined (Ehgartner et al., 2017). RAD describes the ratio of the loose pellet periphery to the whole pellet whereas compactness represents the uniformity of the density of the pellet core.

Combination of size, shape, and compactness   Based on a combination of several properties determined from image analysis, the dimensionless morphology number can be investigated (Wucherpfennig et al., 2011):

$$morphology\ number = \frac{2\ \sqrt{A}\ S}{\sqrt{\pi}\ D\ E},$$

(2.2)

where A is the projected area, S the solidity, D the maximum Feret diameter, and E the elongation (aspect ratio). Perfectly round and convex pellets would result in a morphology number of 1, whereas elongated and/or non-convex pellets would result in lower morphology numbers.

Spatial distribution of hyphal material   An established method to visualize the interior of pellets is to acquire images of slices. In brief, pellets are frozen in embedding medium and then cut into slices with a thickness of about 50 - 100 μm. Images of the slices are taken either with light (Lin et al., 2010; Priegnitz et al., 2012) or confocal laser scanning (Hille et al., 2005, 2009) microscopy. Lin et al. (2010) and Priegnitz et al. (2012) described the spatial distribution of hyphal material only qualitatively by the appearance of dense and loose regions in the pellet. Contrary, Hille et al. (2005, 2009) applied quantitative descriptors. They investigated the hyphal fraction, i.e., the ratio of the volume of hyphae to the total volume, as a function of the pellet radius.

Micromorphology of dispersed hyphae   Because hyphae of more complex structures superimpose, 2D image analysis can be only applied to investigate the micromorphology of mycelia with a few branches. One important property is the total hyphal length, which can be investigated manually with the help of measurement tools implemented in image analysis softwares (Bocking et al., 1999; Kwon et al., 2013). Additionally, it can be determined automatically by the investigation of the mycelial skeleton (Figure 2), which is the centerline of hyphae with a thickness of one pixel (Barry et al., 2015; Cardini et al., 2020; Lecault et al., 2007; Sachs et al., 2019; Schmideder et al., 2018; Vidal-Diez de Ulzurrun et al., 2019). Each pixel of the skeleton can be assigned to be a tip (one neighbor), hyphae (two neighbors), or branch (three neighbors). Four neighboring pixels would be assigned to the junction of two overlapping hyphae. As shown in Figure 2, the number of tips and number of branches can be investigated automatically based on analyses of the skeleton (Barry et al., 2015; Lecault et al., 2007; Sachs et al., 2019; Vidal-Diez de Ulzurrun et al., 2019). However, the number of tips and number of branches are often counted manually (Bocking et al., 1999; Kwon et al., 2013). Dividing the total hyphal length by the number of tips results in the hyphal growth unit

(HGU) (Barry et al., 2015; Bocking et al., 1999; Choy et al., 2011; Colin et al., 2013; Kwon et al., 2013; Sachs et al., 2019). Similar to the HGU, the internodal length (distance between two branches) can be determined as a measure for the branching frequency (Du et al., 2016; Lehmann et al., 2019; Sachs et al., 2019). Further, the hyphal diameter (Choy et al., 2011; Colin et al., 2013; Lehmann et al., 2019) and the branch angle (Du et al., 2016; Lehmann et al., 2019; Yang et al., 1992b) can be investigated.
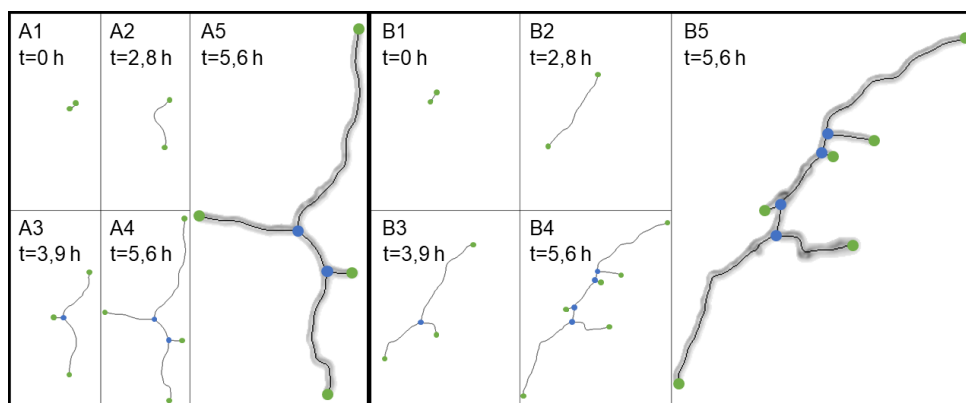
Figure 2: Analysis of morphological development of *Aspergillus niger* mycelia: black marks the centerlines of hypha, green the tips, and blue the branches. A1 - A4) Development of mycelium A. B1 - B4) Development of mycelium B. In A5 and B5, the analyzed centerlines of A4 and B4 are illustrated along with their respective microscopic image. Image analysis procedure was adapted from Schmieder et al. (2018).

2.1.3 Applicability of morphological measurement techniques

Usually, microscopy is applied to determine the morphology of pellets. While, FBRM, laser diffraction, and flow cytometry have become fast alternatives to microscopy, they often lead to less detailed information. In the following, the advantages and limitations of the mentioned measurement techniques are elaborated.

Light microscopy   The state of the art to characterize the morphology is light microscopy (Papagianni, 2014). Today, several open source image analysis tools simplify the offline-analysis of pellets (Barry et al., 2015; Willemse et al., 2018) and dispersed hyphae (Barry et al., 2015; Brunk et al., 2018; Cardini et al., 2020; Sachs et al., 2019; Vidal-Diez de Ulzurrun et al., 2019). Further, the germination of spores (Brunk et al., 2018) and the tip extension and branch formation of dispersed hyphae (Schmieder et al., 2018) can be tracked time-resolved when the spores are fixed in a growth chamber (Figure 2). A combination of these tools, the ubiquitous presence of light microscopes in laboratories, the opportunity to study diverse morphological properties (compare Table 1), and the possibility to investigate hundreds of pellets per time point (Schrinner et al., 2020) will further drive the use of light microscopy to study filamentous microorganisms. However, the superimposition of hyphae hinders the straightforward analysis of the micromorphology of more complex structures such as pellets.

Confocal laser scanning microscopy Contrary to 2D light microscopy, CLSM enables to visualize the 3D morphology. However, CLSM requires a fluorescent signal and is limited to about 50 - 150 μm in penetration depth. Thus, only the periphery can be visualized without cutting the pellets (Hille et al., 2005, 2009; Villena et al., 2010). For unknown reasons, existing studies lack subsequent image analysis to investigate the micromorphology of the pellet periphery. To determine the spatial distribution of the hyphal fraction inside pellets, Hille et al. (2005, 2009) analyzed CLSM measurements of slices. However, the determined hyphal fraction did not reflect the reality, since they used overlays of the acquired z-stacks. Thus, the hyphal fraction was often 100 %, which is impossible even for densest packing. To the author's knowledge there is no approach that analyzes the three-dimensional micromorphology based on CLSM measurements.

Focused beam reflectance measurement FBRM enables the analysis of the chord length and concentration of spores, spore agglomerates, and pellets offline (Pearson et al., 2003, 2004; Whelan et al., 2012) as well as inline (Grimm et al., 2004; Kelly et al., 2006; Lin et al., 2008). Advantages of FBRM are the inline applicability and the potential to measure large quantities of objects. However, information about the shape and periphery of pellets are missing and data interpretation remains challenging.

Laser diffraction To investigate the size distribution of spore agglomerates and pellets, laser diffraction can be applied (Lin et al., 2010; Petersen et al., 2008; Quintanilla et al., 2018; Rønnest et al., 2012; Wucherpfennig et al., 2011). Based on Fraunhofer diffraction theory, the diffraction pattern of a laser beam can be analyzed to calculate the volumetric pellet size distribution that best matches the measured pattern (Lin et al., 2010). Wucherpfennig et al. (2011) applied laser diffraction in a bypass, whereas the other authors took samples before the measurements. Laser diffraction has the advantage to be much faster than more commonly used microscopy (Lin et al., 2010; Petersen et al., 2008; Quintanilla et al., 2018; Rønnest et al., 2012). However, it fails to report properties that describe the shape and periphery of pellets (Petersen et al., 2008; Wucherpfennig et al., 2011) as well as the pellet concentration (Lin et al., 2010). According to Rønnest et al. (2012), the analysis is based on a number of assumptions. For example, the shape of filamentous structures has to be assumed. However, the authors suggested that validation studies could contribute to a reliable technique to analyze size distributions of filamentous microorganisms.

Flow cytometry Ehgartner et al. (2017) described flow cytometry as a fast alternative to microscopy. Further, they envision an online application through automated sampling systems. Similar to image analysis, flow cytometry allows the quantification of the pellet size and the identification of the hairy region of the pellet periphery (Ehgartner et al., 2017; Schrinner et al., 2020; Veiter and Herwig, 2019). In addition, flow cytometry reveals a compactness parameter of pellets. However, information about the projected area is lacking and size exclusion of samples occurs, which can result in an over-representation of small pellets (Veiter and Herwig, 2019).

2.2 Interplay between morphology, transport of nutrients, and metabolic activity of pellets

The interplay between morphology, transport of nutrients, and metabolic activity is a key aspect for the productivity of filamentous pellets (Papagianni, 2004; Veiter et al., 2018; Zacchetti et al., 2018). In general, the optimal morphology varies with the desired product and cannot be generalized (Gibbs et al., 2000; Krull et al., 2010). For example, the pellet form of *Aspergillus niger* is used to produce citric acid, whereas its dispersed form serves for the production of enzymes (Meyer et al., 2016). While pellets have some advantages over dispersed hyphae (Section 1), limited nutrient availability (Cairns et al., 2019b; Krull et al., 2013) might occur within pellets. For example, the concentration of oxygen is known to decrease towards the center of pellets (Hille et al., 2005, 2009). This leads to a reduced growth and metabolic activity in the core (Cairns et al., 2019b; Veiter et al., 2018) and can limit the production of enzymes (Driouch et al., 2010; Veiter et al., 2018). However, reduced metabolic activity in the center of pellets can also increase the production of secondary metabolites (Cairns et al., 2019b; Veiter et al., 2018) such as Penicillin (Cronenberg et al., 1994). This demonstrates that a detailed understanding of the profile of nutrients and the resulting metabolic activity in pellets is of crucial importance.

2.2.1 Spatial distribution and mass transport of nutrients inside pellets

The spatial distribution of nutrients inside pellets is determined by metabolic rates and transport processes through their dense structure (Celler et al., 2012; Cui et al., 1998). In the following section, the focus is on the investigation of nutrient profiles in pellets and mass transport properties of hyphal networks.

Profile of nutrients In general, studies measuring the profile of nutrients are rare. A reason might be the need of complicated experimental setups, where pellets are fixed in defined chambers before the concentration profile of oxygen or glucose can be measured with microelectrodes (Cronenberg et al., 1994; Hille et al., 2005, 2009; Wittier et al., 1986). To guarantee a realistic nutrient transport and keep the morphology intact, the handling of the pellets and microelectrodes as well as the design and control of the chambers are challenging. For example, Hille et al. (2005, 2009) applied a thin microelectrode with a tip diameter similar to the diameter of hyphae.

Experiments unveiled oxygen as prime limiting nutrient in fungal pellets (Cronenberg et al., 1994; Veiter et al., 2018). Measurements of the oxygen profile in pellets greater than 1 mm revealed a restricted availability of oxygen with only the outer 100 - 300 μm being supplied (Cronenberg et al., 1994; Hille et al., 2005, 2009; Wittier et al., 1986). In addition to oxygen, Cronenberg et al. (1994) determined the concentration profile of glucose. Although glucose penetrated *Penicillium chrysogenum* pellets at early cultivation stages almost at bulk level, no glucose consumption was determined in their core. Since fungal metabolism requires oxygen, this was explained by the measured absence of oxygen in the core. At late cultivation stages,

the pellets were prone to fragmentation and autolysis and showed a decreased metabolic activity in the core. While pellets were completely penetrated by oxygen and glucose, glucose consumption still only occurred in the periphery. The authors explained the lost metabolic activity in the core by the irreversible inhibition in early cultivation stages caused by the absence of oxygen.

Especially Cronenberg et al. (1994) demonstrated the interplay between the profile of nutrients and the metabolic activity in pellets. Further, all mentioned studies revealed that concentration profiles in pellets are highly affected by their structure. In addition to the size of pellets, the density plays a decisive role. For example, Hille et al. (2005) observed a much steeper decrease of the oxygen concentration in dense *A. niger* pellets. Moreover, measuring the development of nutrient profiles in inactivated pellets is the only method to investigate their diffusivity, which is be elaborated in the following.

Mass transport of nutrients Many authors suggest diffusion as the only mass transport phenomenon of oxygen and nutrients inside pellets (Cui et al., 1998; King, 1998; Silva et al., 2001). In addition to diffusive transport, convective transport is proposed to contribute to the nutrient-supply of pellets with a loose periphery, especially if they are prone to turbulent flow regimes (Cronenberg et al., 1994; Hille et al., 2009). Because diffusive mass transport was shown to be the most important transport phenomenon inside pellets, its theoretical background is elaborated in the following. The diffusivity of component *i* is described with the effective diffusion coefficient $D_{i,eff}$ (Becker et al., 2011):

$$D_{i,eff} = D_{i,bulk} \cdot k_{eff}, \tag{2.3}$$

where $D_{i,bulk}$ is the diffusion coefficient in the pure bulk medium and k_{eff} determines the reduction to the effective diffusion coefficient. While the effective diffusion factor k_{eff} is dependent on the geometry of the pores, it is independent of the diffusing substance.

Besides measurement of nutrient profiles, Cronenberg et al. (1994) and Hille et al. (2009) investigated the effective diffusivity of *P. chrysogenum* and *A. niger* pellets, respectively. For this purpose, Hille et al. (2009) placed one microelectrode each at the periphery and in a defined depth of inactivated pellets. The inactivation of the pellets prevented the consumption of oxygen. After saturating the medium with nitrogen, the measurement chamber was aerated with pure oxygen and the change of the concentration was recorded by both microelectrodes. Based on the development of the concentrations and Fick's second law, they were able to fit the effective diffusion coefficient. Similar to Hille et al. (2009), Cronenberg et al. (1994) determined the development of the oxygen or glucose concentration by stimulus response experiments inside inactivated pellets to further estimate the effective diffusivity. As expected, dense pellet peripheries resulted in low effective diffusivities. The minimum effective diffusion factor k_{eff} was about 0.4 and 0.6 in the studies of Hille et al. (2009) and Cronenberg et al. (1994), respectively. As Cronenberg et al. (1994) described the morphology of pellet slices only qualitatively, they were not able to correlate the morphology with the effective diffusivity. Contrary, Hille et al. (2009) quantified the morphology of pellet slices with the

radial profile of the hyphal fraction. However, as mentioned in Section 2.1.3, they missed the three-dimensional information of the hyphal network. Thus, hyphae superimposed in two-dimensional projections of slices and the hyphal fraction was often 100 %. That is impossible even for densest packing. Nevertheless, they correlated the effective diffusivity with the local derivation of the hyphal fraction.

To the author's knowledge, Hille et al. (2009) was the only experimental approach to correlate the morphology and diffusivity of hyphal networks. Although studies about fibrous materials revealed that porosity and tortuosity are important drivers of k_{eff} (Tomadakis and Robertson, 2005; Vignoles et al., 2007), modeling approaches of filamentous pellets (Buschulte, 1992; Cui et al., 1998; Lejeune and Baron, 1997; Meyerhoff et al., 1995) either neglect the tortuosity of the hyphal network or assume a constant value to model the diffusivity of nutrients. A detailed list of applied and determined correlations between the morphology and effective diffusion factors of filamentous microorganisms and fibrous materials can be found in Paper II, Table 1.

2.2.2 Metabolic activity

The limited availability of nutrients in central parts of pellets can lead to a physiological heterogeneity inside pellets (Zacchetti et al., 2018) and to a reduced growth and growth-related metabolism (Hille et al., 2009; Zhang and Zhang, 2016). Metabolic activity can be identified by staining and analyzing active as well as inactive regions. In this way, many studies determined metabolic inactive cores and active shell layers of pellets. Staining as indicator of metabolic activity is conducted either with chemicals (Bizukojc and Ledakowicz, 2010; Nieminen et al., 2013; Schrinner et al., 2020; Veiter and Herwig, 2019) or by using fluorescence proteins expressed by the host organism (Driouch et al., 2012, 2010; Tegelaar et al., 2020).

The author of this dissertation contributed to a cooperative study about the metabolic activity in filamentous bacterial pellets (Schrinner et al., 2020), which is not embedded in the results section of this thesis. In this study, active and inactive regions of *Lentzea aerocoloni-genes* pellets were stained with SYTO9 (green fluorescence through intercalation with DNA of predominantly intact and active cells) and propidium iodide (red fluorescence as result from DNA intercalation in inactive cells with compromised membranes), respectively. As illustrated in Figure 3, metabolically different regions of pellet slices were distinguished through the analysis of CLSM images. Because pellet slicing followed by image analysis is of high manual effort, flow cytometry was applied to detect active and inactive fractions of hundreds of stained pellets. While flow cytometry enabled the analysis of a statistically relevant number of pellets, image analysis of pellet slices provided shape information.

Fluorescence staining of active and inactive pellet regions can also be applied to filamentous fungi. Similar to the mentioned study about filamentous bacteria (Schrinner et al., 2020), Veiter and Herwig (2019) analyzed *P. chrysogenum* pellets based on CLSM and flow cytometry. Bizukojc and Ledakowicz (2010) stained growing regions of *Aspergillus terreus* with lactophenol methyl blue. This staining procedure allows to analyze growing regions through
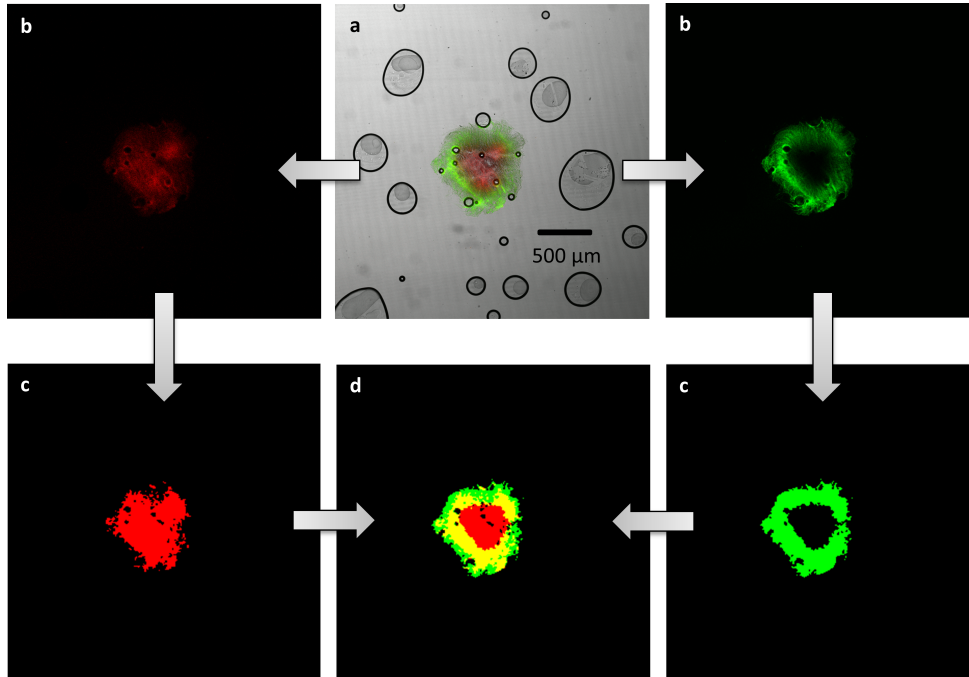
Figure 3: Determination of living (green), dead (red) and a combination of living and dead (yellow) pellet areas. Image analysis was performed based on CLSM measurements of stained *Lentzea aerocolonigenes* pellet slices. (a) Original image with green and red fluorescent areas (black circles are air bubbles that are occasionally enclosed in the sectioning medium). (b) Separation in green fluorescence and red fluorescence. (c) Processed images. (d) Image with living, dead, and a combination of living and dead pellet areas. Figure is from joint publication (Schrinner et al., 2020).

light microscopy of pellet slices. Further, the authors correlated the fraction of active growing regions with the formation of the desired product lovastatin. Instead of activity staining with chemicals, Driouch et al. (2012, 2010) engineered genetically modified *A. niger* strains that co-express green fluorescent protein (GFP) together with the desired product glucoamylase or fructofuranosidase, respectively. Thus, they were able to quantify metabolic active regions based on CLSM images of pellet slices. In Driouch et al. (2012), large pellets were only active in a 200 μm surface layer. The authors concluded that the inner region of large pellets does not contribute to the production of the desired enzymes, which is probably caused by diffusion limitation of oxygen or other nutrients.

In several studies, the volume fraction of the active shell layer and the formation of desired products increased with decreasing pellet diameter (Bizukojc and Ledakowicz, 2010; Driouch et al., 2012, 2010; Tegelaar et al., 2020). However, a correlation between the metabolic activity and the detailed morphology within pellets, e.g., the spatial distribution of hyphal material and the number of (active) tips, is lacking. Additionally, there is no study to date that determines both the nutrient profile and metabolic heterogeneity within pellets.

2.3 Morphological engineering

There is no doubt that the morphology of filamentous microorganisms strongly affects their productivity in submerged cultures. Thus, the precise control of the morphology, i.e., morphological engineering, is of crucial importance (Krull et al., 2013). In this Section, experimental and modeling approaches are described to engineer the morphology of filamentous pellets.

2.3.1 Experimental approaches

In this thesis, it is distinguished between genetic and process engineering approaches to alter the morphology.

Genetics   Two recent reviews highlight genetic aspects that impact the morphogenesis of filamentous fungi (Cairns et al., 2019b; Zhang and Zhang, 2016). In the following, a few exemplary filamentous fungal characteristics are described that can be specifically modified to allow targeted strain development.

As stated earlier, spore agglomeration is one of the driving factors for the formation of pellets. One known factor for spore agglomeration is their hydrophobicity (Zhang and Zhang, 2016). The absence of spore cell wall associated hydrophobins DewA and RodA in *Aspergillus nidulans* knockout mutants reduced the ratio of biomass present as pellets. Further, the average size of pellets decreased (Dynesen and Nielsen, 2003). Fontaine et al. (2010) showed that cell wall 1-3glucans become exposed at the cell surface during spore swelling and induce the agglomeration of germinating *Aspergillus fumigatus* conidia. Additionally, spores of species with 1-3glucan synthase gene (*ags*) in their genome (*A. fumigatus* and *P. chrysogenum*) agglomerate, whereas no spore agglomeration can be observed for organisms without *ags* (*R. oryzae* and *Trichoderma reesii*). Further, *A. niger alb1* knockout mutants are deficient in melanin biosynthesis and showed altered surface structures and charge of spores (Priegnitz et al., 2012). The authors concluded that spore agglomeration differs between the wild type and the mutant in pH-dependent manner due to the changed surface charge.

Besides spore agglomeration, the branching frequency has a strong influence on the morphological development (Cairns et al., 2019b). As shown by several authors, the branching frequency can be genetically modified (Biesebeke et al., 2005; Fiedler et al., 2018; He et al., 2016; Kwon et al., 2013). Fiedler et al. (2018) reported more compact macromorphologies of the hyperbranching phenotype. In addition to the change in morphology, productivity can also be altered by the branching frequency. Especially for the production of enzymes, a high tip to biomass ratio seems to be beneficial (Biesebeke et al., 2005; He et al., 2016). However, in some cases an elevated tip to biomass ratio cannot be correlated with an increased protein titer (Cairns et al., 2019b).

The described genetic modifications prove that the morphology can be influenced specifically by molecular biological approaches. To investigate the impact of genetic approaches on the formation of pellets and the pellet size, morphological measurement techniques shown in Table 1 can be applied. However, the influence on the micromorphology of pellets can of-

ten not be determined. For example, hyperbranching can be quantified for dispersed hyphae based on image analysis, while such methods do not exist for pellets so far.

Process engineering   Several review articles describe process engineering approaches for altering the morphology of filamentous fungal pellets (Böl et al., 2021; Krull et al., 2010, 2013; Veiter et al., 2018). Due to space limitation, only a small overview is presented about approaches concerning inoculation, medium composition, and fluid dynamics.

Inoculation strategies are known for their high impact on the morphological development (Prosser and Tough, 1991; Veiter et al., 2018). Papagianni and Mattey (2006), e.g., inoculated bioreactors with *A. niger* spores in concentrations ranging from 10^4 to 10^9 spores per milliliter and observed a clear transition from pelleted to dispersed macromorphologies. Contrary to *A. niger* (coagulative pellet formation type), non-coagulative pellet formation type *R. stolonifer* (synonym *R. nigricans*) develops larger pellets at lower spore concentrations (Žnidaršič et al., 2000). Besides inoculation with spores, inoculation with pellets can be a promising strategy for *A. niger* cultivations (Wang et al., 2017).

The composition of the medium offers numerous opportunities to influence the morphology. Besides traditional approaches such as the variation of pH (Priegnitz et al., 2012) and nutrient-sources (Papagianni et al., 1999), two approaches are currently coming into focus: the adjustment of the osmolality (Böl et al., 2021; Wucherpfennig et al., 2011) and the addition of particles (Böl et al., 2021; Karahalil et al., 2019). Wucherpfennig et al. (2011) showed that *A. niger* pellets decrease in size with increasing osmolality. The addition of microparticles (diameter mostly < 50 μm (Böl et al., 2021)) can also reduce the size of filamentous pellets and increase enzyme production (Antecka et al., 2016; Karahalil et al., 2019).

According to Krull et al. (2013), the reactor geometry, stirrer shape and size, and dissipated energy are among the fluid dynamic-related criteria affecting the morphology and productivity in stirred tank reactors (STR). They concluded that low power input leads to inadequate nutrient distribution and gas dispersion, whereas high power input can result in cell wall damage. Consequently, high mechanical forces can result in chipping off hyphae from pellets (Cui et al., 1997), which might reseed the fermentation broth. The following studies show that a more profound understanding is required to correlate the power input with the morphology. On the one hand, *A. niger* can grow to large pellets for low stirrer speeds, whereas high stirrer speeds can result in dispersed hyphae (El-Enshasy et al., 2006). On the other hand, an increased mechanical power input can increase the density of the pellet periphery of *A. niger* (Lin et al., 2010). The authors concluded that the increased density of the pellet periphery might limit the mass transport of nutrients. Compared to STR, other reactor types such as air lift column reactors (Gibbs et al., 2000; Xin et al., 2012) and rocking motion reactors (RMR) (Kurt et al., 2018) can reduce shear stress. According to Kurt et al. (2018), RMR can result in higher growth rates and more pelletized *A. niger* structures than STR.

The mentioned process engineering approaches offer numerous opportunities for targeted morphological engineering. In particular, they enable the cultivation of predominantly pelletized or dispersed morphologies and affect the size of pellets. Some studies even showed the

possibility to alter the density of the pellet periphery, which could contribute as a diffusion barrier. However, the impact of process engineering approaches on the micromorphology within pellets has not yet been examined, which is caused by a lack of appropriate methods.

2.3.2 Modeling approaches

Several authors emphasize the demand for mechanistic modeling in order to predict the morphological development for altered cultivation conditions, to reduce elaborate empirical tests, and to improve the fundamental understanding between morphology and productivity (Celler et al., 2012; Grimm et al., 2005; King, 1998; Posch et al., 2013; Veiter et al., 2018). In this thesis, morphological modeling of filamentous pellets is categorized in 1) microscopic approaches, 2) continuum approaches, and 3) population balance modeling (PBM) approaches. Microscopic approaches describe the growth of pellets, considering all positions of hyphae, branches, and tips. Contrary, continuum approaches are less detailed and outline the radial distributions of morphological properties in pellets. While microscopic and continuum approaches predict the development of individual pellets, PBM considers the pellet heterogeneity within a cultivation. As this thesis is based on the morphological characterization of individual pellets, PBMs are not elaborated here. However, Section 6.3 includes a discussion on how such modeling approaches could benefit from the methods and findings of this thesis.

Microscopic approaches　　As shown in Figure 4, microscopic models describe the development of hyphal networks including the location of hyphae, tips, and branches. While two-dimensional approaches consider the growth of filamentous microorganisms on a plane, three-dimensional ones enable the simulation of hyphal networks in submerged cultures. Since this thesis is about filamentous pellets, only three-dimensional models that incorporate the simulation of whole pellets are considered here.

Based on stochastic rules for tip extension and branching, pellets can be simulated starting from a single spore (Celler et al., 2012; Lejeune and Baron, 1997; Meyerhoff et al., 1995; Yang et al., 1992a). For this, microscopic approaches considered following intracellular phenomena: septation of hyphae (Celler et al., 2012; Yang et al., 1992a), distinction into apical, subapical, and hyphal compartments (Celler et al., 2012), and consumption and flow of a component in hyphae that influences the tip extension rate (Yang et al., 1992a). Recent advances in measuring and modeling the intracellular transport of secretory vesicles, which transport cell wall components to the hyphal tips (King, 2015; Kunz et al., 2020), have not been included in three-dimensional microscopic pellet models yet. Contrary, several approaches considered the diffusive mass transport of nutrients from the cultivation broth through the hyphal network of pellets (Celler et al., 2012; Lejeune and Baron, 1997; Meyerhoff et al., 1995). For this, the authors assumed spherical symmetry and computed the transport and consumption of nutrients based on partial differential equations. To prevent hyphae from growing into each other, collision detection can be included (Celler et al., 2012). Another phenomenon that can be considered in microscopic models is the abrasion of pellets due to shear forces (Celler et al., 2012; Meyerhoff et al., 1995). However, the development of coagulative pellets has not been

addressed sufficiently yet. While only Lejeune and Baron (1997) considered the development of pellets from spore agglomerates, these simulations were limited to 100 randomly placed spores. Hence, this was not realistic for coagulative pellet formation.

Most breakthroughs of microscopic approaches were achieved in the nineties including three-dimensional representation, intracellular processes, diffusive mass transport of nutrients into pellets, and abrasion of pellets. However, stagnation in model development can be observed. That might be caused by the absence of experimental data for model validation. Especially the hyphal network of the pellet interior cannot be quantified sufficiently to compare simulated and cultivated pellets (Sections 2.1.2 and 2.1.3). Additionally, the models lack well-founded correlations between the structure and the diffusivity for the computation of the nutrient supply (Section 2.2.1).
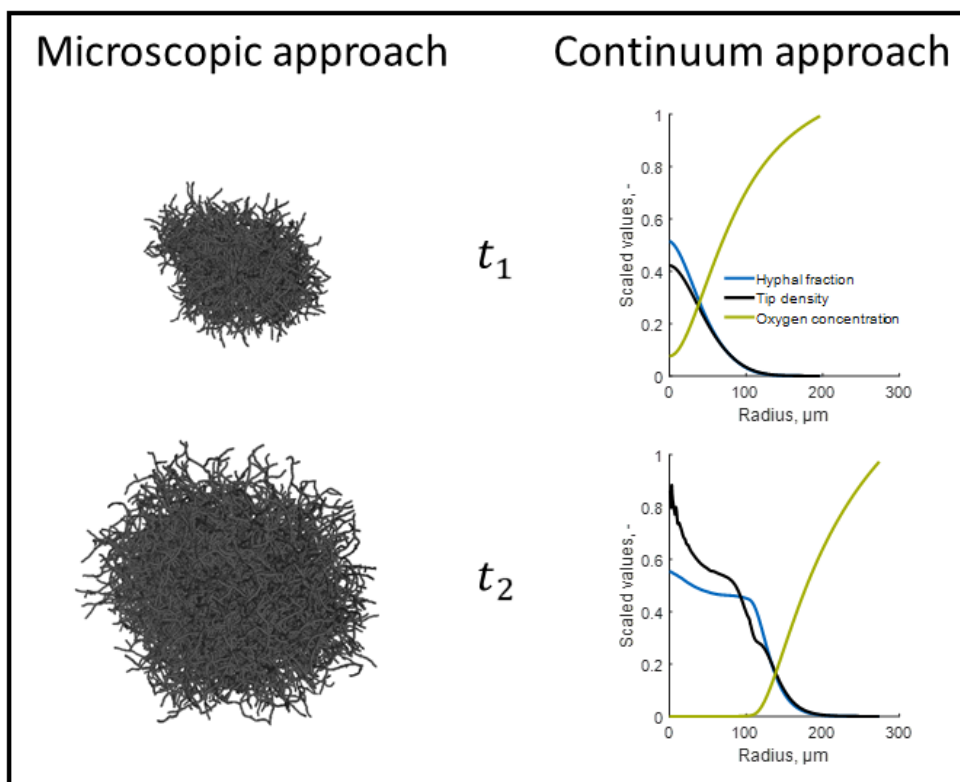
Figure 4: Morphological modeling of pellets. Microscopic approach: own work based on Celler et al. (2012); Continuum approach: own work based on Buschulte (1992).

Continuum approaches First continuum approaches to model pellet growth were based on the cube root relation for the development of the fungal biomass concentration in cultivations (Emerson, 1950; Pirt, 1966). The cube root relation is based on the hypothesis that pellet growth occurs only in the periphery. Contrary, the pellet center is assumed to consist of non-growing mycelium, into which oxygen does not diffuse. In later studies, the oxygen-limitation inside pellets was confirmed experimentally (Cronenberg et al., 1994; Hille et al., 2005; Wittier et al., 1986). Additionally, image analysis of pellet slices revealed the spatial heterogeneity of the hyphal material inside pellets qualitatively (Hille et al., 2005; Lin et al.,

2010; Priegnitz et al., 2012). However, the cube root relation does not consider spatial hetero-geneities of the hyphal fraction inside pellets. Buschulte (1992) and Meyerhoff et al. (1995) overcame this limitation. Their approaches assumed spherical symmetry of pellets concerning the spatial distribution of hyphal material and nutrients (Figure 4). Similar to microscopic approaches (Celler et al., 2012; Lejeune and Baron, 1997), transport and consumption of oxygen inside pellets was computed based on partial differential equations. In this way, the inactivation of mycelial growth in the pellet center can be addressed based on the nutrient profile. According to King (1998), a description with continuous variables for the biomass, such as concentrations of hyphae and tips seems meaningful. The approach introduced by Buschulte (1992) considers the radial concentrations of hyphae, tips, oxygen, and other sub-strates inside pellets during their growth and is based on coupled partial differential equations for these concentrations. With a so called layer model, Meyerhoff et al. (1995) described a simplification of the approach of Buschulte (1992). This approach divides the pellet in a few spherical shells and assumes constant values for hyphal fraction, tips, and nutrients inside these shells. To reduce computational time, this model intentionally omits partial differential equations except for the transport of nutrients into the pellet. Compared to a microscopic model similar to Yang et al. (1992a), the continuum approach resulted in an about 60 - 100 fold reduction of the demands for computing capacity (Meyerhoff et al., 1995).

While the computational time of continuum approaches is lower compared to microscopic ones, the level of detail remains high. Especially the morphological development of spherical symmetric pellets can be well described. Although continuum approaches seem promising to optimize filamentous fungal bioprocesses, recent advances are missing. To the author's knowledge, the model of Buschulte (1992) is still the most detailed approach. Similar to microscopic approaches, continuum ones lack sufficient validation procedures, which might be the reason for the stagnation in model development. Validation procedures would require radial profiles of morphological properties and substrates and a well-founded law for the diffusive mass transport through filamentous fungal networks. However, these properties are difficult or even impossible to measure with current techniques (Sections 2.1.2, 2.1.3, and 2.2.1).

3 Problem definition

Although pellets are often exploited in industrial processes using filamentous fungi, their inner structure and the resulting diffusion barrier for nutrients, oxygen, and secreted metabolites remained largely unexplored. The following knowledge gaps regarding the micromorphology and diffusivity of filamentous fungal pellets were identified based on the theoretical background.

Method to analyze the micromorphology of whole intact pellets does not exist. The micromorphology within pellets is known to have a high impact on the productivity of bioprocesses using filamentous fungi. Although many methods have been developed to investigate the macromorphology and periphery of pellets, there is no non-destructive approach to visualize the three-dimensional micromorphology of whole pellets. Further, no method exists for the analysis of 3D images of filamentous fungal networks. Methods to visualize and analyze the micromorphology of whole intact pellets would open new paths towards morphological engineering. For example, the impact of genetic and process engineering approaches on the morphology of pellets could be investigated in utmost detail. Additionally, existing morphological modeling approaches without suitable micromorphological input from experiments could be validated and improved.

Correlation between the three-dimensional structure and the diffusivity of pellets is not described. The supply with nutrients and oxygen is crucial for the metabolic activity and product formation in pellets. Studies revealed that the transport of nutrients and oxygen through dense hyphal networks is mainly driven by diffusion. However, a well-founded correlation between the micromorphology and the diffusivity through fungal pellets is lacking in literature. Such a correlation would enable the prediction of the diffusive transport of nutrients, oxygen, and secreted metabolites in filamentous fungal pellets and thus, contribute to the targeted design of pellet morphologies.

4 Methods for problem solving

The problem definition illustrates that new methods are required to reveal the micromorphology and diffusivity of filamentous pellets. Therefore, the following methods have been developed. A detailed description of all methods can be found in the embedded papers.

Method to visualize whole intact pellets three-dimensionally. Applying X-ray microcomputed tomography (μCT) measurements, it became feasible to visualize the three-dimensional (3D) network of hyphae forming filamentous fungal pellets. While this technique enabled the non-destructive visualization of whole pellets with several hundred micrometers in diameter, the hyphae with diameters down to 3 μm were resolved.

Method to analyze three-dimensional images of pellets. To quantify the micromorphology of whole pellets, automated image analysis was conducted on the acquired μCT images. After binarization of the hyphal network, the centerlines of hyphae were determined and used to locate tips and branches. This procedure enabled the investigation of morphological properties such as the hyphal length, number of tips, number of branches, hyphal growth unit (HGU), and porosity of whole pellets. Additionally, the spatial distributions of the hyphal fraction, tip density, and branch density were determined.

Method to correlate structure and diffusivity of pellets. Diffusion computations were conducted through numerous representative sub-volumes per μCT measured pellet. The computations resulted in a diffusivity for each sub-volume, which is a measure for the geometrical diffusion hindrance and independent of the diffusing substance. Correlation analysis between the diffusivities and the structures of several hundred *Aspergillus niger* sub-volumes unveiled a diffusion-law with respect to the solid hyphal fraction.

Method to determine a universal law for the diffusion through mycelial networks. To consider the broad morphological range of filamentous fungi, the structures and diffusivities of both μCT measured and simulated pellets were correlated based on the method described above. While μCT measured pellets from four fungal species already showed strongly differing morphologies, Monte Carlo simulated pellets covered the broad morphological range of filamentous microorganisms. To obtain the required 3D structures of the simulated pellets, an existing microscopic model was extended and implemented. Analysis of all measured and simulated pellets unveiled a universal law for the diffusion of nutrients, oxygen, and secreted metabolites with the solid hyphal fraction as the only independent variable.

5 Results

5.1 Paper I: An X-ray microtomography-based method for detailed analysis of the three-dimensional morphology of fungal pellets (Schmideder et al., 2019a)

Summary

Although the micromorphology of filamentous fungal pellets is strongly linked to the productivity in bioprocesses, there is no method to visualize the detailed three-dimensional morphology of whole intact pellets. Further, no method for the analysis of three-dimensional images of filamentous fungal networks exists to date. To enable the non-destructive visualization of whole pellets, we developed a protocol based on X-ray microcomputed tomography (µCT). Exemplarily, we investigated pellets of *Aspergillus niger* and *Penicillium chrysogenum*. The binarization of the images enabled the determination of the hyphal network within whole pellets. Based on the binarized hyphal network, skeletonization was conducted to investigate the location of tips and branches as well as the total hyphal length. Thus, the cumulative morphological properties total hyphal length, total tip number, total branch number, porosity, and hyphal growth unit of whole pellets can be determined. Additionally, multiple hypotheses about the morphological development of fungal pellets can be drawn from the spatial distributions of the hyphal fraction, tip density, and branch density. Based on µCT measurements and image analysis, the outcome of experimental morphological engineering approaches on pellet structures can be investigated in unprecedented detail. Further, the determined three-dimensional morphology will serve as valuable input to validate and improve existing morphological modeling approaches. As shown in Paper II and III, the structure of analyzed pellets can also be used to compute the resulting diffusion barrier for nutrients, oxygen, and secreted metabolites.

Author contributions

Stefan Schmideder did the conception and design of the study and wrote the manuscript, which was edited and approved by all authors. Heiko Briesen and Vera Meyer supervised the study. Lars Barthel and Ludwig Niessen cultivated and freeze-dried fungal pellets. Stefan Schmideder and Michaela Thalhammer developed a protocol for µCT measurements. Stefan Schmideder, Tiaan Friedrich, and Tijana Kovačević developed 3D image analysis of µCT measurements. Stefan Schmideder analyzed the results. Stefan Schmideder, Lars Barthel, Heiko Briesen, and Vera Meyer interpreted the results.

ARTICLE

WILEY | BIOTECHNOLOGY BIOENGINEERING

An X-ray microtomography-based method for detailed analysis of the three-dimensional morphology of fungal pellets

Stefan Schmieder[1] | Lars Barthel[2] | Tiaan Friedrich[1] | Michaela Thalhammer[1] | Tijana Kovačević[1] | Ludwig Niessen[3] | Vera Meyer[2] | Heiko Briesen[1]

[1]Technical University of Munich, School of Life Sciences Weihenstephan, Chair of Process Systems Engineering, Freising, Germany

[2]Department of Applied and Molecular Microbiology, Institute of Biotechnology, Technische Universität Berlin, Berlin, Germany

[3]Lehrstuhl für Technische Mikrobiologie, Technical University of Munich, Freising, Germany

Correspondence
Heiko Briesen, Technical University of Munich, Gregor-Mendel-Straße 4, 85354 Freising, Germany.
Email: heiko.briesen@tum.de

Abstract

Filamentous fungi are widely used in the production of biotechnological compounds. Since their morphology is strongly linked to productivity, it is a key parameter in industrial biotechnology. However, identifying the morphological properties of filamentous fungi is challenging. Owing to a lack of appropriate methods, the detailed three-dimensional morphology of filamentous pellets remains unexplored. In the present study, we used state-of-the-art X-ray microtomography (μCT) to develop a new method for detailed characterization of fungal pellets. μCT measurements were performed using freeze-dried pellets obtained from submerged cultivations. Three-dimensional images were generated and analyzed to locate and quantify hyphal material, tips, and branches. As a result, morphological properties including hyphal length, tip number, branch number, hyphal growth unit, porosity, and hyphal average diameter were ascertained. To validate the potential of the new method, two fungal pellets were studied—one from *Aspergillus niger* and the other from *Penicillium chrysogenum*. We show here that μCT analysis is a promising tool to study the three-dimensional structure of pellet-forming filamentous microorganisms in utmost detail. The knowledge gained can be used to understand and thus optimize pellet structures by means of appropriate process or genetic control in biotechnological applications.

KEYWORDS

filamentous fungi, image analysis, pellets, three-dimensional morphological quantification, X-ray microtomography

1 | INTRODUCTION

Filamentous fungi are microorganisms with a high capability to produce primary metabolites, proteins, secondary metabolites, and biopolymers. Over a century of research on filamentous fungi has led to the development of diverse biotechnological applications, including the production of organic acids, enzymes, antibiotics, and exopolysaccharides (Cairns, Nai, & Meyer, 2018; Meyer, 2008; Meyer et al., 2016). When filamentous fungi are cultivated in a submerged culture, they develop different macromorphologies, such as dispersed mycelia consisting of nonaggregated hyphae, clumps of loosely aggregated hyphae, and densely packed compact spherical structures called pellets (Pirt, 1966). Such morphology is determined by the fungal species and the cultivation conditions, including the fermenter geometry, agitation systems, cultivation mode (batch, fed-batch, or continuous), type and concentration of substrates, pH, and temperature (Papagianni, 2004). The preferable fungal morphology strongly depends on the aim of the respective bioprocess (Gibbs, Seviour, & Schmid, 2000). For example, the industrial cell factory *Aspergillus niger* is used in its pellet form to produce citric acid and in its dispersed form to produce enzymes (Meyer et al., 2016).

Because fungal morphology is of considerable importance, it is vital to thoroughly study the structure of hyphal aggregates. Light microscopy is sufficient enough to analyze and characterize disperse mycelium and small aggregates owing to their simple geometry. However, more sophisticated tools are essential for analyzing the complex morphology of densely packed pellet structures. The inner pellet region often differs from its outer region. Densely packed pellets result in oxygen limitation in the inner region, thereby making the pellets prone to reduced growth or even autolysis (Ehgartner, Herwig, & Fricke, 2017; Hille, Neu, Hempel, & Horn, 2006). Many techniques have been developed to study the inner pellet region. A relatively simple method is the analysis of pellet slices by using light microscopy (Lin, Scholz, & Krull, 2010). A more advanced technique for the same purpose is the use of confocal laser scanning microscopy. By using this technique, cryomicrotome slices of previously frozen and dyed fungal pellets, with a thickness of 40–60 μm, are scanned three-dimensionally and then evaluated with image analysis, giving a hyphal distribution for small cutouts of the pellet (Hille, Neu, Hempel, & Horn, 2005). Applying viability staining in combination with confocal laser scanning microscopy, active and inactive pellet regions can be detected (Nieminen, Webb, Smith, & Hoskisson, 2013). Further information can be obtained using cryo-scanning electron microscopy with whole pellets, revealing the difference between highly intertwined superficial hyphae and a densely packed deep mycelium (Villena & Gutiérrez-Correa, 2007). In addition to these single-sample examination methods, flow cytometry can be used to elucidate the core compactness of numerous fungal pellets in short time (Ehgartner et al., 2017).

In fungal biotechnology, three pellet-forming mechanisms are generally distinguished: coagulative, noncoagulative, and hyphal element agglomerating (Veiter, Rajamanickam, & Herwig, 2018). Coagulative formation comprises two steps. Numerous spores aggregate because of electrostatic and hydrophobic interactions and then the aggregated spores begin to germinate and form pellets (Zhang & Zhang, 2016). A typical representative of this is A. niger. In noncoagulative formation, the spores germinate before they start to form pellets, meaning that, theoretically, a single spore forms a pellet. Species that commonly form noncoagulative pellets include Rhizopus oryzae and Mortierella vinacea (Zhang & Zhang, 2016). Some fungi, such as Penicillium chrysogenum show both, coagulative and non-coagulative pellet formation, and are therefore categorized into the hyphal element agglomerating type. In this case, the agglomeration of different hyphal elements leads to hyphal clumps and subsequent pellet formation (Veiter et al., 2018).

Modeling approaches have been developed to predict the morphology of filamentous pellets in submerged cultures (King, 1998, 2015; Meyer, Fiedler, Nitsche, & King, 2015). Many modeling approaches include locating the hyphae, tips, and branches in filamentous pellets (Celler, Picioreanu, vanLoosdrecht, & vanWezel, 2012; Lejeune & Baron, 1997; Yang, King, Reichl, & Gilles, 1992). Others assume spherical symmetry of pellets and consider morphological properties, such as the hyphal length density and tip density dependent on the radius (Buschulte, 1992; Meyerhoff, Tiller,

& Bellgardt, 1995). However, these modeling approaches have not been fully validated yet owing to the significant lack of knowledge of three-dimensional pellet morphologies.

This study thus introduces a new method for a detailed investigation of the morphological properties of filamentous pellets and is structured as follows: In Section 2, the preparation of fungal pellets and the microtomography (μCT) measurements are described. The applied μCT measurements offer a nondestructive way to visualize complex morphologies and are applied intensively in medical and biological research as well as material science (Salvo et al., 2003; Stock, 2008). Since the subsequent data processing of fungal pellets cannot be clearly separated into the methodological development of the image processing and the results of this processing, Section 3 is introduced. By applying three-dimensional image analysis, the locations of hyphae, tips, and branches were determined. To demonstrate the potential of the described method, two freeze-dried fungal pellets from submerged cultivations from A. niger and P. chrysogenum, respectively, were investigated in detail in the Section 4. Based on the processed data of the fungal pellets, morphological properties like the hyphal length, number of tips, number of branches, hyphal growth unit (HGU), porosity, and average diameter of hyphae were investigated.

2 | MATERIALS AND METHODS

2.1 | Pellet preparation

Conidiospores of P. chrysogenum strain MUM17.85 (Micoteca da Universidade do Minho, Braga, Portugal) and A. niger strain MF22.4 (Fiedler, Barthel, Kubisch, Nai, & Meyer, 2018) were obtained from agar plate cultures by using standard procedures for filamentous fungi (Bennett & Lasure, 1991). The spores were grown in liquid cultivation media for P. chrysogenum (yeast carbon base; Difco, Franklin Lakes, NJ) and A. niger (complete medium; Meyer, Ram, & Punt, 2010) for 24–48 hr until pelleted structures became visible. Single pellets were then carefully removed by pipetting and were washed three times with water. Samples were frozen in liquid nitrogen while pellets were floating in water to preserve their structure and were subsequently freeze-dried. A FreeZone device (Labcono, Kansas City, MO) was used to freeze dry the A. niger pellet at 0.014 mbar and −55°C for 24 hr. The freeze-drying of the P. chrysogenum pellet was performed using a FreeZone 2,5 PLUS device (Labconco) at 0.002 mbar and ambient temperature for 24 hr. To prevent the freeze-dried pellets from absorbing water, the samples were stored in sealed Eppendorf tubes for further use. To investigate the influence of the applied freeze-drying process on the morphology of filamentous pellets, we compared the same pellets in two states: wet (immediately after fermentation) and freeze-dried. Light microscope images of wet and freeze-dried A. niger and P. chrysogenum pellets are shown in Figures S1–S5. After 48 hr fermentation of A. niger and P. chrysogenum, the diameter of freeze-dried pellets decreased by 9% and 10% on average, respectively. The pellet diameter has been calculated on base of the outermost hyphae of the
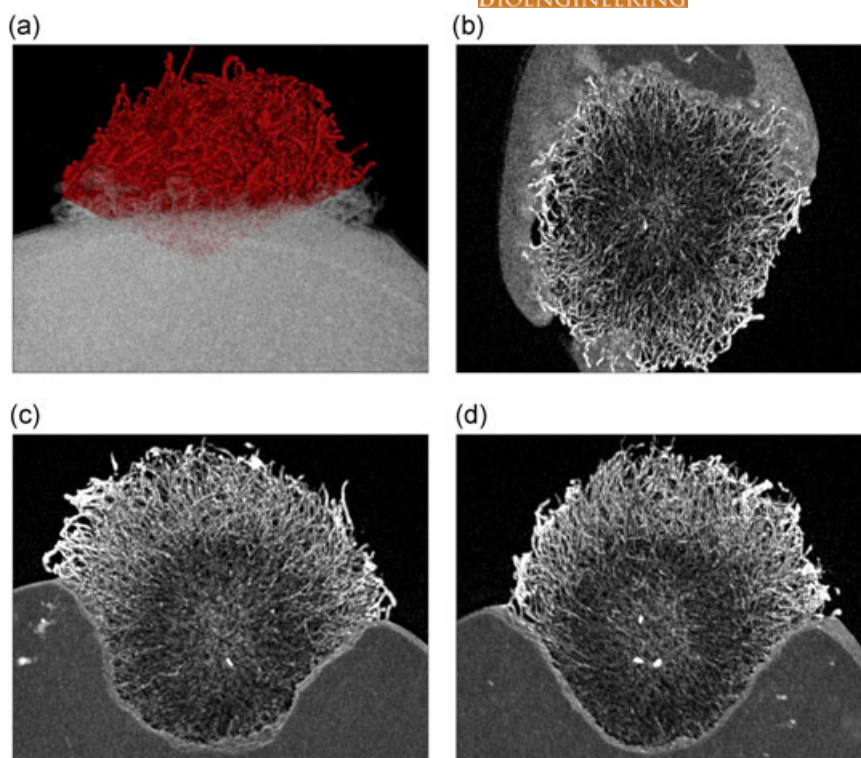
FIGURE 1 μCT image of *A. niger* pellet; two-dimensional projections of a three-dimensional image. (a) Whole pellet with XZ-orientation; red object represents the analyzed cone of the pellet; transparent white object represents the remaining pellet and fixation material. (b–d) Slices (100 μm) of different orientations; center of the slices is the pellet center; image processed with basic rendering only; (b) XY-orientation; (c) YZ-orientation; (d) XZ-orientation [Color figure can be viewed at wileyonlinelibrary.com]

pellets. The fermentation of *P. chrysogenum* for 24 hr resulted in looser pellets (Figure S3) and a decrease in the dried pellet diameter of 13%. In addition, we measured the diameter of wet and freeze-dried hyphae at the pellet periphery of *P. chrysogenum* pellets manually with FIJI. The average diameter of wet hyphae was 3.6 μm, whereas freeze-dried hyphae had an average diameter of 3.5 μm. In addition, the freeze-dried samples do still exhibit hairy regions in the outer part of the pellets (Figures S4 and S5).

2.2 | X-ray microtomography

Three-dimensional images of the fungal pellets were acquired using a custom-built X-ray microtomography system (XCT-1600HR; Matrix Technologies, Feldkirchen, Germany). Between the open tube and the detector, the fungal pellets were fixed on a sample holder, which rotated during the measurement. The tube of the μCT system generates a cone beam. Thus, two-dimensional projections were obtained from various angles. The projections were reconstructed using a custom-designed software (Matrix Technologies) that uses CERA (Siemens, Munich, Germany) to receive three-dimensional images. Because freeze-dried filamentous pellets have a low density, low energy (60 kV, 25 μA) was used to generate the cone beam. The three-dimensional images had a resolution of 1 μm (i.e., the edge length of the voxels was 1 μm). To fix the *A. niger* pellet on top of the sample holder, an instant adhesive (UHU, Bühl, Germany) was used. Partial embedding of the *A. niger* pellet in the instant adhesive guaranteed structural stability. For the *P. chrysogenum* pellet, a double-sided tape (Tesa, Norderstedt, Germany) was sufficient to guarantee structural stability.

3 | DATA PROCESSING

This section describes the detection of tips, branches, and hyphal material in pellets by using image analysis. The analysis was conducted with the μCT images of the *A. niger* (Figure 1) and the *P. chrysogenum* pellet (Figure 2) acquired as described in Section 2.

3.1 | Preprocessing

Preprocessing aimed to generate binarized three-dimensional images with the hyphal material as foreground. Thereby, voxels originating from noisy data and sample fixation materials must be separated from the pellet.

Both fixation materials, the instant adhesive for *A. niger* and the double-sided adhesive tape for *P. chrysogenum*, showed gray values similar to those of the pellets. Because of this, the automated segmentation of the pellet turned out to be difficult to implement. To achieve successful segmentation, the images were cropped. Part of the *A. niger* pellet enclosed in the instant adhesive was deformed. For further investigation, a conically shaped section was cropped from the raw data using MATLAB (version R2016a; MathWorks, Natick, MA), resulting in a structure not affected by the fixation material (Figure 1a). This cone was used to represent the whole pellet. According to visual observations, the tip of the cone was assumed to be the center of the pellet. The opening angle of the cone was chosen to be 65°. The *P. chrysogenum* pellet was cropped by cutting off a small XY-orientated slice at the bottom of the three-dimensional image with the software MAVI (version 1.4.1; Fraunhofer ITWM, Kaiserslautern, Germany). After cropping, the 16-bit grayscale
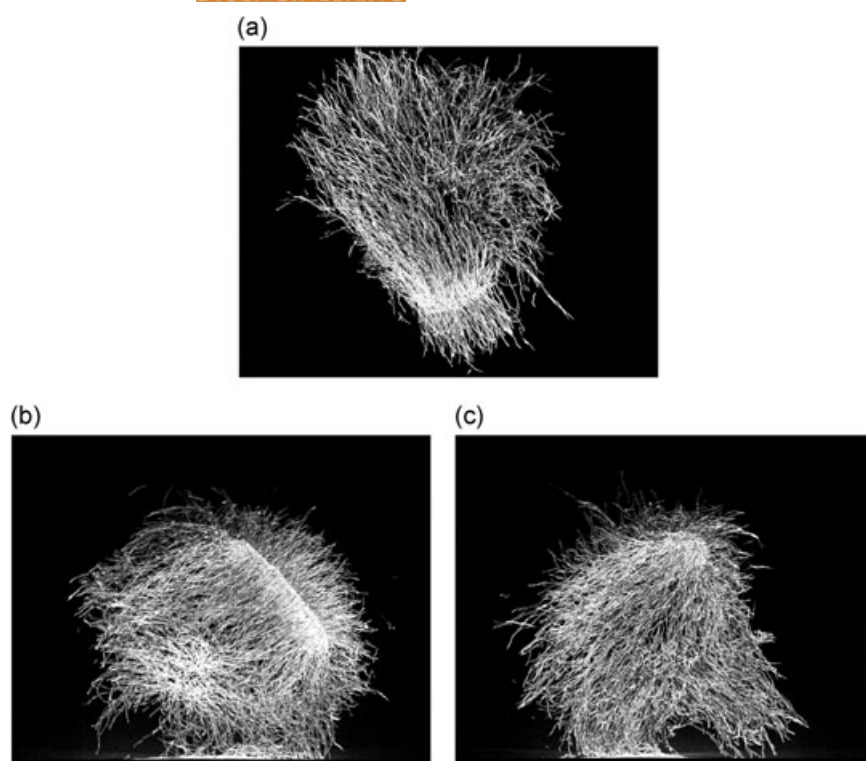
FIGURE 2 µCT image of *a P. chrysogenum* pellet; two-dimensional projections of three-dimensional image; slices (100 µm) of different orientations; center of the slices is the pellet center; image processed with basic rendering only. (a) XY-orientation; (b) YZ-orientation; (c) XZ-orientation

images (i.e., voxels of µCT images exhibiting gray values between 0 and 65,535) were binarized to differentiate between the hyphae and background (Figure 3a,b). The binarization was performed using MAVI by setting a gray value threshold that was calculated using Otsu's method (Otsu, 1979). The voxels with gray values higher than the gray value threshold were designated as hyphal material. Small interconnected objects, which were not part of the pellet, were eliminated. This was achieved by labeling neighboring voxels with MAVI and deleting all but the largest object. It has to be mentioned that MATLAB or FIJI could also be applied to the preprocessing steps conducted in MAVI. However, the three-dimensional rendering performance of MAVI was highly superior, which enabled to visualize the conducted processing steps immediately.

3.2 | Skeletonization

Since there exists no established three-dimensional skeletonization method for filamentous microorganisms, we adopted and adapted a procedure that has been already successfully applied for two-dimensional image analysis. Barry, Williams, and Chan (2015) published an ImageJ plugin for the morphological analysis of light microscope images of filamentous microorganisms. In their two-dimensional skeletonization procedure, they also applied an iterative thinning method, as we chose for our three-dimensional skeletoniza-tion. An advantage of the usage of an iterative thinning algorithm is its computational efficiency. Skeletonization alternatives, such as methods based on Voronoi Covariance Measurement (Grélard, Baldacci, Vialard, & Domenger, 2017) would result in significantly higher computation times. However, computational efficiency is

crucial for the analysis of the high data volume of the µCT measurements. In the present work, skeletonization was achieved using the plugin "Skeletonize (2D/3D)" for FIJI/ImageJ (Schneider, Rasband, & Eliceiri, 2012; Schindelin et al., 2012). This plugin is based on the three-dimensional thinning algorithm by Lee, Kashyap, and Chu (1994) and Homann (2007). The basic procedure is to erode the object's surface iteratively until only the centerline remains. To analyze the obtained skeleton voxels of the three-dimensional image, the FIJI plugin "Analyze Skeleton (2D/3D)" (Arganda-Carreras, Fernández-González, Muñoz-Barrutia, & Ortiz-De-Solorzano, 2010) was used. Depending on their direct neighbors, the skeleton voxels can be categorized into three different classes: tips, "normal" hyphae, and branch voxels. The tips are endpoints of the skeleton with only one neighbor. "Normal" hyphae are skeleton voxels with two neighbors, and branch voxels are skeleton voxels with at least three neighbors. As illustrated in Figure 3c,d, the plugin labels each voxel of the skeleton as either a hyphal voxel (red), a branch voxel (green), or a tip (yellow). In addition, the plugin calculates the total hyphal length of the pellet based on the number and location of skeleton voxels.

3.3 | Postprocessing

To correct minor issues arising because of preprocessing and skeletonization, three postprocessing steps were applied to the skeleton using MATLAB.

The first issue concerns incorrect short junctions, appearing due to surface roughness (Figure 4a,b). The deletion of such short junctions is a commonly described issue when working with skeletons (e.g. Barry, Chan, & Williams, 2009; Grélard et al., 2017). To delete

FIGURE 3 Image processing steps for a small region of the *P. chrysogenum* pellet; images are rendered with VGSTUDIO MAX. (a) Raw image: CT data with a low threshold for gray values. (b) Preprocessed image: for binarization, threshold for gray values is applied; additionally, small connected objects are deleted. (c) Skeletonized image. (d) Analyzed image: analysis of the skeleton; tips are marked yellow and branches green [Color figure can be viewed at wileyonlinelibrary.com]
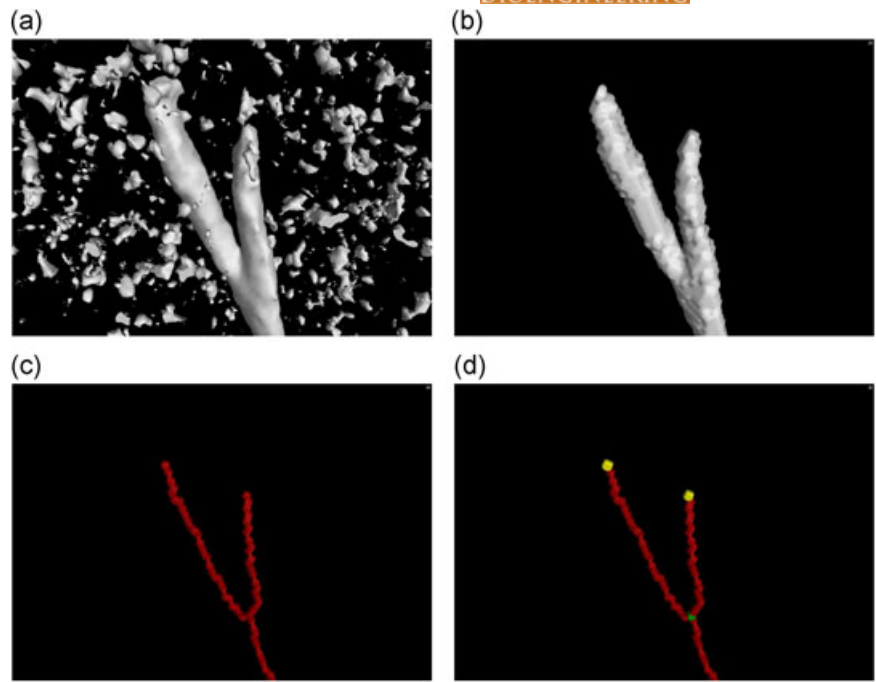

FIGURE 4 Postprocessing steps for small regions of *P. chrysogenum* pellet; transparent white objects illustrate the binarized three-dimensional data, red objects the skeleton, yellow markers the tips, and green markers the branches. (a) Without postprocessing: coarse surface of binarized hyphae results in short junction. (b) Postprocessing: short junction resulting from coarse surface of binarized hyphae is deleted. (c) Without postprocessing: overlapping hyphae result in branch. (d) Postprocessing: incorrect branch is deleted. (e) Without postprocessing: close parallel hyphae can cause bridges imitating branches. (f) Postprocessing: incorrect branches are deleted [Color figure can be viewed at wileyonlinelibrary.com]
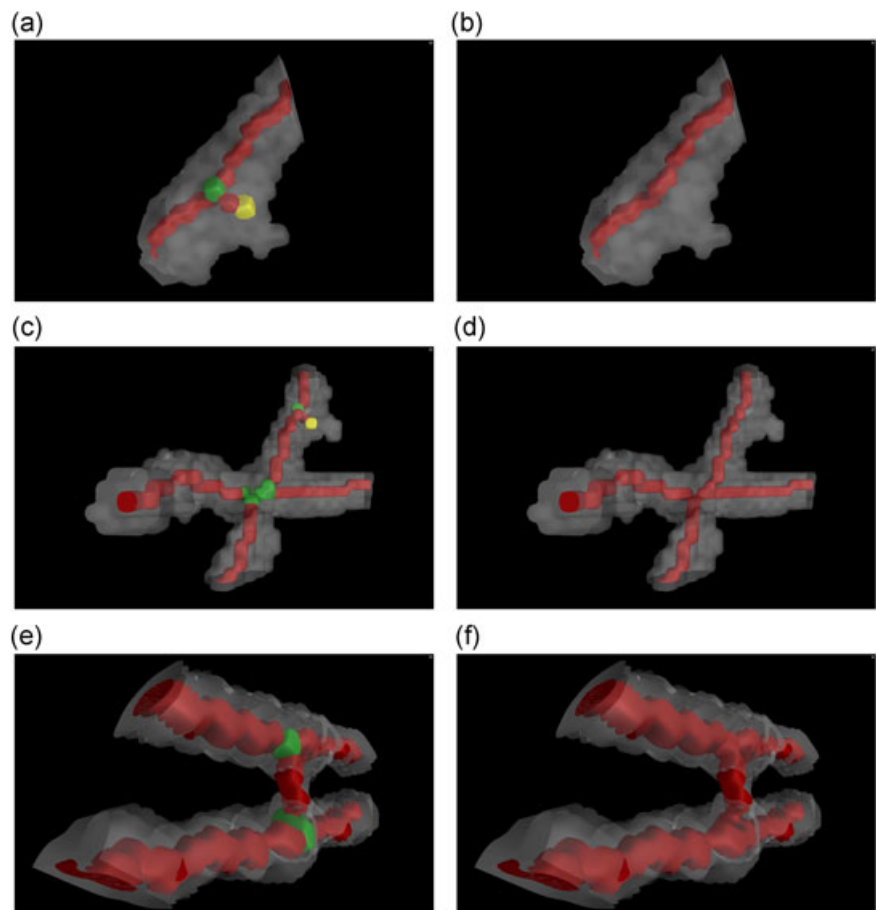
such junctions, geodesic distance transform (MATLAB function "bwdistgeodesic") was used, which can measure the distance between a pair of voxels obtained by traversing only the foreground voxels. Here, the distance was measured as quasi-Euclidean, approximating the actual distance between each pair of the neighboring voxels on the path. First, this procedure ascertained the distance $x_{min,branch}$ to the closest branch voxel for each hyphal (skeleton) voxel. Afterward, the procedure was used to find the
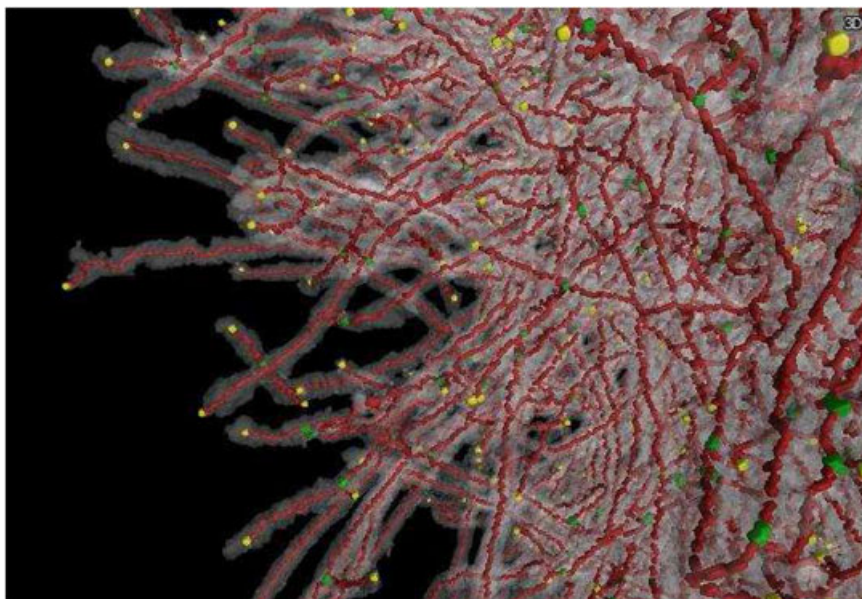
FIGURE 5 Skeletonized region of *P. chrysogenum* pellet: white transparent object illustrates the binarized three-dimensional data, red object the skeleton, yellow markers the tips, and green markers the branches [Color figure can be viewed at wileyonlinelibrary.com]

distance $x_{min,tip}$ to the closest tip voxel. After this, $x_{sum,tip+branch} = x_{min,tip} + x_{min,branch}$ for each voxel of the skeleton was calculated. Tip and "normal" hyphae voxels of the skeleton with $x_{sum,tip+branch} \leq x_{threshold}$ were deleted. Branch voxels of the skeleton with $x_{sum,tip+branch} \leq x_{threshold}$ were changed to "normal" hyphae voxels. With 4 μm, $x_{threshold}$ was set to a value close to the hyphal diameter (Nielsen, 1993; Packer, Keshavarz-Moore, Lilly, & Thomas, 1992).

In addition, overlapping hyphae misleadingly resulted in branches. This could be easily corrected because overlapping hyphae result in four hyphal tubes, whereas a true branching hypha generates three hyphal tubes connected to the branch (Figure 4c,d). Hence, the number of hyphal tubes connected to the branch were counted, and a branch was defined as correct, only if it was connected to three hyphal tubes.

Binarization of close parallel hyphae may occasionally be misinterpreted as branches because of small bridges between the hyphae. The connection between two parallel hyphae can be caused by two effects: the fusion between hyphae (Read & Lichius, 2009) or misinterpreting noisy data by image analysis. The investigation of the actual origin could be the focus of future studies. In both cases, the branches are not caused by branching itself. Hence, the last postprocessing step changed the incorrect branches to "normal" hyphae (Figure 4e,f). Branches closer to another branch at a distance of less than 6.5 μm (*P. chrysogenum*) or 5.5 μm (*A. niger*) were defined as incorrect. These thresholds were chosen to be 2 μm higher than the average hyphal diameters (Nielsen, 1993; Packer et al., 1992). Overall, this processing step prevented an overestimation of the number of branches.

3.4 | Determination of the local hyphal fraction

The newly defined morphological property, "local hyphal fraction" (LHF), is a measure of the local accumulation of hyphal material in filamentous pellets. The LHF is the ratio between the volume of hyphal material and the total volume with regard to a specified local volume. Binarized images of the pellets included hyphal voxels and voxels corresponding to empty space. The LHF was determined by applying an appropriate filter to the binarized images. For each voxel, the filter counted the hyphal voxels in its neighborhood. To obtain an average of the neighborhood, a cube with an edge length of 61 voxels was used, with the center of the cube containing the target voxel. The LHF of a voxel is the number of hyphal voxels of the cube divided by the total number of voxels of the cube. Thus, a voxel with an LHF of 0.3 implies that the region of the target voxel has a porosity of 70%, and the remaining 30% of the region is filled with hyphal voxels. Applying this filter method, the LHF of each pellet voxel was calculated.

To enable visualization of the LHFs at different points, these values are shown on spherical shells with varying radius. For each sphere, the LHFs are shown on 4,800 equally-distributed points, as illustrated in Figure 9. The points were obtained by the HEALPix discretization (Gorski et al., 2005), which provides 4,800 representative coordinates at the sphere surface. Thus, the value of the LHF of the closest voxel of the pellet was assigned to the representative coordinate of the sphere.

4 | RESULTS AND DISCUSSION

In this study, we demonstrate the potential of our μCT measurement and three-dimensional image analysis system to investigate the morphology of filamentous pellets. Exemplarily, two pellets have been investigated in detail: one *A. niger* (Figure 1) and one *P. chrysogenum* (Figure 2) pellet. *A. niger* represents the coagulative type for pellet formation and *P. chrysogenum* the hyphal element agglomerating type. The investigation of the pellets is based on final binarized (Figure 3a,b), skeletonized (Figure 3c,d), and post-processed (Figure 4) pellets. The
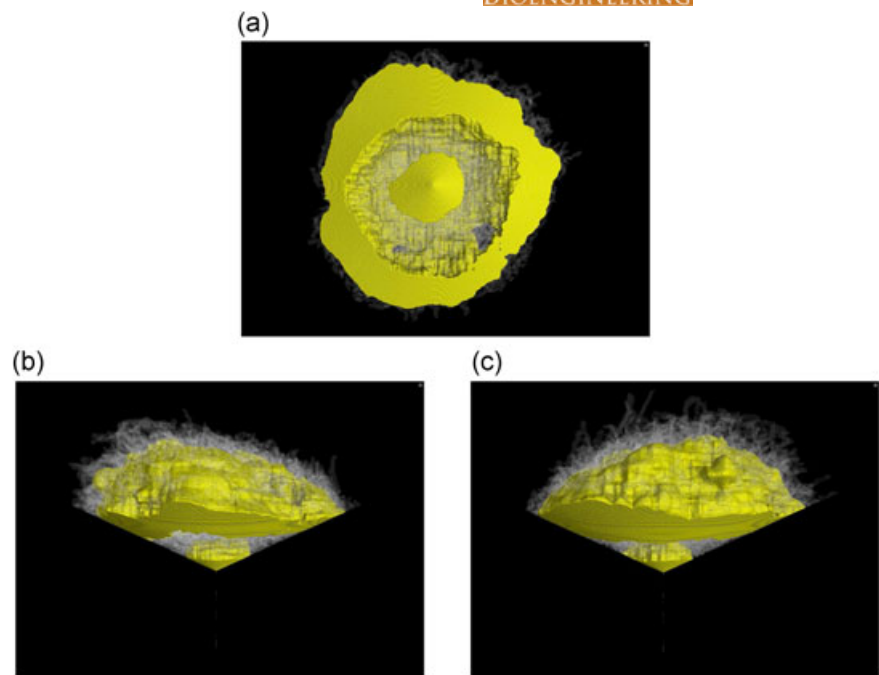
FIGURE 6 Regions with high hyphal fractions of the cone of the *A. niger* pellet illustrated for three different perspectives; white: binarized cone of *A. niger* pellet; yellow: regions with a hyphal fraction higher than 0.20. (a) Bottom perspective. (b) Right perspective. (c) Front perspective [Color figure can be viewed at wileyonlinelibrary.com]

FIGURE 7 Regions with high hyphal fractions of *P. chrysogenum* pellet illustrated for three different perspectives; white: binarized *P. chrysogenum* pellet; yellow: regions with a hyphal fraction higher than 0.20. (a) Bottom perspective. (b) Right perspective. (c) Front perspective [Color figure can be viewed at wileyonlinelibrary.com]
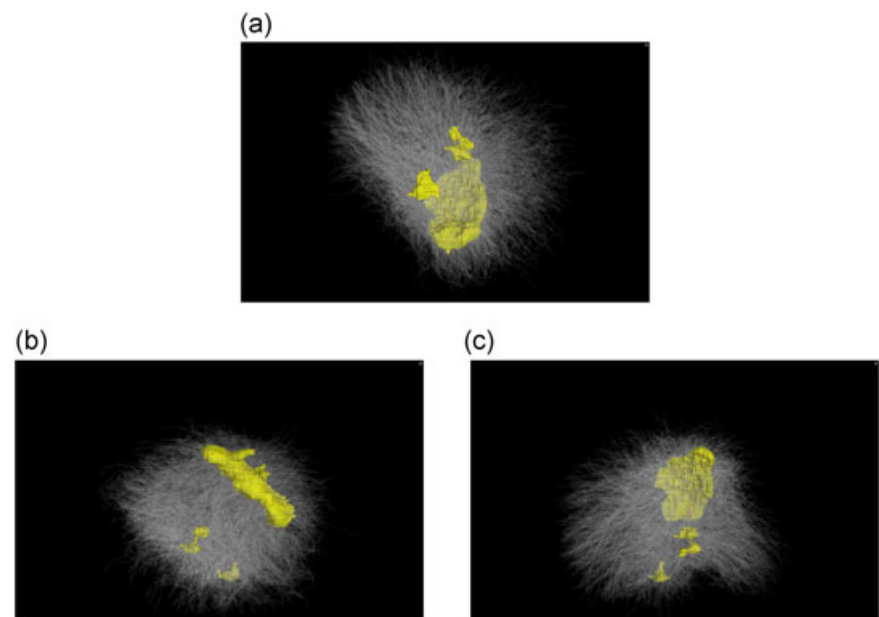
mentioned operation steps are described and discussed in detail in Section 3. Figure 5 displays a processed region of the *P. chrysogenum* pellet.

4.1 | Global morphology of pellets

The final processed images were used to calculate pellet diameter, porosity, total hyphal length, average hyphal diameter, total tip number, total branch number, HGU, and hyphal branch unit (HBU). In the case of the *A. niger* pellet, a conical section of the pellet not affected by the fixation material was analyzed (Figure 1a). To determine the morphology of the whole pellet, the other part of the

pellet was assumed to exhibit the same properties as the studied portion. This approach was selected because visual observation of the *A. niger* showed spherical symmetry (Figure 1 and see below). As the *P. chrysogenum* pellet was not affected by the fixation material, it was possible to analyze the complete pellet.

The diameter of the pellet d_{Pellet} was estimated as the volume equivalent diameter of the convex hull of the respective pellet: $d_{\text{Pellet}} = \sqrt[3]{\frac{6 \cdot V_{\text{ConvHull}}}{\pi}}$. The porosity, ϵ, was defined by the volume of the hyphal material V_{Hyphae} and the volume of the convex hull of the pellet: $\epsilon = 1 - \frac{V_{\text{Hyphae}}}{V_{\text{ConvHull}}}$. The total hyphal length L_{Hyphae}, total tip number, and total branch number were determined as described earlier. Based on the volume of the hyphal material and the total
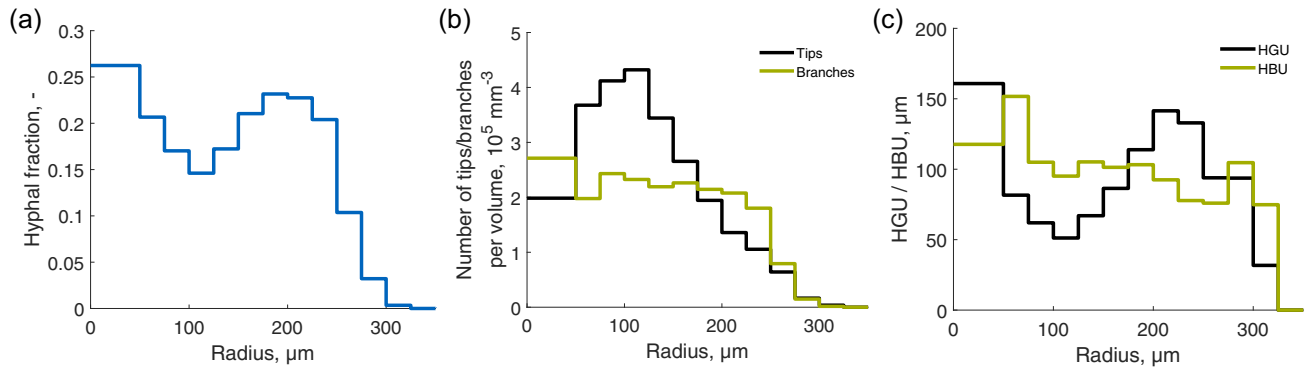
FIGURE 8 Morphological properties of spherically symmetric *A. niger* pellet dependent on radius; morphological properties are calculated for shells. The width of shells is 25 μm and the inner sphere has a radius of 50 μm. (a) Hyphal fraction. (b) Number of tips/branches per volume. (c) Hyphal growth unit (HGU): hyphal length in micrometer per number of tips; hyphal branch unit (HBU): hyphal length in micrometer per number of branches [Color figure can be viewed at wileyonlinelibrary.com]
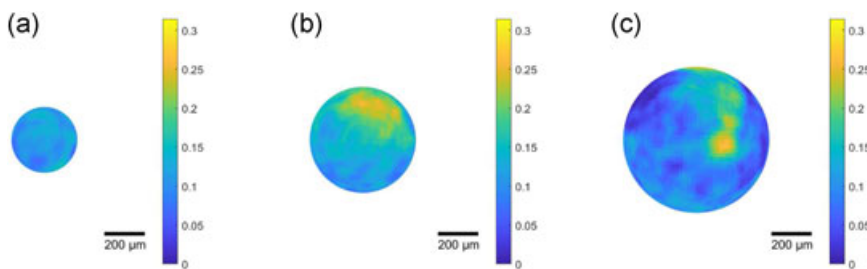

FIGURE 9 Local hyphal fraction of *P. chrysogenum* pellet for different distances from the pellet center: (a) 150 μm. (b) 250 μm. (c) 350 μm [Color figure can be viewed at wileyonlinelibrary.com]

hyphal length, the average diameter of hyphae d_{Hyphae} was calculated as $d_{\text{Hyphae}} = \sqrt{\frac{4 \cdot V_{\text{Hyphae}}}{\pi \cdot L_{\text{Hyphae}}}}$. The HGU and HBU were estimated as follows:

$$HGU = \frac{\text{Total hyphal length}}{\text{Total number of tips}} \quad (1)$$

$$HBU = \frac{\text{Total hyphal length}}{\text{Total number of branches}}. \quad (2)$$

The morphological properties of the analyzed *A. niger* pellet and *P. chrysogenum* pellet are listed in Table 1. The *A. niger* pellet has a diameter of 633 μm, a porosity of 0.87, and an average hyphal diameter of 3.8 μm. The *P. chrysogenum* pellet has a diameter of 1085 μm, a porosity of 0.94, and an average diameter of 4.1 μm.

These diameters of the hyphae correspond to those described in the literature (Colin, Baigorí & Pera, 2013; Morrison & Righelato, 1974; Nielsen, 1993; Packer et al., 1992). Since the average hyphal diameter was calculated on the basis of the volume of the hyphal material and the total hyphal length, our image data suggest that they are sufficiently precise to deduce biologically meaningful information. The HGU and HBU, respectively, were 95 μm and 93 μm for *A. niger* and 150 μm and 135 μm for *P. chrysogenum*. Considering a single pellet, the HGU and HBU should be in a similar range because each new branch results in one new tip. With 95 μm, the *A. niger* pellet showed an HGU in a range comparable to literature (Colin et al., 2013). By contrast, the *P. chrysogenum* pellet, with an HGU of 150 μm, showed a higher HGU value than mentioned in the literature (29–99 μm; Morrison & Righelato, 1974). The reported

value, however, has been obtained for disperse mycelia and loose clumps and therefore cannot be directly compared with the present study. Nevertheless, we emphasize that future studies involving μCT measurements of fungal pellets need a large sample size for analysis to obtain statistically significant data.

It is clear that μCT analysis is a powerful tool to estimate morphological properties of fungal pellets, including total hyphal length, total tip number, total branch number, HGU, and HBU. To our knowledge, this is the first study to do so. Moreover, properties such as porosity and average hyphal diameter can be estimated on the basis of information obtained for a complete pellet. The determination of pellet's porosity via light microscopic analysis of pellet cross sections (Hille et al., 2005; Lin et al., 2010) was to date possible only with low accuracy due to the thickness of the applied slices. Applying confocal laser scanning microscopy (Villena, Fujikawa, Tsuyumu, &

TABLE 1 Morphological properties of the fungal pellets

	A. niger	*P. chrysogenum*	unit
Diameter of pellet	633	1,085	μm
Porosity	0.87	0.94	–
Total hyphal length	1,472,998	2 995,557	μm
Average diameter of hyphae	3.8	4.1	μm
Total number of tips	15,425	20,000	–
Total number of branches	15,768	22,123	–
Hyphal growth unit	95	150	μm
Hyphal branch unit	93	135	μm

Gutiérrez-Correa, 2010) or flow cytometry (Ehgartner et al., 2017), only superficial parts of pellets have been investigated.

4.2 | Distribution of hyphal material within pellet structures

Next, we checked whether the three-dimensional distribution of fungal biomass within a pellet can be used to deduce information about the pellet's genesis and development during submerged cultivation. To determine the regions with a high biomass content, three-dimensional distribution of the LHF was calculated, as described in Section 3.4. Subsequently, a threshold value for the LHF was set. As a result, only the regions of the pellet with a higher LHF than the set threshold remained.

The threshold for the hyphal fraction of the conical section of the *A. niger* pellet was set to 0.20 (Figure 6), which was chosen to be close to the maximum hyphal fraction. Two regions with high hyphal fractions were observed: a smaller region in the pellet's center and a larger region in the outer part. The regions with high hyphal fractions show spherical symmetry with the cone tip at the center, which was reflected in Figure 1, confirming that the *A. niger* pellet was spherically symmetric. The dense region in the pellet's center was possibly a result of agglomeration events involving the conidia and germ tubes. These early agglomeration events are common pellet-building mechanisms seen in filamentous microorganisms of the coagulative type, including *A. niger* Zhang & Zhang, 2016.

With 0.20 as the threshold of the LHF of the *P. chrysogenum* pellet, the value was also set close to the maximum LHF. Figure 7 shows three regions with high hyphal fractions: one large region and two small ones. Although the *P. chrysogenum* pellet on its own is spherical, no spherical symmetry was visible for the location of the regions with high hyphal fractions. Considering the three regions with high hyphal fractions, it can be supposed that the *P. chrysogenum* pellet was a product of the agglomeration of three hyphal clumps. This is a typical pellet-formation mechanism for filamentous microorganisms of the hyphal element agglomerating type, including *P. chrysogenum* (Nielsen, Johansen, Jacobsen, Krabben, & Villadsen, 1995; Veiter et al., 2018).

Our data show that analyzing hyphal fractions provides new insights into the symmetry of fungal pellets and hypotheses can be deduced with respect to their evolution. This knowledge can be used to rationally engineer aggregation events by appropriate process control and/or by genetic modifications to obtain final pellet structures with improved productivities during industrial processes.

4.3 | Radial morphology of spherically symmetric pellets

Spherically symmetric pellets offer the opportunity to characterize morphological properties along their radii. Thus, the morphological properties of shells of the *A. niger* pellet were analyzed. Again, only a cone of the pellet not affected by the fixation material was studied (compare Figure 1a). To determine the morphology of the entire pellet, the remainder part of the pellet was assumed to exhibit

properties identical to those of the cone. The width of shells was set to 25 μm. The inner sphere had a radius of 50 μm. To determine the hyphal fraction of a shell, the hyphal volume of the shell was divided by the total volume of the shell. In addition, the number of branches and tips per shell were divided by the total volume of shells. To obtain the HGU and HBU, the hyphal length of the shells was divided by the number of tips and branches.

Figure 8a shows that the hyphal fraction of the *A. niger* pellet contained two maxima. One maximum was in the pellet center, and the other one at a distance 200 μm outside the center. These observations are in accordance with the investigation of the regions with a high hyphal fraction in Section 4.2. Between the two maxima, a local minimum with a hyphal fraction of about 0.15 could be observed at 100–125 μm. Starting from the second local maximum at 200 μm, the hyphal fraction decreased, until the edge of the pellet was reached at a radius between 300 and 325 μm.

With $2.8 \cdot 10^5$ branches per mm^3, the branching density was highest at the pellet center. From there, the branching density gradually decreased to $1.9 \cdot 10^5$ branches per mm^3 at a radius of 250 μm. Then, the branching density decreased rapidly toward the edge of the pellet. With $2.0 \cdot 10^5$ tips per mm^3, the tip density had a local minimum at the pellet center. From there, the tip density increased until the maximum tip density of $4.2 \cdot 10^5$ tips per mm^3 was reached between 100 and 125 μm. From there, the tip density decreased towards the edge of the pellet.

HGU and HBU result from the hyphal length of shells and the corresponding number of tips and branches. It is clear that HBU does not vary strongly along the radius and has values between 80 and 120 μm. Therefore, it can be assumed that the number of branches is directly proportional to the hyphal length for the whole pellet. By contrast, the HGU varies strongly along the radius, which is why the number of tips is not directly proportional to the hyphal length.

4.4 | Nonsymmetry of pellets

Finally, a method to detect and illustrate nonsymmetry of filamentous pellets is presented. Exemplarily, the method was applied to the *P. chrysogenum* pellet. Thereby, the LHF was calculated as described in Section 3.4. The mass center of the pellet was calculated based on the hyphal volume elements. By using the HEALPIX algorithm, the LHF for different distances from the pellet center was determined. Figure 9 shows the LHFs for three different distances from the center.

As shown, the LHF varied strongly for all illustrated distances from the pellet center. At a distance of 150 μm from the center, the LHF varied between 0.075 and 0.15. At a distance of 250 μm, the range of the LHF was between 0.075 and 0.3. At a distance of 350μm, the LHF varied even more strongly, with values between 0 and 0.3.

4.5 | Critical evaluation of the μCT-based method

The new method to determine morphological properties with μCT measurements and subsequent three-dimensional image analysis has considerable benefits compared with existing methods. For the first

time, hyphal material, tips, and branches can be located and quantified for entire filamentous pellets. Thus, it is also the first time, that the following properties of entire pellets are reported: total hyphal length, total tip number, total branch number, HGU, and the newly defined parameter HBU. With the applied technique, the inner part of the fungal pellet can be studied along with the outer part, which is nearly impossible with light microscopy. This fact makes it difficult to validate the here newly introduced method with existing methods. However, applying light microscopy, the influence of the freeze-drying process has been evaluated. As shown in the Figures S1–S3, the freeze-drying does not appear to significantly modify either the size of the pellets or hyphal thickness. A limitation of the new method is the high costs of µCT measurements. In addition, three-dimensional image analysis to obtain morphological properties follows an elaborate workflow that requires special computational expertize. As any other image analysis technique, the here-described three-dimensional one has potential sources of errors/inaccuracies, such as the selection of the gray value threshold and the selection of the two parameters of the postprocessing steps. Compared with other methods, such as microscopy and flow cytometry, the sample number is low and the measurement rather time-consuming. µCTs have also lower voxel resolutions compared with pixels of microscopic approaches.

5 | CONCLUSIONS

The present study describes a new method to determine the morphological properties of the pellets of filamentous fungi. Freeze-dried fungal pellets were analyzed using µCT measurements and three-dimensional image analysis. µCT produces three-dimensional images, which is why the inner part of the fungal pellet can be studied along with the outer part. To our knowledge, this is the first time that total hyphal length, total tip number, total branch number, and HGU of entire pellets can be determined with a single technique. Morphological properties, such as porosity and average diameter of the hyphae, can be studied in higher detail than ever before by using our method. By elucidating the spatial morphological distribution, multiple hypotheses regarding the morphological development of fungal pellets can be formulated. Summarizing, compared with established methods, the new method has significant advantages in analyzing the morphology of entire pellets, including the hyphal network with the location of hyphal material, tips, and branches. Main disadvantages are the low sample number and high costs of the new method.

CONFLICT OF INTERESTS

The authors declare that they have no conflict of interests.

ORCID

Stefan Schmieder http://orcid.org/0000-0003-4328-9724

REFERENCES

Arganda-Carreras, I., Fernández-González, R., Muñoz-Barrutia, A., & Ortiz-De-Solorzano, C. (2010). 3D reconstruction of histological sections: Application to mammary gland tissue. *Microscopy Research and Technique, 73,* 1019–1029. https://doi.org/10.1002/jemt.v73:11

Barry, D. J., Chan, C., & Williams, G. A. (2009). Morphological quantification of filamentous fungal development using membrane immobilization and automatic image analysis. *Journal of Industrial Microbiology & Biotechnology, 36,* 787. https://doi.org/10.1007/s10295-009-0552-9

Barry, D. J., Williams, G. A., & Chan, C. (2015). Automated analysis of filamentous microbial morphology with AnaMorf. *Biotechnology Progress, 31,* 849–852. https://doi.org/10.1002/btpr.2087

Bennett, J. W., & Lasure, L. L. (1991). *More gene manipulations in fungi.* Cambridge, MA: Academic Press.

Buschulte, T. K. (1992). Mathematische Modellbildung und Simulation von Zellwachstum, Stofftransport und Stoffwechsel in Pellets aus Streptomyceten (PhD thesis). Stuttgart, Germany: Fakultät Verfahrenstechnik der Universität Stuttgart.

Cairns, T. C., Nai, C., & Meyer, V. (2018). How a fungus shapes biotechnology: 100 years of *Aspergillus niger* research. *Fungal Biology and Biotechnology, 5,* 13. https://doi.org/10.1186/s40694-018-0054-5

Celler, K., Picioreanu, C., vanLoosdrecht, M. C., & vanWezel, G. P. (2012). Structured morphological modeling as a framework for rational strain design of streptomyces species. *Antonie Van Leeuwenhoek, 102,* 409–423. https://doi.org/10.1007/s10482-012-9760-9

Colin, V. L., Baigorí, M. D., & Pera, L. M. (2013). Tailoring fungal morphology of *Aspergillus niger* MYA 135 by altering the hyphal morphology and the conidia adhesion capacity: Biotechnological applications. *AMB Express, 3,* 27. https://doi.org/10.1186/2191-0855-3-27

Ehgartner, D., Herwig, C., & Fricke, J. (2017). Morphological analysis of the filamentous fungus *Penicillium chrysogenum* using flow cytometry: The fast alternative to microscopic image analysis. *Applied Microbiology and Biotechnology, 101,* 7675–7688. https://doi.org/10.1007/s00253-017-8475-2

Fiedler, M. R., Barthel, L., Kubisch, C., Nai, C., & Meyer, V. (2018). Construction of an improved *Aspergillus niger* platform for enhanced glucoamylase secretion. *Microbial Cell Factories, 17,* 95. https://doi.org/10.1186/s12934-018-0941-8

Gibbs, P., Seviour, R., & Schmid, F. (2000). Growth of filamentous fungi in submerged culture: Problems and possible solutions. *Critical Reviews in Biotechnology, 20,* 17–48. https://doi.org/10.1080/07388550091144177

Gorski, K. M., Hivon, E., Banday, A., Wandelt, B. D., Hansen, F. K., Reinecke, M., & Bartelmann, M. (2005). Healpix: A framework for high-resolution discretization and fast analysis of data distributed on the sphere. *The Astrophysical Journal, 622,* 759. https://doi.org/10.1086/apj.2005.622.issue-2

Grélard, F., Baldacci, F., Vialard, A., & Domenger, J.-P. (2017). New methods for the geometrical analysis of tubular organs. *Medical Image Analysis, 42,* 89–101. https://doi.org/10.1016/j.media.2017.07.008

Hille, A., Neu, T., Hempel, D., & Horn, H. (2005). Oxygen profiles and biomass distribution in biopellets of *Aspergillus niger*. *Biotechnology and Bioengineering*, *92*, 614–623. https://doi.org/10.1002/bit.20628

Hille, A., Neu, T. R., Hempel, D. C., & Horn, H. (2006). Effect of morphology on transport of matter and conversion in *Aspergillus niger*-pellets. *Chemie Ingenieur Technik*, *78*, 627–632. https://doi.org/10.1002/cite.200600018

Homann, H. (2007). Implementation of a 3D thinning algorithm. *Insight Journal*, *421*

King, R. (1998). Mathematical modelling of the morphology of streptomyces species, *Relation between morphology and process performances* (95–124). New York, NY: Springer.

King, R. (2015). A framework for an organelle-based mathematical modeling of hyphae. *Fungal Biology and Biotechnology*, *2*, 1. https://doi.org/10.1186/s40694-015-0014-2

Lee, T.-C., Kashyap, R. L., & Chu, C.-N. (1994). Building skeleton models via 3-D medial surface axis thinning algorithms. *CVGIP: Graphical Models and Image Processing*, *56*, 462–478. https://doi.org/10.1006/cgip.1994.1042

Lejeune, R., & Baron, G. V. (1997). Simulation of growth of a filamentous fungus in 3 dimensions. *Biotechnology and Bioengineering*, *53*, 139–150. https://doi.org/10.1002/(sici)1097-0290(19970120)53:2<139::aid-bit3>3.3.co;2-e

Lin, P.-J., Scholz, A., & Krull, R. (2010). Effect of volumetric power input by aeration and agitation on pellet morphology and product formation of *Aspergillus niger*. *Biochemical Engineering Journal*, *49*, 213–220. https://doi.org/10.1016/j.bej.2009.12.016

Meyer, V. (2008). Genetic engineering of filamentous fungi: Progress, obstacles and future trends. *Biotechnology Advances*, *26*, 177–185. https://doi.org/10.1016/j.biotechadv.2007.12.001

Meyer, V., Ram, A. F., & Punt, P. J. (2010). Genetics, genetic manipulation, and approaches to strain improvement of filamentous fungi, *Manual of industrial microbiology and biotechnology* (3rd ed., 318–329). Washington, DC: American Society of Microbiology.

Meyer, V., Fiedler, M., Nitsche, B., & King, R. (2015). The cell factory *Aspergillus* enters the big data era: Opportunities and challenges for optimising product formation, *Filaments in bioprocesses* (pp.91–132). New York, NY: Springer.

Meyer, V., Andersen, M. R., Brakhage, A. A., Braus, G. H., Caddick, M. X., Cairns, T. C., & Head, R. M. (2016). Current challenges of research on filamentous fungi in relation to human welfare and a sustainable bioeconomy: A white paper. *Fungal Biology and Biotechnology*, *3*, 6. https://doi.org/10.1186/s40694-016-0024-8

Meyerhoff, J., Tiller, V., & Bellgardt, K.-H. (1995). Two mathematical models for the development of a single microbial pellet; part 2: Simulation of the pellet growth of *Penicillium chrysogenum* by a fast method equivalent to a morphological detailed description. *Bioprocess Engineering*, *12*, 305–313. https://doi.org/10.1007/BF00369507

Morrison, K., & Righelato, R. (1974). The relationship between hyphal branching, specific growth rate and colony radial growth rate in *Penicillium chrysogenum*. *Microbiology*, *81*, 517–520. https://doi.org/10.1099/00221287-81-2-517

Nielsen, J. (1993). A simple morphologically structured model describing the growth of filamentous microorganisms. *Biotechnology and Bioengineering*, *41*, 715–727. https://doi.org/10.1002/bit.260410706

Nielsen, J., Johansen, C. L., Jacobsen, M., Krabben, P., & Villadsen, J. (1995). Pellet formation and fragmentation in submerged cultures of *Penicillium chrysogenum* and its relation to penicillin production. *Biotechnology Progress*, *11*, 93–98. https://doi.org/10.1021/bp00031a013

Nieminen, L., Webb, S., Smith, M. C., & Hoskisson, P. A. (2013). A flexible mathematical model platform for studying branching networks: Experimentally validated using the model actinomycete, *Streptomyces coelicolor*. *PloS One*, *8*, e54316. https://doi.org/10.1371/journal.pone.0054316

Otsu, N. (1979). A threshold selection method from gray-level histograms. *IEEE Transactions on Systems, Man, and Cybernetics*, *9*, 62–66. https://doi.org/10.1109/TSMC.1979.4310076

Packer, H., Keshavarz-Moore, E., Lilly, M., & Thomas, C. (1992). Estimation of cell volume and biomass of *Penicillium chrysogenum* using image analysis. *Biotechnology and Bioengineering*, *39*, 384–391. https://doi.org/10.1002/bit.260390404

Papagianni, M. (2004). Fungal morphology and metabolite production in submerged mycelial processes. *Biotechnology Advances*, *22*, 189–259. https://doi.org/10.1016/j.biotechadv.2003.09.005

Pirt, S. (1966). A theory of the mode of growth of fungi in the form of pellets in submerged culture. *Proceedings of the Royal Society of London*, *166*, 369–373. https://doi.org/10.1098/rspb.1966.0105

Read, N. D., Lichius, A., Shoji, J.-Y., & Goryachev, A. B. (2009). Self-signalling and self-fusion in filamentous fungi. *Current Opinion in Microbiology*, *12*, 608–615. https://doi.org/10.1016/j.mib.2009.09.008

Salvo, L., Cloetens, P., Maire, E., Zabler, S., Blandin, J. J., Buffière, J. -Y., & Josserond, C. (2003). X-ray micro-tomography an attractive characterisation technique in materials science. *Nuclear Instruments and Methods in Physics Research B: Beam Interactions with Materials and Atoms*, *200*, 273–286. https://doi.org/10.1016/S0168-583X(02)01689-0

Schindelin, J., Arganda-Carreras, I., Frise, E., Kaynig, V., Longair, M., Pietzsch, T., & Cardona, A. (2012). Fiji: An open-source platform for biological-image analysis. *Nature Methods*, *9*, 676. https://doi.org/10.1038/nmeth.2019

Schneider, C. A., Rasband, W. S., & Eliceiri, K. W. (2012). NIH image to ImageJ: 25 years of image analysis. *Nature Methods*, *9*, 671. https://doi.org/10.1038/nmeth.2089

Stock, S. R. (2008). *Microcomputed tomography: Methodology and applications*. Boca Raton, FL: CRC Press.

Veiter, L., Rajamanickam, V., & Herwig, C. (2018). The filamentous fungal pellet: Relationship between morphology and productivity. *Applied Microbiology and Biotechnology*, 1–10. https://doi.org/10.1007/s00253-018-8818-7

Villena, G., & Gutiérrez-Correa, M. (2007). Morphological patterns of *Aspergillus niger* biofilms and pellets related to lignocellulolytic enzyme productivities. *Letters in Applied Microbiology*, *45*, 231–237. https://doi.org/10.1111/j.1472-765X.2007.02183.x

Villena, G., Fujikawa, T., Tsuyumu, S., & Gutiérrez-Correa, M. (2010). Structural analysis of biofilms and pellets of *Aspergillus niger* by confocal laser scanning microscopy and cryo scanning electron microscopy. *Bioresource Technology*, *101*, 1920–1926. https://doi.org/10.1016/j.biortech.2009.10.036

Yang, H., King, R., Reichl, U., & Gilles, E. D. (1992). Mathematical model for apical growth, septation, and branching of mycelial microorganisms. *Biotechnology and Bioengineering*, *39*, 49–58. https://doi.org/10.1002/bit.260390109

Zhang, J., & Zhang, J. (2016). The filamentous fungal pellet and forces driving its formation. *Critical Reviews in Biotechnology*, *36*, 1066–1077. https://doi.org/10.3109/07388551.2015.1084262

SUPPORTING INFORMATION

Additional supporting information may be found online in the Supporting Information section at the end of the article.

Supplementary Materials for Paper I: An X-ray microtomography-based method for detailed analysis of the three-dimensional morphology of fungal pellets
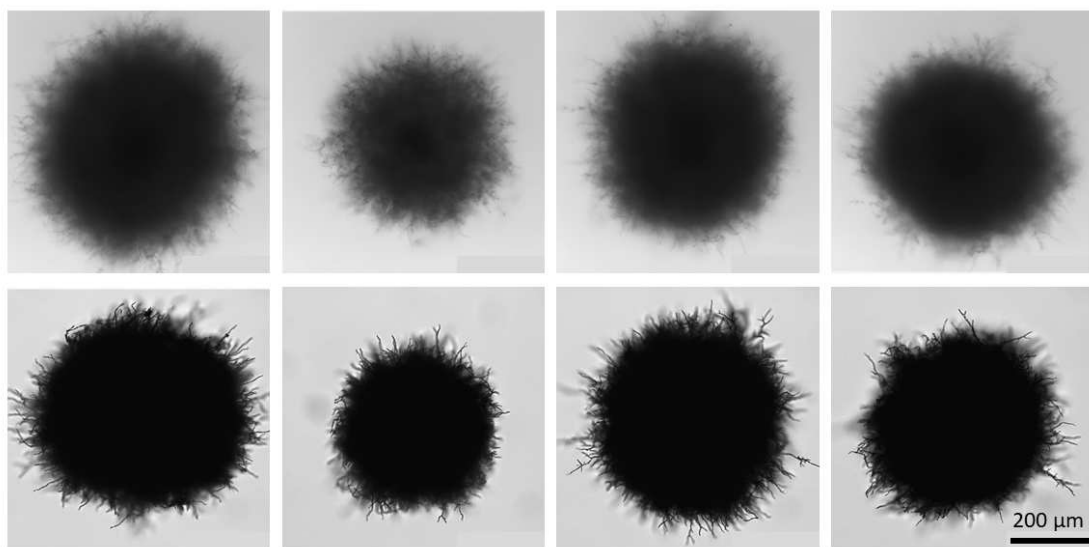

Figure S1: Light microscope images of *A. niger* pellets after 48 h fermentation: the upper row shows the "wet" states of pellets, whereas the lower row shows the freeze-dried states; Columns contain microscope images of the same pellet for the two states "wet" and freeze-dried.

Figure S2: Light microscope images of *P. chrysogenum* pellets after 48 h fermentation: the upper row shows the "wet" states of pellets, whereas the lower row shows the freeze-dried states; Columns contain microscope images of the same pellet for the two states "wet" and freeze-dried.
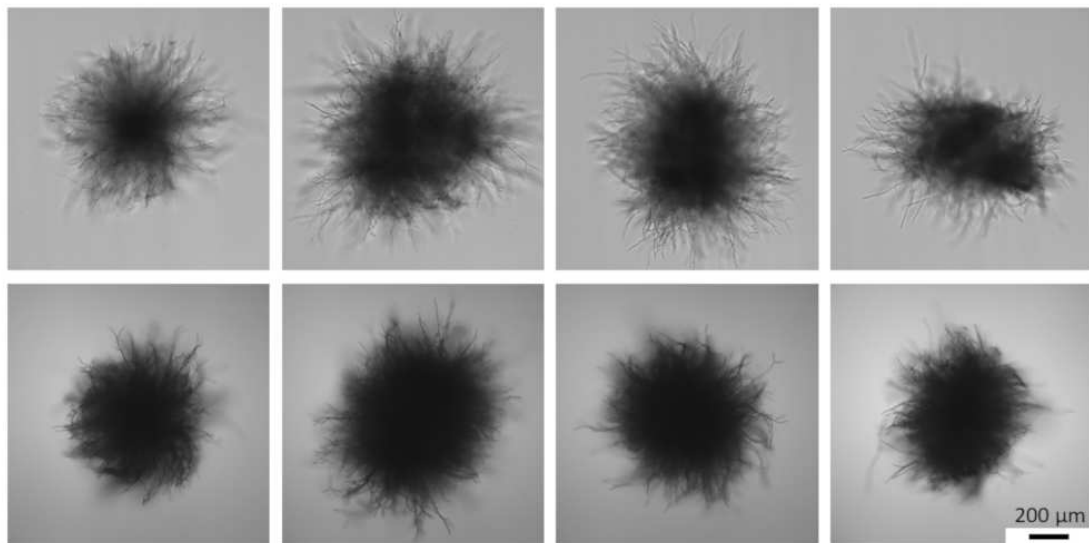
Figure S3: Light microscope images of *P. chrysogenum* pellets after 24 h fermentation: the upper row shows the "wet" states of pellets, whereas the lower row shows the freeze-dried states; Columns contain microscope images of the same pellet for the two states "wet" and freeze-dried.
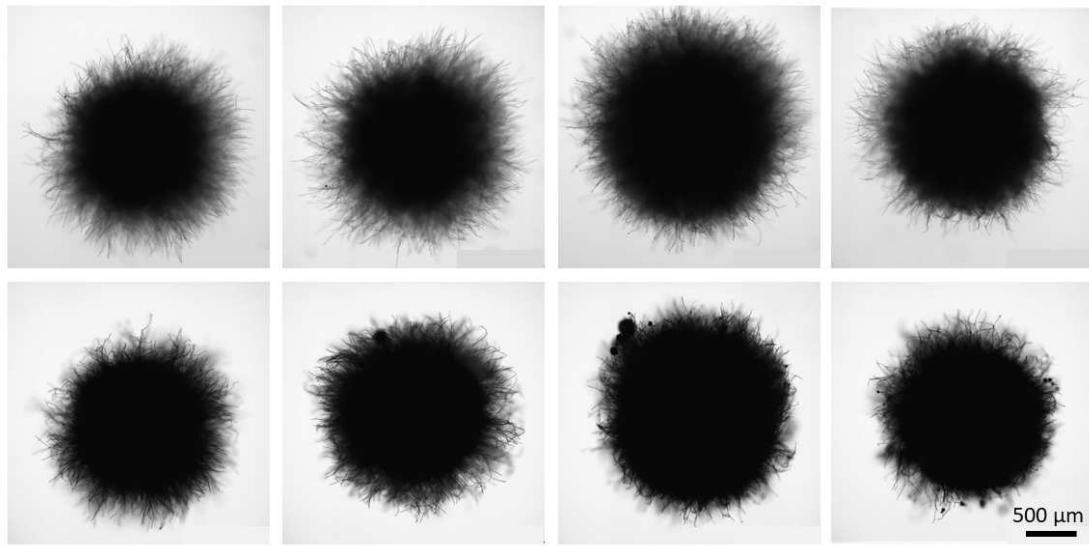
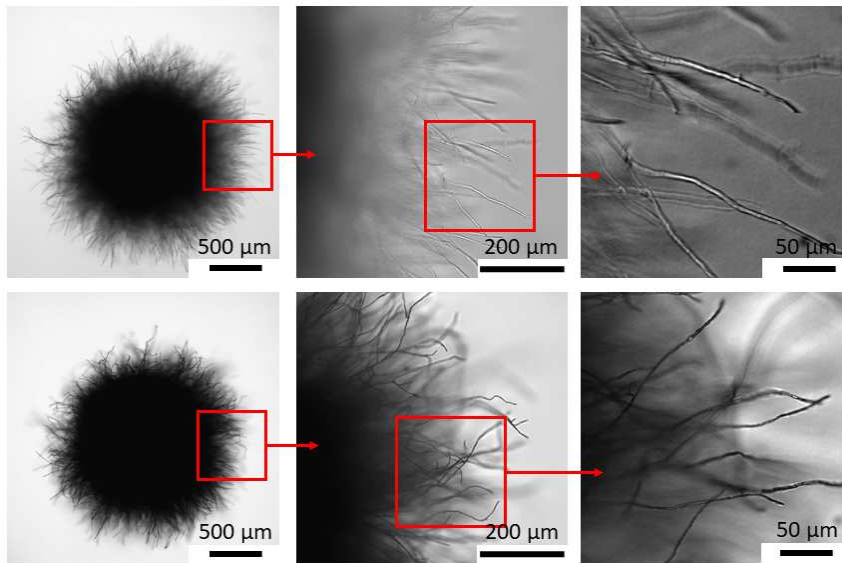Figure S4: Light microscope images of a *P. chrysogenum* pellet applying high resolutions: the upper row shows the "wet" state of the pellet, whereas the lower row shows the freeze-dried state.
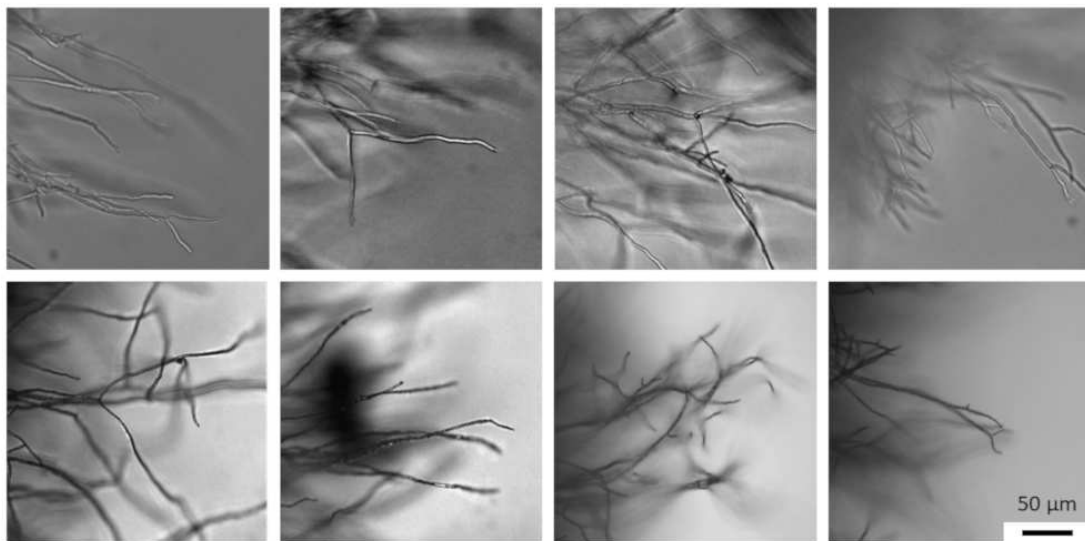

Figure S5: Light microscope images of outer regions of different *P. chrysogenum* pellets applying high resolutions: the upper row shows the "wet" state of pellets, whereas the lower row shows the freeze-dried state.

5.2 Paper II: From three-dimensional morphology to effective diffusivity in filamentous fungal pellets (Schmideder et al., 2019b)

Summary

The supply of pellets with nutrients and oxygen strongly influences their growth and productivity. While the consumption of nutrients and oxygen is required for fungal metabolism, their transport into pellets is mainly driven by diffusion. Although the dense hyphal network is known to limit the diffusive mass transport of nutrients, oxygen, and secreted metabolites, a well-founded correlation between structure and diffusivity does not exist. In this study, we computed the effective diffusivities through a few hundred representative sub-volumes of five *Aspergillus niger* pellets. The three-dimensional structures of the pellets were determined with μCT measurements and image analysis described in Paper I. Based on the diffusion computations, we obtained a correlation between effective diffusivity and solid hyphal fraction. This correlation is inspired by material laws for fibers, consistent with theoretical expectations, and shows an excellent fit to the investigated *A. niger* pellets. While the correlation uncovered discrepancies with previously assumed laws for filamentous fungi, it showed some similarities to laws for randomly oriented fibers. The findings of this study enable the prediction of the diffusive transport of nutrients, oxygen, and secreted metabolites in filamentous fungal pellets. This knowledge will improve morphological engineering of pellets, and thus, contribute to increased productivities in bioprocesses. Restrictions of the applied μCT system demanded the application of a fixed resolution for the measurements. Further, pellets originated from a single experimental setup, which resulted in comparable pellet-micromorphologies. However, both resolution and micromorphology can alter the diffusivity. These limitations were overcome in Paper III.

Author contributions

Stefan Schmideder did the conception and design of the study and wrote the manuscript, which was edited and approved by all authors. Heiko Briesen and Vera Meyer supervised the study. Lars Barthel cultivated and freeze-dried fungal pellets. Stefan Schmideder and Henri Müller conducted μCT measurements and image analysis. Stefan Schmideder set up morphological simulations and diffusion computations. Stefan Schmideder and Heiko Briesen interpreted the results. Stefan Schmideder and Lars Barthel proposed a workflow for bioprocess development.

ARTICLE

BIOTECHNOLOGY
BIOENGINEERING WILEY

From three-dimensional morphology to effective diffusivity in filamentous fungal pellets

Stefan Schmideder[1] │ Lars Barthel[2] │ Henri Müller[1] │ Vera Meyer[2] │
Heiko Briesen[1]

[1]Chair of Process Systems Engineering, Technical University of Munich, Freising, Germany

[2]Department of Applied and Molecular Microbiology, Institute of Biotechnology, Technische Universität Berlin, Berlin, Germany

Correspondecne
 Heiko Briesen, Technical University of Munich, Chair of Process Systems Engineering, 85354 Freising, Germany.
Email: heiko.briesen@tum.de

Abstract

Filamentous fungi are exploited as cell factories in biotechnology for the production of proteins, organic acids, and natural products. Hereby, fungal macromorphologies adopted during submerged cultivations in bioreactors strongly impact the productivity. In particular, fungal pellets are known to limit the diffusivity of oxygen, substrates, and products. To investigate the spatial distribution of substances inside fungal pellets, the diffusive mass transport must be locally resolved. In this study, we present a new approach to obtain the effective diffusivity in a fungal pellet based on its three-dimensional morphology. Freeze-dried *Aspergillus niger* pellets were studied by X-ray microcomputed tomography, and the results were reconstructed to obtain three-dimensional images. After processing these images, representative cubes of the pellets were subjected to diffusion computations. The effective diffusion factor and the tortuosity of each cube were calculated using the software GeoDict. Afterwards, the effective diffusion factor was correlated with the amount of hyphal material inside the cubes (hyphal fraction). The obtained correlation between the effective diffusion factor and hyphal fraction shows a large deviation from the correlations reported in the literature so far, giving new and more accurate insights. This knowledge can be used for morphological optimization of filamentous pellets to increase the yield of biotechnological processes.

KEYWORDS
Aspergillus niger, effective diffusion, filamentous fungal pellets, tortuosity, X-ray microcomputed tomography

1 │ INTRODUCTION

Filamentous fungi are widely used cell factories for the production of a variety of compounds such as enzymes, organic acids, or antibiotics (Meyer, 2008). As just one example, plant-biomass-degrading enzymes produced by filamentous fungi, have a global market value of € 4.7 billion (Meyer et al., 2016). During submerged cultivation, filamentous fungi adopt different macromorphological entities such as non-aggregated hyphae (disperse mycelia), loosely aggregated hyphal clumps, and densely aggregated spherical structures (pellets; Pirt, 1966). This morphology is influenced by the fungal species and cultivation parameters (Papagianni, 2004). Depending on the predominant morphology in a submerged fungal culture, the substances produced by the organism can differ significantly. As fungal growth and protein secretion are coupled processes, it is for example known that the highest protein secretion normally occurs during rapid hyphal growth, which takes place in disperse mycelia and the outer layers of fungal pellets where nutrient supply is not limited (Cairns, Zheng, Zheng, Sun, & Meyer, 2019). On the

other hand, the production of secondary metabolites peaks when the producing organism shows an extremely low or zero growth (Brakhage, 2013). These conditions can be observed for example in the dense center of fungal pellets, where the restricted diffusion of oxygen and nutrients leads to limitations, thus inhibiting growth (Veiter, Rajamanickam, & Herwig, 2018). This demonstrates that a detailed understanding of the limitations and diffusion processes in fungal pellets is of crucial importance for many biotechnological applications.

The effective diffusion coefficient is required to calculate the diffusive mass transport. For component i in a porous medium, this parameter can be expressed as (Becker, Wieser, Fell, & Steiner, 2011)

$$D_{i,\text{eff}} = D_{i,\text{bulk}} \cdot k_{\text{eff}}, \tag{1}$$

where $D_{i,\text{bulk}}$ is the diffusion coefficient of component i in the bulk medium without geometrical hindrance and k_{eff} describes the reduction of the free bulk diffusion $D_{i,\text{bulk}}$ to the effective diffusion $D_{i,\text{eff}}$ and is solely dependent on the pore geometry and independent of the diffusing substance i (Becker et al., 2011). Hereafter, k_{eff} is called the effective diffusion factor. In the case of diffusion in filamentous pellets, $D_{i,\text{bulk}}$ corresponds to the molecular diffusion coefficient of components such as oxygen, glucose, or products in the fermentation

medium and is strongly dependent on the medium, diffusing substance, and process conditions such as temperature. Temperature-dependent bulk diffusion coefficients for glucose, oxygen, and several other compounds in aqueous solutions can be estimated, for example, from Yaws (2014). The geometrically caused reduction of the diffusion, k_{eff}, can be expressed as (Epstein, 1989):

$$k_{\text{eff}} = \frac{\epsilon}{\tau^2}, \tag{2}$$

where the porosity, ϵ, is defined as the ratio of volume of voids to the total volume. The tortuosity, τ, is a geometrical parameter and can be taken as the ratio of the average pore length to the length of the porous medium along the major flow or diffusion axis. Thus, in general it is > 1 (Epstein, 1989).

So far, no experimental or modeling approaches to exactly predict the diffusive mass transport inside whole fungal pellets are available. Several modeling approaches of filamentous microorganisms consider the diffusive mass transport of oxygen and/or substrates like glucose (Buschulte, 1992; Celler, Picioreanu, van Loosdrecht, & van Wezel, 2012; Cui, Van der Lans, & Luyben, 1998; Lejeune & Baron, 1997; Meyerhoff, Tiller, & Bellgardt, 1995; Table 1). They include effective diffusion coefficients that are dependent on the molecular

TABLE 1 Applied correlations between effective diffusion coefficients ($D_{i,\text{eff}}$), effective diffusion factor (k_{eff}), bulk diffusion coefficients ($D_{i,\text{bulk}}$), porosity (ϵ), hyphal fraction ($c_h = 1 - \epsilon$), solid fraction (ϕ), and tortuosity (τ) in the literature to model the diffusive transport mechanisms

Eq. for k_{eff} in $D_{i,\text{eff}} = D_{i,\text{bulk}} k_{\text{eff}}$	Origin structure	Diffusion direction	Field	Source
$1 - c_h$	–	–	Filamentous microorganisms	Celler et al. (2012)
	–	–	Filamentous microorganisms	Cui et al. (1998) adopted from Van't Riet and Tramper (1991)
	–	–	Filamentous microorganisms	Buschulte (1992) adopted from Aris (1975)
$\frac{(1 - c_h)}{\tau}$ with $\tau = 2$	–	–	Filamentous microorganisms	Lejeune and Baron (1997)
$\frac{2 - 2c_h}{2 + c_h}$	–	–	Filamentous microorganisms	Meyerhoff et al. (1995) adopted from Neale and Nader (1973)
$\exp(-2.8c_h)$	–	–	Filamentous microorganisms	Buschulte (1992) adopted from Vorlop (1984)
$\left(1 - \dfrac{2\phi}{1 + \phi - \frac{0.30583\,\phi^4}{1 - 1.40296\,\phi^8} - 0.01336\,\phi^8}\right)$	–	Perpendicular to fibers	Square array of parallel fibers	Perrins et al. (1979)
$\frac{\epsilon}{\tau^2}$ with $\tau^2 = \exp(1.16(1 - \epsilon))$	Simulated	Perpendicular to fibers	Nonoverlapping parallel fibers	Tomadakis and Sotirchos (1993), Tomadakis and Robertson (2005)
$\frac{\epsilon}{\tau^2}$ with $\tau^2 = \left(\frac{1 - 0.33}{\epsilon - 0.33}\right)^{0.707}$	Simulated	Perpendicular to fibers	Overlapping parallel fibers	Tomadakis and Sotirchos (1991)
$\frac{\epsilon}{\tau^2}$ with $\tau^2 = \left(\frac{1 - 0.04}{\epsilon - 0.04}\right)^{0.107}$	μCT	Parallel to fibers	Parallel carbon fibers	Vignoles et al. (2007)
$\frac{\epsilon}{\tau^2}$ with $\tau^2 = \left(\frac{1 - 0.04}{\epsilon - 0.04}\right)^{0.465}$	μCT	Perpendicular to fibers	Parallel carbon fibers	Vignoles et al. (2007)
$\frac{\epsilon}{\tau^2}$ with $\tau^2 = \left(\frac{1 - 0.037}{\epsilon - 0.037}\right)^{0.661}$	Simulated	All directions	Overlapping nonparallel fibers	Tomadakis and Sotirchos (1991)
$1.05\epsilon^3$	Simulated	All directions	Overlapping nonparallel fibers	He et al. (2017)

diffusion coefficient, tortuosity, and porosity/hyphal fraction. Thereby, the hyphal fraction, $c_h = 1 - \epsilon$, is defined as the ratio of the volume of hyphae to the total volume. It is important to note that the modeling approaches published so far (Buschulte, 1992; Celler et al., 2012; Cui et al., 1998; Lejeune & Baron, 1997; Meyerhoff et al., 1995) either neglect the tortuosity of the hyphal structure or assume a constant tortuosity for different porosities. These simplifications may be caused by the absence of information about the tortuosity. In the materials science of fibers, correlations between the porosity and the effective diffusion factor for bulk diffusion that include knowledge about the tortuosity have been described. Perrins, McKenzie, and McPhedran (1979) derived an analytic expression for ideal square arrays of parallel fibers, Tomadakis and Sotirchos (1991) a correlation for random distributed overlapping parallel fibers, Tomadakis and Sotirchos (1993) and Tomadakis and Robertson (2005) a relation for random distributed nonoverlapping parallel fibers, Tomadakis and Sotirchos (1991) and He, Guo, Li, Pan, and Wang (2017) a relation for 3D random distributed overlapping fibers, and Vignoles, Coindreau, Ahmadi, and Bernard (2007) a correlation for parallel fibrous carbon–carbon composite preforms (Table 1). The only published experimental approach to predict the diffusive mass transport is based on the measurement of oxygen concentrations using microelectrodes inside fungal pellets (Hille, Neu, Hempel, & Horn, 2009; Wittier, Baumgartl, Lübbers, & Schügerl, 1986). The researchers correlated the mass transport of oxygen into the pellets with microscopic information from cryo-slices. However, the microscopy images of the cryo-slices missed the three-dimensional information of the hyphal network and hyphae superimposed in the two-dimensional projections. Therefore, the appropriate correlation between pellet morphology and diffusion was not possible in this experimental approach. We could recently overcome the limitations of two-dimensional image generation by performing X-ray microcomputed tomography (μCT) measurements on whole fungal pellets (Schmieder et al., 2019). The investigated *Aspergillus niger* pellet showed a very complex three-dimensional structure. With a diameter of 633 μm, the *A. niger* pellet had a hyphal length of 1.5 m and 15,425 tips in total.

In materials science, μCT measurements and subsequent mass-transfer computations matured into a widely used method to determine the effective diffusivity of porous/fibrous materials. Exemplarily, Panerai et al. (2017), Becker et al. (2011), Coindreau, Mulat, Germain, Lachaud, and Vignoles (2011), and Foerst et al. (2019) investigated the effective diffusivity of fibrous insulators, fuel cell media, carbon-carbon composites, and maltodextrin solutions, respectively. Thereby, μCT appeared as a non-destructive technique to measure three-dimensional micro-structures.

In this study, we computed the effective diffusivity of *A. niger* pellets based on the micro-structural characterization gained from μCT measurements and subsequent image analysis. The newly developed technique for fungal pellets combines the experimental acquisition of three-dimensional images with the locally resolved calculation of the effective diffusion coefficient and tortuosity within this structure for the first time. This results in an unprecedented potential for the determination of diffusion processes inside fungal pellets.

2 | MATERIALS AND METHODS

2.1 | Preparation of pellets

The *A. niger* hyperbranching strain MF22.4, which has been shown to be a better protein-secretion strain than the wild-type strain (due to deletion of the racA gene; Fiedler, Barthel, Kubisch, Nai, & Meyer, 2018), was used in this study. Pellets were obtained by submerged cultivation of MF22.4 for 48 hr and freeze-drying following the previously described protocol (Schmieder et al., 2019).

2.2 | X-ray microcomputed tomography

To obtain three-dimensional images of the freeze-dried filamentous pellets, μCT measurements were performed based on the method reported by Schmieder et al. (2019). Two-dimensional projections from different angles were reconstructed to generate three-dimensional images with a custom-designed software (Matrix Technologies, Feldkirchen, Germany) that uses CERA (Siemens, Munich, Germany). The image resolution was 1 μm (i.e., the edge length of the voxels was 1 μm), and to generate the beam, 60 kV and 25 μA were applied. Depending on the size of the pellets, 1-5 pellets can be measured with one μCT-measurement (3 hr including the time for image reconstruction). An instant adhesive (UHU, Bühl, Germany) was used to fix the freeze-dried fungal pellets on top of a sample holder. In contrast to the previous study (Schmieder et al., 2019), in this case, the instant adhesive dried 5 min before placing the pellets on top of the holder. This procedure resulted in a smooth surface of the instant adhesive, while it remained sticky enough to fix the pellets. The smooth surface facilitated the segmentation of the instant adhesive in the subsequent image processing.

2.3 | Image processing

Image processing aimed at differentiating between hyphal material and background. The background included the instant adhesive used for sample fixation, the air between the hyphae, and small impurities. In general, image processing is leaned to the one reported in the section "Preprocessing" by Schmieder et al. (2019)). The image processing result for one pellet is exemplarily illustrated in Figure 1.

As the instant adhesive showed similar gray values as the pellets, we did not implement an automated segmentation. Instead, the instant adhesive at the bottom of the pellets was cropped manually using the commercial software VGSTUDIO MAX (version 3.2, Volume Graphics GmbH, Heidelberg, Germany) in a first processing step. The further image processing steps were carried out automatically using MATLAB (version 2018a, MathWorks, Natick, MA). To differentiate between hyphae and air voxels, a threshold – calculated by Otsu's method (Otsu, 1979) – was applied on the gray value images. Finally, small connected objects with a maximum size of 1,000 μm^3 were deleted to eliminate objects that were not part of the pellet. The processed three-dimensional pellets were used for further diffusion computations.
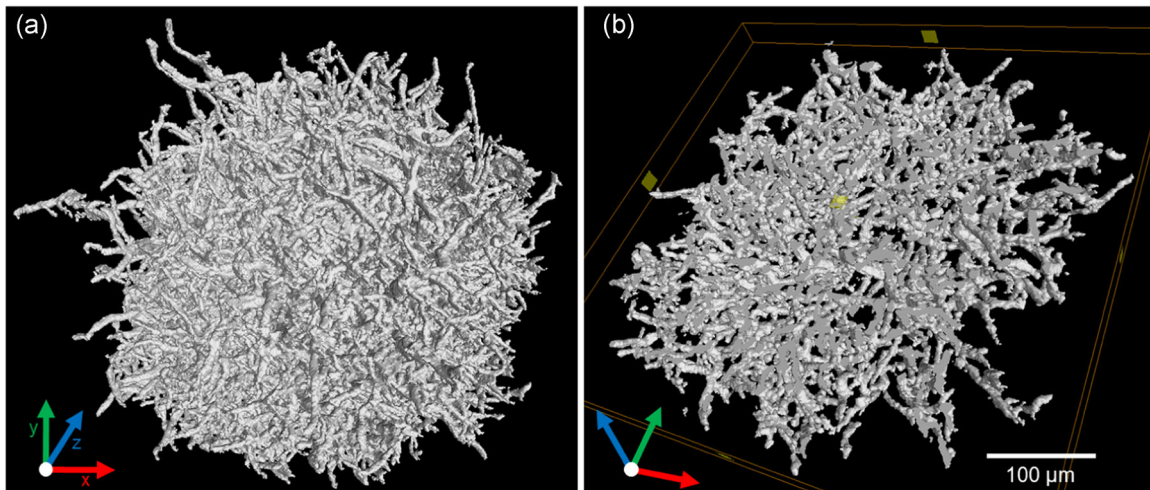
FIGURE 1 Processed three-dimensional µCT image of an *Aspergillus niger* pellet. The images were rendered using VGSTUDIO MAX. (a) Projection of the whole pellet. (b) Projection of a central slice with a depth of 25 µm [Color figure can be viewed at wileyonlinelibrary.com]

2.4 | Representative cubes for diffusion computations of *A. niger* pellets

To compute the spatially resolved effective diffusivity in fungal pellets, we extracted representative cubic sub-volumes of the processed three-dimensional images. The diffusive mass transport was computed, as described in Section 2.6 using these cubes. The centers of the cubes used for diffusion computations were selected along the main axis originating from the calculated mass center of the *A. niger* pellets. The distance between the centers of the cubes along the main axis was set to 25 µm. In Figure 2, the distance between the cubes was increased for the sake of clarity. To identify the influence of the cube-size on the diffusion computations, the edge length of the cubes was varied to 30, 50, 70, and 90 µm.

2.5 | Beam-Pellet

A common assumption for the effective diffusion coefficient of filamentous microorganisms is the direct proportionality to the porosity ε (Buschulte, 1992; Celler et al., 2012; Cui et al., 1998; Silva, Gutierrez, Dendooven, Hugo, & Ochoa-Tapia, 2001):

$$D_{i,\text{eff}} = D_{i,\text{bulk}} \cdot \epsilon. \tag{3}$$

Thereby, the effective diffusion factor k_{eff} is assumed to be equal to the porosity, and the tortuosity is neglected. To imitate a filamentous spherical object, where the tortuosity can be nearly neglected, we simulated a so-called "Beam-Pellet," which was used to validate the
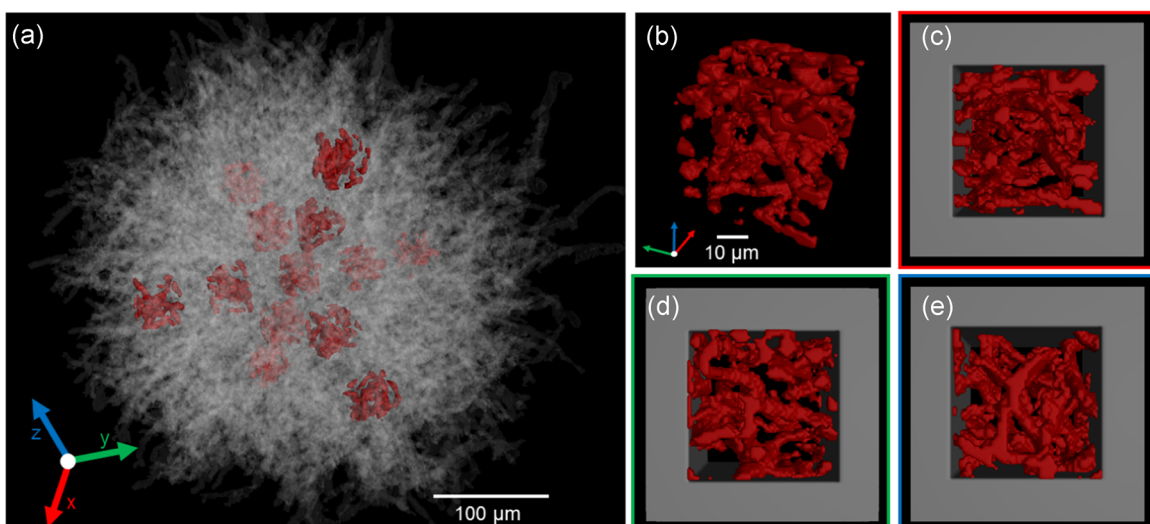
FIGURE 2 Processed three-dimensional µCT image of the *Aspergillus niger* pellet of Figure 1 and cubes for the diffusion computations: (a) Transparent: projection of a whole pellet; red: exemplary cubes that were used for the diffusion computations. (b–e) Morphology of a single cube from different viewing directions; the gray boundaries in (c–e) illustrate the boundaries parallel to the diffusion computation. (b) Cube without illustration of boundaries for the diffusion computations. (c) Cube for diffusion in the *x*-direction. (d) Cube for diffusion in the *y*-direction. (e) Cube for diffusion in the *z*-direction [Color figure can be viewed at wileyonlinelibrary.com]

method of the diffusion computation and critically scrutinize the tortuosity neglect in the literature.

The "Beam-Pellet" (Figure 3) was built up from equally sized filaments (in diameter and length) with their origin in the pellet center and having a radial orientation. To guarantee a uniform distribution of the filaments in space, their orientation was calculated using the HEALPIx (hierarchical equal area iso-latitude pixelization) discretization (Gorski et al., 2005). In this way, 50,700 representative, equally distributed points were calculated on the pellet surface; all of them were connected to the pellet center. Then, the connected lines were dilated with MATLAB to obtain a "Beam-Pellet" with a defined diameter of the filaments. The diameter was chosen to be 3 μm, similar to the average hyphal diameter of *A. niger* (Colin, Baigorí, & Pera, 2013; Nielsen, 1993; Schmieder et al., 2019). To investigate the influence of the image resolution on the subsequent diffusion computations, similar "Beam-Pellets" with different resolutions were simulated. Starting from a "Beam-Pellet" with a radius of 700 voxels and a dilation of one voxel, the resolution of the filaments was increased. Thereby, the number of filaments was kept constant, whereas the radius of the "Beam-Pellet" was set to 1,167, 1,633, 2,567, and 3,500 voxels and the dilation was set to 2, 3, 5, and 7 voxels, respectively. Thus, the "Beam-Pellets" only differed in the scaling and the resolution of the filaments. The effective diffusivity of the "Beam-Pellet" was analyzed, as described in Section 2.6. This analysis required cubes that represent the whole pellet. Similar to the case of the *A. niger* pellets, cubes located along the main axes were chosen to investigate the effective diffusivity (Figure 3). Identical to the final analysis of the *A. niger* pellets, the cube-edge length was set to 50 μm, and the cubes were selected along the main axis. Thus, the cube edge length was 50 voxels for the "Beam-Pellet" with a radius of 700 voxels and a dilation of one voxel. To guarantee that the same

structure (50 μm × 50 μm × 50 μm) was analyzed for higher resolutions, we increased the cube edge length to 83, 117, 183, and 250 voxels, respectively. In Figure 4, the same representative cube is shown for different resolutions.

2.6 | Computation of the effective diffusivity

To compute the effective diffusion factor and tortuosity of filamentous structures (Equation (2)), the module DiffuDict of the commercial software GeoDict (Becker et al., 2011; Velichko, Wiegmann, & Mücklich, 2009; Wiegmann & Zemitis, 2006; Math2Market Gmbh, Kaiserslautern, Germany) was used. As DiffuDict allows for the voxel-based solution of transport equations, the processed three-dimensional image data of the μCT measurements as well as the simulated "Beam-Pellet," could be used for the diffusion computations. DiffuDict requires cubic domains for the diffusion computations, and therefore, cubic sub-volumes of the filamentous pellets were extracted from the three-dimensional images for further analysis. The selections of representative sub-volumes are described in Sections 2.4 and 2.5 for *A. niger* pellets and the "Beam-Pellet," respectively. Conceptually, as shown in Figures 2c–e and 3c–e, the diffusion computations in DiffuDict were executed in one of the three main axes for each computation. As the representative cubes were chosen along the main axes, we were able to apply three computations on each cube and could thus analyze the effective diffusivity of each cube in the radial and in two tangential directions. The computational effort to obtain the diffusivity of one cube in the three directions was about 1 min for cubes with 50 × 50 × 50 voxels with an Intel Xeon E5-1660 CPU (3.7 GHz). The details of the computations are described in the following.
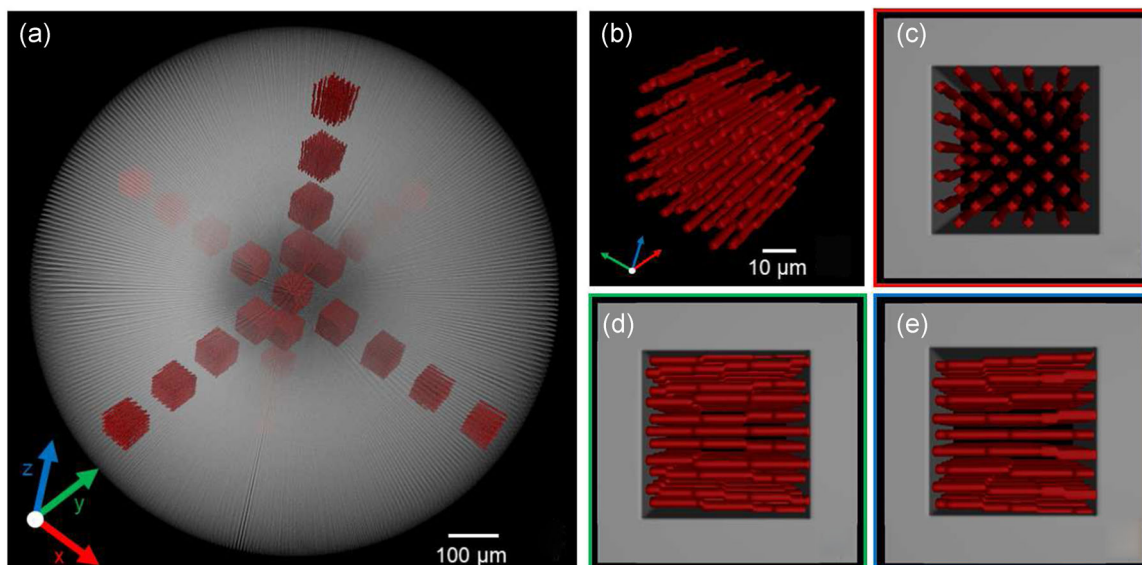
FIGURE 3 Simulated "Beam-Pellet" and cubes for diffusion computations: (a) Transparent: projection of the whole pellet; red: exemplary cubes that were used for the diffusion computations. (b–e) Morphology of a single cube from different viewing directions; the gray boundaries in (c–e) illustrate the boundaries parallel to the diffusion computation. (b) Cube without illustration of boundaries for the diffusion computations. (c) Cube for diffusion in the *x*-direction. (d) Cube for diffusion in the *y*-direction. (e) Cube for diffusion in the *z*-direction [Color figure can be viewed at wileyonlinelibrary.com]

FIGURE 4 Same representative cube of "Beam-Pellets" with different resolutions: (a) Three voxels per filament (dilation 1). (b) Five voxels per filament (dilation 2). (c) Seven voxels per filament (dilation 3). (d) 15 voxels per filament (dilation 7) [Color figure can be viewed at wileyonlinelibrary.com]
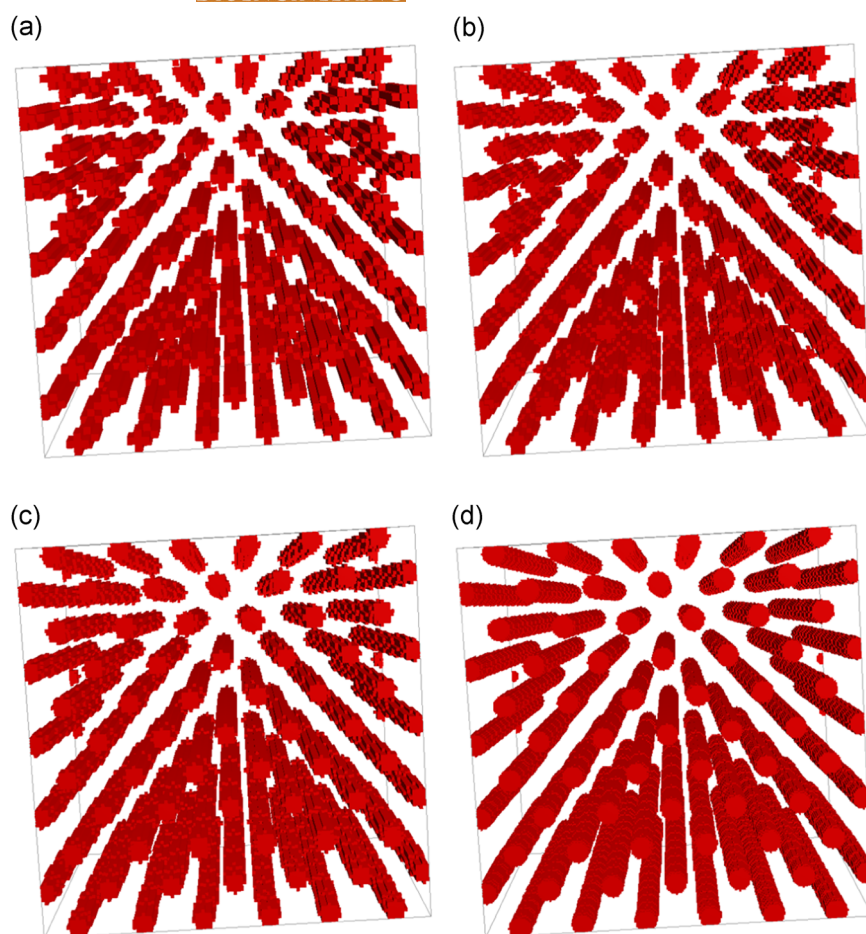
We computed the diffusion in the space/liquid between the hyphae (porous medium). The predominant diffusion regime in liquids is bulk diffusion (Becker et al., 2011; Panerai et al., 2017), that is, mass transport is mainly driven by collisions between fluid molecules. In our approach, we neglected surface effects on the solid–liquid interface that could influence diffusion. One possible effect could be surface diffusion, that is molecules can diffuse on the surface of pores. This phenomenon is known to be an important transport mechanism in reversed-phase liquid chromatography. However, predictions are difficult and depend on the temperature, surface concentration, and surface chemistry (Medveď & Černý, 2011; Miyabe & Guiochon, 2010). Electrical double-layers on solid–liquid interfaces could change the diffusivity through porous media, especially the diffusivity of ions (Gabitto & Tsouris, 2017). In the present study we assumed pure bulk diffusion. In the case of pure bulk diffusion, the diffusion in the pores can be modeled by the Laplace equation, with Neumann boundary conditions on the pores-to-solids boundaries and a concentration drop of the diffusing component in the diffusion direction (Becker et al., 2011). Thus, we applied bulk diffusion in DiffuDict and applied a concentration drop of the diffusing component between the inlet and outlet. To avoid a bias in the diffusion computations, we chose Dirichlet boundary conditions on the in- and outlet and symmetric boundary conditions on the other four faces. Computing the total diffusion flux through the porous structures and applying Fick's law, DiffuDict calculates the effective diffusion factor (Becker et al., 2011; Wiegmann & Zemitis, 2006). According to Equation (2), the tortuosity can be calculated from the porosity and the effective diffusion factor. Therefore, both the effective diffusion factor and the tortuosity were calculated for each representative sub-volume of the filamentous pellets.

3 | RESULTS AND DISCUSSION

3.1 | Effective diffusivity of the "Beam-Pellet"

The "Beam-Pellet" introduced in Section 2.5 (Figure 3) imitates a hypothetical filamentous pellet that grew only in the radial direction and is similar but not identical to parallel fibers. We compared the diffusion behavior of the "Beam-Pellet" with literature correlations for the diffusion through parallel fibers to validate the diffusion computations. Additionally, we critically scrutinized the literature assumption that $k_{eff} = \epsilon$ (Buschulte, 1992; Celler et al., 2012; Silva et al., 2001; Van't Riet & Tramper, 1991), where the tortuosity is neglected and the effective diffusion factor is assumed to be only dependent on the porosity.
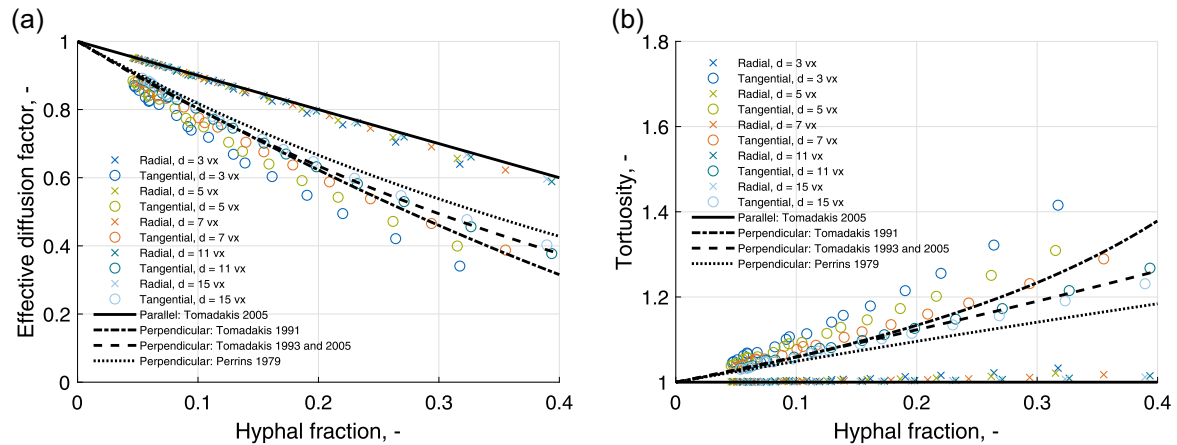
FIGURE 5 Diffusion computations of "Beam-Pellets" in the radial and tangential directions and comparison to existing literature correlations for parallel fibers (Table 1). The "Beam-Pellets" differ in the fiber-diameter in voxels, whereas the diameter in μm stayed constant (Figure 4). Each data point results from a single diffusion computation of a cubic sub-volume with a cube-edge length of 50 μm. Crosses and circles correspond to computed diffusion properties in the radial and tangential directions, respectively. The black lines represent literature correlations. The hyphal fraction corresponds to the ratio of the volume of hyphae to the total volume in the cubic sub-volumes [Color figure can be viewed at wileyonlinelibrary.com]

The results of the diffusion computations on the "Beam-Pellet" are shown in Figure 5 for the hyphal fraction range 0.05–0.4. A hyphal fraction of 0.4 was the maximum value for the *A. niger* pellets investigated in this study. Figure 5a shows the relation between the hyphal fraction of cubic sub-volumes and their corresponding effective diffusion factor. In the radial diffusion direction, the effective diffusion factor decreased almost linearly with increasing hyphal fractions. The radial effective diffusion factors showed a similar behavior as that of the often applied assumption for filamentous microorganisms: $k_{eff} = \epsilon$ (Buschulte, 1992; Celler et al., 2012; Silva et al., 2001; Van't Riet & Tramper, 1991). This formula is the prediction of the "law of mixtures" for the flow along parallel fibers (Tomadakis & Robertson, 2005). In the tangential directions, the effective diffusion factors were much smaller than their radial counterparts – and the slope was by no means in the order of minus one. Figure 5b shows the tortuosities for the radial and tangential diffusions, and it can be seen that they increase with increasing hyphal fractions. As expected, the tortuosities in the tangential diffusion direction were much higher than their radial counterparts.

To investigate the influence of the image resolution on the diffusion computations, we simulated "Beam-Pellets" with different resolutions (Section 2.5). With increasing resolutions, the effective diffusion factor increased and the tortuosity decreased, which was probably caused by the increased circularity of the filaments (Figure 4). As shown in Figure 3 and 4, representative cubes of the "Beam-Pellets" closely resemble parallel nonoverlapping fibers. Literature correlations for bulk diffusion through parallel fibers (Perrins et al., 1979; Tomadakis & Sotirchos, 1991, 1993; Tomadakis & Robertson, 2005) suggest, that the applied diffusion computations underestimate the diffusivity in the case of low resolutions. With increased resolutions, the computed diffusion results approach the literature correlations. However, it has to be mentioned that the literature correlations are for a square array of parallel fibers (Perrins et al., 1979), parallel random distributed overlapping fibers

(Tomadakis & Sotirchos, 1991), and random distributed nonoverlapping fibers (Tomadakis & Robertson, 2005; Tomadakis & Sotirchos, 1993) and thus similar but not identical to our "Beam-Pellets."

In contrast to the tangential diffusion paths, the radial paths of the "Beam-Pellet" were not winding (Figure 3). In theory, increased path lengths result in an increased tortuosity and a decreased diffusion factor (Epstein, 1989). This behavior could be observed for the "Beam-Pellet" in the radial and tangential diffusion directions as well. The small difference between the computed radial effective diffusion factors/tortuosities and the "law of mixtures" for the flow along parallel fibers (Tomadakis & Robertson, 2005) $k_{eff} = \epsilon$ was evoked by the radial direction of the filaments of the "Beam-Pellet." Thus, the filaments were not completely parallel to each other. Further investigations with simulated perfectly parallel filaments resulted in $k_{eff} = \epsilon$ and a constant tortuosity of one (data now shown).

To sum up, the diffusion behavior of the "Beam-Pellet" was consistent with the diffusion theory described by Epstein (1989) and could be used to verify the applied diffusion computations. The comparison to literature correlations about the diffusivity of parallel fibers suggests that our diffusion computations of fibers with a low image resolution tend to underestimate the diffusivity, whereas high resolutions approach the literature correlations. The radial diffusion behavior of the "Beam-Pellet" illustrated the often applied literature assumption for filamentous microorganisms: $k_{eff} = \epsilon$ (Buschulte, 1992; Celler et al., 2012; Silva et al., 2001; Van't Riet & Tramper, 1991). However, the morphology of the idealized "Beam-Pellet" (Figure 3) was very different from the μCT data of *A. niger* pellets (Figure 2). Thus, the actual correlation between the effective diffusivity and the hyphal fraction of *A. niger* pellets was investigated in further detail.

3.2 | Effective diffusivity of *A. niger* pellets

Contrary to the "Beam-Pellet" (Figure 3), in the case of the *A. niger* pellets, the voids, that is, the spaces between the hyphae (Figure 2),
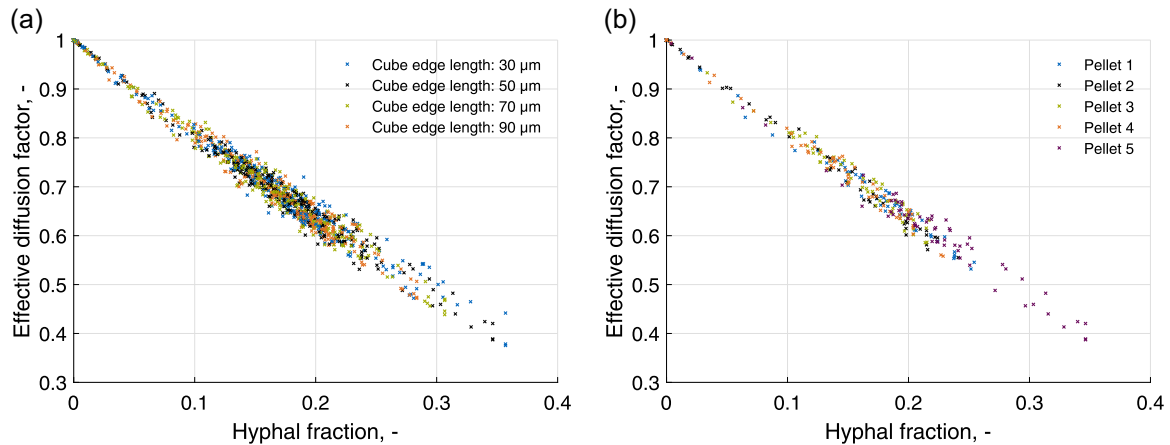
FIGURE 6 Correlations between the radial effective diffusion factor and hyphal fraction (ratio of the volume of hyphae to the total volume) for five *Aspergillus niger* pellets. Each data point results from a single diffusion computation of a cubic sub-volume: (a) Diffusion computations with different cube sizes. (b) The cube-edge length was 50 μm; each color represents the investigated cubes of one pellet [Color figure can be viewed at wileyonlinelibrary.com]

are strongly winded. According to Epstein (1989) that should result in an increased tortuosity, and therefore, in a decreased effective diffusivity. The tortuosity and effective diffusion factors of five *A. niger* pellets are investigated in this section. The diameters of the pellets were between 410 and 570 μm.

To investigate the influence of the size of the cubic sub-volumes on the diffusion computations, the edge length of the cubes was varied. Figure 6a shows the relation between the effective diffusion factor and the hyphal fraction for different cube sizes. The data include the diffusion computations of the five investigated *A. niger* pellets in the radial direction for cube-edge lengths of 30, 50, 70, and 90 μm. Generally, the effective diffusion factors for different cube-edge lengths showed similar behavior. When no hyphal material is present, that is, when the hyphal fraction is zero, the effective diffusion factor is one, and thus, the diffusion is not geometrically hindered. With increasing hyphal fraction, the effective diffusion factor decreases. The applied cube-edge lengths did not have a high

impact on the diffusion results. Thus, a cube-edge length of 50 μm was applied for further computations in this study. Figure 6b) shows the effective diffusion factors of the five *A. niger* pellets studied herein for a cube-edge length of 50 μm. It can be seen that the values for the different pellets varied only slightly. As five pellets were investigated, this very subtle scattering of the data points implies that the method is quite reproducible when applied to different pellets obtained from the same cultivation sample.

Figure 7 shows the results of the diffusion computations for the five studied *A. niger* pellets in the radial and tangential directions for a cube-edge length of 50 μm. Figure 7a shows that the computed effective diffusion factors of the *A. niger* pellets were much smaller than the values expected from the literature assumption $k_{eff} = \epsilon$, and therefore, also much smaller than the values obtained for the investigated "Beam-Pellet." A slight anisotropy was observed when comparing the radial and tangential diffusion directions because the effective diffusion factors in the radial direction were slightly higher
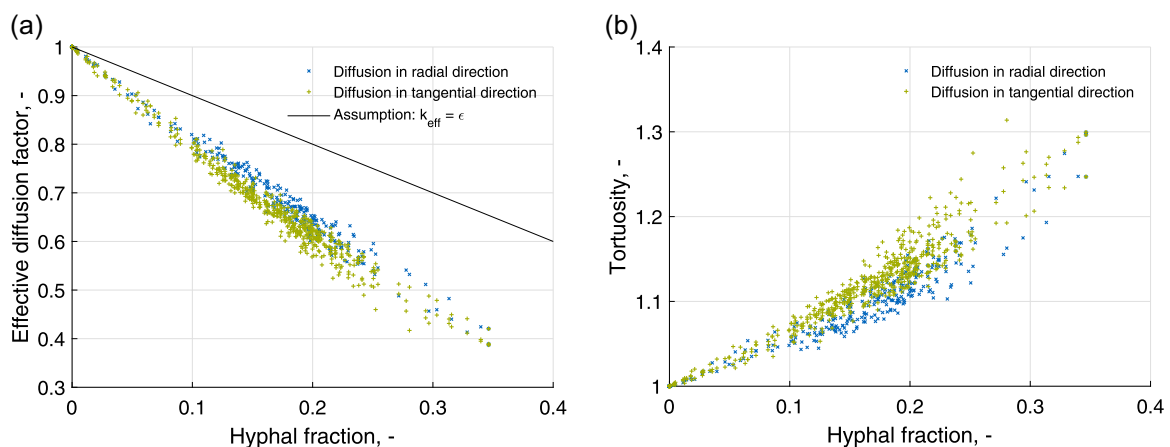
FIGURE 7 Diffusion computations of five *Aspergillus niger* pellets in the radial and tangential directions. Each data point results from a single diffusion computation of a cubic sub-volume with a cube-edge length of 50 μm; k_{eff} is the effective diffusion factor and ϵ is the porosity: (a) The blue and green data points correspond to effective diffusion factors in the radial and tangential directions, respectively; the black line represents the literature assumption $k_{eff} = \epsilon$. (b) The blue and green data points represent the tortuosities in the radial and tangential directions, respectively [Color figure can be viewed at wileyonlinelibrary.com]

than their counterparts in the tangential direction. In the absence of hyphal material, that is, when the hyphal fraction is zero, the tortuosity is one (Figure 7b). With increasing hyphal fraction, the tortuosity increases as well. Again, a slight difference was observed between the radial and tangential diffusion directions, with the radial diffusion computations resulting in lower tortuosities than their tangential counterparts. According to Equation (2), the lower tortuosities explain the higher effective diffusion factors in the radial direction. In the model assumption $k_{eff} = -c_h + 1 = \varepsilon$, the tortuosity is assumed to be constantly one. This simplification explains the differences between our computed effective diffusion factors for the *A. niger* pellets and the values expected from the literature (Figure 7a) as well as those reported for the "Beam-Pellet" in the previous section.

The local hyphal fraction range of the five investigated *A. niger* pellets was 0–0.4. To the best of our knowledge, there are no reports in the literature, in which the hyphal fraction of filamentous pellets is higher than the maximum hyphal fraction measured in this study, for example, Cui, Van der Lans, and Luyben (1997, 1998) reported average hyphal fractions between 0.07 and 0.30 for whole *Aspergillus awamori* pellets. Thus, the hyphal fraction ranges of the investigated *A. niger* pellets could already be representative for realistic pellets.

3.3 | Correlation between effective diffusivity and hyphal fraction

The diffusion computations of the five investigated *A. niger* pellets (Section 3.2) are compared to literature assumptions (Table 1) for the correlation between the effective diffusion factor (k_{eff}) and the hyphal fraction (c_h)/solid fraction/porosity ($\varepsilon = 1 - c_h$) of filamentous microorganisms (Figure 8a) and fibers (Figure 8b). As the diffusion of spherical pellets should be driven mainly by radial diffusion, we have investigated it herein. Additionally, a new modeling approach was

introduced to correlate the effective diffusion factor and the hyphal fraction.

The computed diffusion factors differed strongly from the assumption $k_{eff} = \varepsilon$, which has been used for simulation/modeling studies of filamentous microorganisms by Celler et al. (2012), Buschulte (1992), and Silva et al. (2001). In fact, the computed effective diffusion factors were far below the expected values. In those previous models, the effective diffusion factor was assumed to be only dependent on the porosity of the material, while neglecting the tortuosity. Thus, the difference between our computed effective diffusion factors and previous assumptions (Buschulte, 1992; Celler et al., 2012; Silva et al., 2001) was not surprising. The second linear literature assumption for filamentous microorganisms was $k_{eff} = \varepsilon/2$ (Lejeune & Baron, 1997). In their work, Lejeune and Baron (1997) considered the tortuosity to be consistently 2, without explaining that assumption. As shown, their model differed strongly from the computed data. Their model would result in a geometrically hindered diffusion for a hyphal fraction of zero. Thus, especially for low hyphal fractions, that assumption seems to be untenable. In their growth modeling approach for filamentous microorganisms, Meyerhoff et al. (1995) applied a nonlinear correlation between the effective diffusion factor and the hyphal fraction: $k_{eff} = (2 - c_h)/(2 + c_h)$. This approach seemed to approximate our computed data better than the two previous model assumptions from the literature. Additionally, the effective diffusion factor is 1 and 0 for hyphal fractions of 0 and 1, respectively. In theory, these conditions should be fulfilled. However, the model seemed to overestimate the effective diffusion factors. Besides the assumption $k_{eff} = \varepsilon$, Buschulte (1992) deduced a second model for filamentous microorganisms: $k_{eff} = e^{-2.8c_h}$. In comparison with the other literature assumptions for filamentous microorganisms, this approach fitted our computed data best. However, in the hyphal fraction range of 0–0.4, the model seemed to underestimate the computed data. Additionally, for a hyphal fraction of 1, the model would result in an effective diffusion factor of
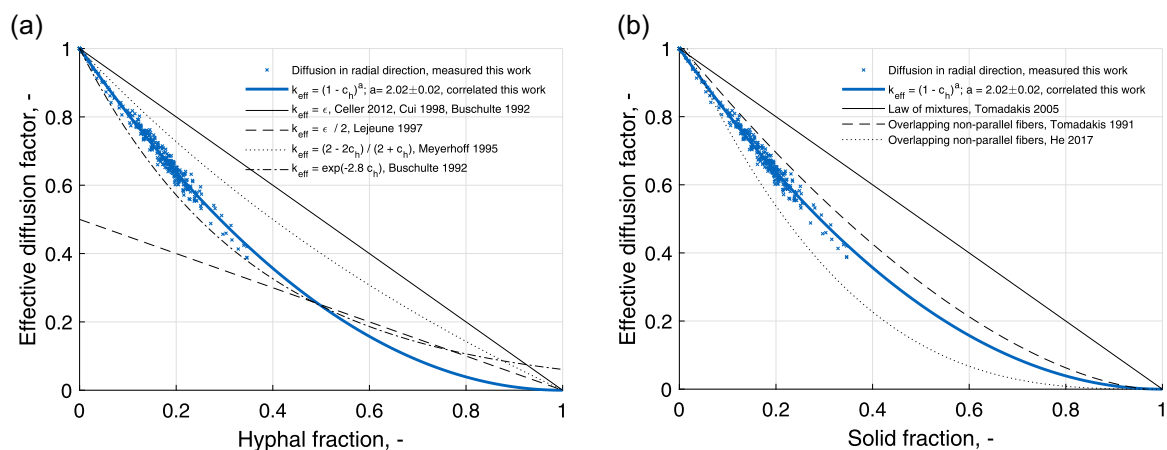
FIGURE 8 Correlations between hyphal fraction (c_h)/solid fraction/porosity ($\varepsilon = 1 - c_h$) and effective diffusion factor (k_{eff}). The blue data points correspond to the computed effective diffusion factors of five *Aspergillus niger* pellets in the radial direction, with the cube-edge length for the diffusion calculations being 50 μm. The solid bold blue line shows the new correlation between the hyphal fraction and the effective diffusion factor; the black lines represent existing correlations in the literature (Table 1) for (a) filamentous microorganisms and (b) 3D random distributed overlapping fibers [Color figure can be viewed at wileyonlinelibrary.com]

0.06. In theory, for a hyphal fraction of 1, the effective diffusion factor has to be 0 (Epstein, 1989).

The correlations for 3D random distributed overlapping fibers (Figure 8b) fitted our data better than the correlations existing for filamentous microorganisms. Our data fall in between the correlation of Tomadakis and Sotirchos (1991) and He et al. (2017). In both studies, the computation of the effective diffusivity was well validated for other structures like parallel fibers. However, they differ significantly. Tomadakis and Sotirchos (1991) applied a modification of Archie's law (Archie, 1942) to correlate the tortuosity factor $\tau^2 = ((1 - \epsilon_p)/(\epsilon - \epsilon_p))^\alpha$, with the percolation porosity $\epsilon_p = 0.037$ and $\alpha = .661$. It has to be mentioned that the modification of Archie's law also fitted well for Vignoles et al. (2007) for bulk diffusion of μCT-generated images of parallel fibrous carbon-carbon composite preforms. The percolation porosity was $\epsilon_p = 0.04$ and $\alpha = 0.107/\alpha = 0.465$ for diffusion parallel/perpendicular to the fibers, respectively. According to Nam and Kaviany (2003), the effective diffusivity of isotropic structures is often estimated using a power function of porosity. Thus, He et al. (2017) fitted their diffusion results of 3D random distributed overlapping fibers and found $k_{eff} = \alpha\epsilon^n$, with $\alpha = 1.05$ and $n = 3$.

To overcome the limitations and/or inaccuracies in the correlations between the effective diffusion factor and hyphal fraction for filamentous microorganisms and to obtain a relation with only one fitting parameter, we propose a new correlation:

$$k_{eff} = (1 - c_h)^a, \tag{4}$$

where a is the only fitting parameter. This rather simple expression guarantees theory-consistent effective diffusion factors of 1 and 0 at hyphal fractions of 0 and 1, respectively, and provides an excellent fit to our data. Minimizing the error squares, $a = 2.02 \pm 0.02$ (with 95% confidence bounds):

$$k_{eff} = (1 - c_h)^{2.02 \pm 0.02}. \tag{5}$$

In conclusion, the literature assumptions for modeling diffusion in filamentous pellets failed to fit our computed results, whereas correlations for fibers in material science fitted our data better. Thus, we set up a nonlinear equation (5) approach with only one fitting parameter, which is a special case for the power function of porosity, for $\alpha = 1$ as well as for the modified Archie's law, when $\epsilon_p = 0$. This approach modeled the correlation between the effective diffusion factor and the hyphal fraction for five investigated *A. niger* pellets quite well.

3.4 | Proposed workflow in bioprocess development

Depending on the product of interest, a saturation or a limitation of substrates inside fungal pellets is pursued (Veiter et al., 2018). To predict the spatial distribution of substrates inside pellets, the effective diffusivity through the fibrous network has to be known (Buschulte, 1992; Celler et al., 2012). Thus, our newly proposed

method to determine the effective diffusivity of filamentous fungal pellets with μCT measurements and subsequent diffusion computations through the three-dimensional morphology has considerable benefits for bioprocess development. We propose the following idealized workflow to achieve an optimal/suitable pellet morphology:

(1) Generate pellets through experiments or simulations
   a) Cultivate different strains at different process conditions; apply μCT measurements and subsequent image analysis of pellets (Schmieder et al., 2019)
   b) Simulate various three-dimensional pellet-networks with algorithms similar to Celler et al. (2012); model calibration could be carried out based on μCT measurements with subsequent image analysis (Schmieder et al., 2019)
(2) Compute the correlation between the hyphal fraction and the effective diffusivity for each existing and simulated pellet of Step 1, as described in the present study
(3) Compute the proportion of substrate-limited and substrate-saturated regions of each pellet based on the consumption- and diffusion-terms of models such as Buschulte (1992)); apply correlation of the hyphal fraction and effective diffusivity in diffusion terms (this study; Step 2)
(4) Assemble data base of experimentally or simulatively generated pellets including substrate-supply and morphological features
(5) Select optimal/suitable pellet for the desired process from data base
(6) Realize optimal/suitable pellet in bioprocess, for example, through the upscale of previous experiments (Step 1a), genetic modifications, or process control

Obviously, some of these steps have to be investigated and elaborated in much more detail to reach the proposed optimum macromorphology through this workflow. However, we consider the investigation of the effective diffusivity as an important step towards morphological engineering. In our study, we investigated five pellets of one process and the correlation between the effective diffusivity and hyphal fraction scattered only slightly. Thus, we propose, that our method is at least reproducible for a certain strain at certain process conditions. If the observed correlation between the hyphal fraction and the effective diffusivity is representative for the applied *A. niger* strain in general, other fungal strains, and/or theoretically all filamentous microorganisms should be the focus of future studies. Thereby, as described, μCT measurements are suitable to detect the three-dimensional morphology used for diffusion computations. However, other three-dimensional methods such as confocal laser scanning microscopy of pellets slices or even simulated pellets are also conceivable to explore other strains and processes.

4 | CONCLUSIONS

The findings described in this manuscript unveil the actual relation between the hyphal fraction (c_h, i.e., the ratio between the volume of

hyphae and the total volume) and the effective diffusion factor (k_{eff}) and tortuosity inside filamentous fungal pellets. They also uncover a discrepancy with the assumptions made in the literature for filamentous microorganisms so far. We propose a new correlation, which is inspired by correlations for fibers, rather simple, consistent with theoretical expectations, and shows an excellent fit to the investigated *A. niger* pellets: keff=$(1 - c_h)^2$. Our μCT images resulted in hyphae with a diameter of approximately five voxels. As indicated in Section 3.1 and Figure 5, that might lead to a slight underestimation of the diffusivity. For future studies of fibers/filamentous microorganisms, we recommend μCTs, that could resolve fibers/hyphae to a diameter of approximate 11 voxels. Alternatively, a correction factor could be calculated based on diffusion computations of simulated filamentous pellets. The method described in this study is not limited to *A. niger* but can also be applied to a variety of fungal species as well as to other organisms forming filamentous structures. It is conceivable to use the described workflow not only based on μCT data, but also on other three-dimensional data such as confocal laser scanning microscopy (CLSM) images of smaller structures and pellet slices, or even simulated pellets. The computed diffusion parameters, and thus the diffusion rates of substrates and products inside fungal pellets, could in combination with a consumption and production model, be applied to predict the actual metabolic flux inside filamentous pellets. With this information, it would be possible to propose an ideal fungal macromorphology for the production of a certain substance, which could then be achieved by genetic engineering and control of the process parameters during fermentation.

CONFLICT OF INTERESTS

The authors declare that there is no conflict of interests.

ORCID

Stefan Schmieder http://orcid.org/0000-0003-4328-9724
Lars Barthel http://orcid.org/0000-0001-8951-5614
Henri Müller http://orcid.org/0000-0002-4831-0003
Vera Meyer http://orcid.org/0000-0002-2298-2258
Heiko Briesen http://orcid.org/0000-0001-7725-5907

REFERENCES

Archie, G. E. (1942). The electrical resistivity log as an aid in determining some reservoir characteristics. *Transactions of the AIME*, *146*(01), 54–62. https://doi.org/10.2118/942054-g

Aris, R. (1975). *The mathematical theory of diffusion and reaction in permeable catalysts*. Clarendon Press.

Becker, J., Wieser, C., Fell, S., & Steiner, K. (2011). A multi-scale approach to material modeling of fuel cell diffusion media. *International Journal of Heat and Mass Transfer*, *54*(7-8), 1360–1368. https://doi.org/10.1016/j.ijheatmasstransfer.2010.12.003

Brakhage, A. A. (2013). Regulation of fungal secondary metabolism. *Nature Reviews Microbiology*, *11*(1), 21. https://doi.org/10.1038/nrmicro2916

Buschulte, T. K. (1992). *Mathematische Modellbildung und Simulation von Zellwachstum, Stofftransport und Stoffwechsel in Pellets aus Streptomyceten*. PhD thesis, Fakultät Verfahrenstechnik der Universität Stuttgart.

Cairns, T. C., Zheng, X., Zheng, P., Sun, J., & Meyer, V. (2019). Moulding the mould: Understanding and reprogramming filamentous fungal growth and morphogenesis for next generation cell factories. *Biotechnology for Biofuels*, *12*(1), 77. https://doi.org/10.1186/s13068-019-1400-4

Celler, K., Picioreanu, C., van Loosdrecht, M. C., & van Wezel, G. P. (2012). Structured morphological modeling as a framework for rational strain design of streptomyces species. *Antonie Van Leeuwenhoek*, *102*(3), 409–423.

Coindreau, O., Mulat, C., Germain, C., Lachaud, J., & Vignoles, G. L. (2011). Benefits of x-ray cmt for the modeling of c/c composites. *Advanced Engineering Materials*, *13*(3), 178–185. https://doi.org/10.1002/adem.201000233

Colin, V. L., Baigorí, M. D., & Pera, L. M. (2013). Tailoring fungal morphology of *Aspergillus niger* MYA 135 by altering the hyphal morphology and the conidia adhesion capacity: Biotechnological applications. *AMB Express*, *3*, 27. https://doi.org/10.1186/2191-0855-3-27

Cui, Y., Van der Lans, R., Luyben, K., et al. (1997). Effect of agitation intensities on fungal morphology of submerged fermentation. *Biotechnology and Bioengineering*, *55*(5), 715–726.

Cui, Y., Van der Lans, R., Luyben, K., et al. (1998). Effects of dissolved oxygen tension and mechanical forces on fungal morphology in submerged fermentation. *Biotechnology and Bioengineering*, *57*(4), 409–419.

Epstein, N. (1989). On tortuosity and the tortuosity factor in flow and diffusion through porous media. *Chemical Engineering Science*, *44*(3), 777–779. https://doi.org/10.1016/0009-2509(89)85053-5

Fiedler, M. R., Barthel, L., Kubisch, C., Nai, C., & Meyer, V. (2018). Construction of an improved *Aspergillus niger* platform for enhanced glucoamylase secretion. *Microbial Cell Factories*, *17*, 95. https://doi.org/10.1186/s12934-018-0941-8

Foerst, P., de Carvalho, T. M., Lechner, M., Kovacevic, T., Kim, S., Kirse, C., & Briesen, H. (2019). Estimation of mass transfer rate and primary drying times during freeze-drying of frozen maltodextrin solutions based on x-ray μ-computed tomography measurements of pore size distributions. *Journal of Food Engineering*, https://doi.org/10.1016/j.jfoodeng.2019.05.002

Gabitto, J., & Tsouris, C. (2017). Surface transport processes in charged porous media. *Journal of Colloid and Interface Science*, *498*, 91–104. https://doi.org/10.1016/j.jcis.2017.03.009

Gorski, K. M., Hivon, E., Banday, A., Wandelt, B. D., Hansen, F. K., Reinecke, M., & Bartelmann, M. (2005). Healpix: A framework for high-resolution discretization and fast analysis of data distributed on the sphere. *The Astrophysical Journal*, *622*, 759. https://doi.org/10.1086/apj.2005.622.issue-2

He, X., Guo, Y., Li, M., Pan, N., & Wang, M. (2017). Effective gas diffusion coefficient in fibrous materials by mesoscopic modeling. *International*

Journal of Heat and Mass Transfer, 107, 736–746. https://doi.org/10.1016/j.ijheatmasstransfer.2016.11.097

Hille, A., Neu, T., Hempel, D., & Horn, H. (2009). Effective diffusivities and mass fluxes in fungal biopellets. *Biotechnology and Bioengineering, 103*(6), 1202–1213.

Lejeune, R., & Baron, G. V. (1997). Simulation of growth of a filamentous fungus in 3 dimensions. *Biotechnology and Bioengineering, 53,* 139–150. https://doi.org/10.1002/(sici)1097-0290(19970120)53:2<139::aid-bit3>3.3.co;2-e

Medveď, I., & Černỳ, R. (2011). Surface diffusion in porous media: A critical review. *Microporous and Mesoporous Materials, 142*(2-3), 405–422. https://doi.org/10.1016/j.micromeso.2011.01.015

Meyer, V. (2008). Genetic engineering of filamentous fungi: Progress, obstacles and future trends. *Biotechnology Advances, 26,* 177–185. https://doi.org/10.1016/j.biotechadv.2007.12.001

Meyer, V., Andersen, M. R., Brakhage, A. A., Braus, G. H., Caddick, M. X., Cairns, T. C., & Head, R. M. (2016). Current challenges of research on filamentous fungi in relation to human welfare and a sustainable bio-economy: A white paper. *Fungal Biology and Biotechnology, 3,* 6. https://doi.org/10.1186/s40694-016-0024-8

Meyerhoff, J., Tiller, V., & Bellgardt, K.-H. (1995). Two mathematical models for the development of a single microbial pellet; part 1: Detailed morphological model based on the description of individual hyphae. *Bioprocess Engineering, 12*(6), 305–313.

Miyabe, K., & Guiochon, G. (2010). Surface diffusion in reversed-phase liquid chromatography. *Journal of Chromatography A, 1217*(11), 1713–1734. https://doi.org/10.1016/j.chroma.2009.12.054

Nam, J. H., & Kaviany, M. (2003). Effective diffusivity and water-saturation distribution in single-and two-layer pemfc diffusion medium. *International Journal of Heat and Mass Transfer, 46*(24), 4595–4611. https://doi.org/10.1016/S0017-9310(03)00305-3

Neale, G. H., & Nader, W. K. (1973). Prediction of transport processes within porous media: Diffusive flow processes within an homogeneous swarm of spherical particles. *AIChE Journal, 19*(1), 112–119. https://doi.org/10.1002/aic.690190116

Nielsen, J. (1993). A simple morphologically structured model describing the growth of filamentous microorganisms. *Biotechnology and Bioengineering, 41,* 715–727. https://doi.org/10.1002/bit.260410706

Otsu, N. (1979). A threshold selection method from gray-level histograms. *IEEE Transactions on Systems, Man, and Cybernetics, 9,* 62–66. https://doi.org/10.1109/tsmc.1979.4310076

Panerai, F., Ferguson, J. C., Lachaud, J., Martin, A., Gasch, M. J., & Mansour, N. N. (2017). Micro-tomography based analysis of thermal conductivity, diffusivity and oxidation behavior of rigid and flexible fibrous insulators. *International Journal of Heat and Mass Transfer, 108,* 801–811. https://doi.org/10.1016/j.ijheatmasstransfer.2016.12.048

Papagianni, M. (2004). Fungal morphology and metabolite production in submerged mycelial processes. *Biotechnology advances, 22*(3), 189–259.

Perrins, W., McKenzie, D. R., & McPhedran, R. (1979). Transport properties of regular arrays of cylinders. *Proceedings of the Royal Society of London. A. Mathematical and Physical Sciences, 369*(1737), 207–225. https://doi.org/10.1098/rspa.1979.0160

Pirt, S. (1966). A theory of the mode of growth of fungi in the form of pellets in submerged culture. *Proceedings of the Royal Society of London, 166,* 369–373. https://doi.org/10.1098/rspb.1966.0105

Schmieder, S., Barthel, L., Friedrich, T., Thalhammer, M., Kovačević, T., Niessen, L., & Briesen, H. (2019). An x-ray microtomography-based method for detailed analysis of the three-dimensional morphology of

fungal pellets. *Biotechnology and Bioengineering,* https://doi.org/10.1002/bit.26956

Silva, E. M. E., Gutierrez, G. F., Dendooven, L., Hugo, J. I., & Ochoa-Tapia, J. A. (2001). A method to evaluate the isothermal effectiveness factor for dynamic oxygen into mycelial pellets in submerged cultures. *Biotechnology Progress, 17*(1), 95–103. https://doi.org/10.1021/bp0001361

Tomadakis, M. M., & Robertson, T. J. (2005). Viscous permeability of random fiber structures: Comparison of electrical and diffusional estimates with experimental and analytical results. *Journal of Composite Materials, 39*(2), 163–188. https://doi.org/10.1177/0021998305046438

Tomadakis, M. M., & Sotirchos, S. V. (1991). Effects of fiber orientation and overlapping on knudsen, transition, and ordinary regime diffusion in fibrous substrates. *MRS Online Proceedings Library Archive, 250,* https://doi.org/10.1557/proc-250-221

Tomadakis, M. M., & Sotirchos, S. V. (1993). Effective diffusivities and conductivities of random dispersions of nonoverlapping and partially overlapping unidirectional fibers. *The Journal of chemical physics, 99*(12), 9820–9827. https://doi.org/10.1063/1.465464

Van't Riet, K., & Tramper, J. (1991). *Basic bioreactor design.* CRC Press.

Veiter, L., Rajamanickam, V., & Herwig, C. (2018). The filamentous fungal pellet: Relationship between morphology and productivity. *Applied Microbiology and Biotechnology,* 1–10. https://doi.org/10.1007/s00253-018-8818-7

Velichko, A., Wiegmann, A., & Mücklich, F. (2009). Estimation of the effective conductivities of complex cast iron microstructures using fib-tomographic analysis. *Acta Materialia, 57*(17), 5023–5035. https://doi.org/10.1016/j.actamat.2009.07.004

Vignoles, G. L., Coindreau, O., Ahmadi, A., & Bernard, D. (2007). Assessment of geometrical and transport properties of a fibrous c/c composite preform as digitized by x-ray computerized microtomography: Part ii. heat and gas transport properties. *Journal of materials research, 22*(6), 1537–1550. https://doi.org/10.1557/jmr.2007.0216

Vorlop, K.-D. (1984). *Entwicklung von Verfahren zur Polymerfixierung von Mikroorganismen und Anwendung der Biokatalysatoren zur Spaltung von Penicillin G und Synthese von L-Tryptophan.* PhD thesis, Naturwissenschaftliche Fakultät der Technischen Universität Carolo-Wilhemina zu Braunschweig.

Wiegmann, A., & Zemitis, A. (2006). *EJ-HEAT: A fast explicit jump harmonic averaging solver for the effective heat conductivity of composite materials.* Fraunhofer Institute ITWM.

Wittier, R., Baumgartl, H., Lübbers, D. W., & Schügerl, K. (1986). Investigations of oxygen transfer into Penicillium chrysogenum pellets by microprobe measurements. *Biotechnology and Bioengineering, 28*(7), 1024–1036. https://doi.org/10.1002/bit.260280713

Yaws, C. L. (2014). *Transport properties of chemicals and hydrocarbons.* William Andrew.

How to cite this article: Schmieder S, Barthel L, Müller H, Meyer V, Briesen H. From three-dimensional morphology to effective diffusivity in filamentous fungal pellets. *Biotechnology and Bioengineering.* 2019;1–12. https://doi.org/10.1002/bit.27166

5.3 Paper III: Universal law for diffusive mass transport through mycelial networks (Schmideder et al., 2021)

Summary

In Paper II, we determined a law for the diffusivity through the hyphal network of one fungal strain at defined process conditions. However, there are numerous fungal species capable of forming pellets with strongly differing morphologies. To consider the broad morphological range of filamentous fungi, we investigated the correlation between the effective diffusivity and the structure of 66 μCT measured pellets from four fungal species (*Aspergillus niger*, *Penicillium chrysogenum*, *Rhizopus oryzae*, and *Rhizopus stolonifer*) and 3125 Monte Carlo simulated pellets. Simulated pellets allowed the variation of following morphological properties in ranges known to exist for filamentous microorganisms: branching frequency, hyphal diameter, branch angle, maximum growth angle, and number of initial spores. As image resolution is known to have an influence on diffusion computations, it was varied for simulated structures. Thus, the simulated pellets overcame the limitations of Paper II, where the results were based on one experimental set up and a fixed resolution for μCT measurements. Based on diffusion computations through the mentioned simulated and measured pellets, we determined a universal law, which unveiled that only one independent variable, the hyphal fraction, affects the diffusivity. Because the simulations even considered the morphology of filamentous bacteria, we propose that our law can be used to compute the diffusion of molecules through any filamentous pellet. Concentrations of molecules inside pellets are affected by metabolic rates and the transport through the dense network. As the transport can now be calculated, the estimation of metabolic rates within pellets becomes feasible.

Author contributions

Stefan Schmideder did the conception and design of the study and wrote the manuscript, which was edited and approved by all authors. Heiko Briesen and Vera Meyer supervised the study. Lars Barthel and Ludwig Niessen cultivated filamentous fungi and prepared pellets for μCT measurements. Henri Müller and Stefan Schmideder performed μCT measurements of pellets. Stefan Schmideder, Henri Müller, and Tiaan Friedrich performed image analysis. Stefan Schmideder and Tiaan Friedrich set up the code for morphological Monte Carlo simulations. Stefan Schmideder performed the diffusion computations and analyzed the results. Stefan Schmideder, Henri Müller, Lars Barthel, and Heiko Briesen interpreted the results.

ARTICLE

Universal law for diffusive mass transport through mycelial networks

Stefan Schmideder[1] | Henri Müller[1] | Lars Barthel[2] | Tiaan Friedrich[1] |
Ludwig Niessen[3] | Vera Meyer[2] | Heiko Briesen[1]

[1]School of Life Sciences Weihenstephan, Chair of Process Systems Engineering, Technical University of Munich, Freising, Germany

[2]Institute of Biotechnology, Faculty III Process Sciences, Chair of Applied and Molecular Microbiology, Technische Universität Berlin, Berlin, Germany

[3]School of Life Sciences Weihenstephan, Chair of Technical Microbiology, Technical University of Munich, Freising, Germany

Correspondence
Heiko Briesen, Technical University of Munich, Chair of Process Systems Engineering, Gregor-Mendel-Str. 4, 85354 Freising, Germany.
Email: heiko.briesen@tum.de

Funding information
Deutsche Forschungsgemeinschaft, Grant/Award Numbers: 198187031, 315305620, 315384307, 427889137

Abstract

Filamentous fungal cell factories play a pivotal role in biotechnology and circular economy. Hyphal growth and macroscopic morphology are critical for product titers; however, these are difficult to control and predict. Usually pellets, which are dense networks of branched hyphae, are formed during industrial cultivations. They are nutrient- and oxygen-depleted in their core due to limited diffusive mass transport, which compromises productivity of bioprocesses. Here, we demonstrate that a generalized law for diffusive mass transport exists for filamentous fungal pellets. Diffusion computations were conducted based on three-dimensional X-ray micro-tomography measurements of 66 pellets originating from four industrially exploited filamentous fungi and based on 3125 Monte Carlo simulated pellets. Our data show that the diffusion hindrance factor follows a scaling law with respect to the solid hyphal fraction. This law can be harnessed to predict diffusion of nutrients, oxygen, and secreted metabolites in any filamentous pellets and will thus advance the rational design of pellet morphologies on genetic and process levels.

KEYWORDS

diffusive mass transport, filamentous fungal pellets, three-dimensional morphological measurements and simulations, X-ray microcomputed tomography

1 | INTRODUCTION

Fungal biotechnology is key for the transition from a petroleum-based economy into a bio-based circular economy. A thinktank consisting of leading European and American researchers and global business leaders concluded that this biotech sector can help to achieve 10 of the United Nations' 17 sustainable development goals (Meyer et al., 2020). Filamentous fungi are the only microorganisms that can fully degrade renewable lignocellulosic biomass and sustainably transform it into food, feed, chemicals, fuels, commodities, textiles, composite materials, antibiotics, and other drugs (Meyer et al., 2020). Their ability to perform complex posttranslational

modifications (Wang et al., 2020), their greatly expanded natural protein secretion apparatus (Ward, 2012), and the enormous potential of the secondary metabolome to produce bioactive molecules (Brakhage, 2013; Keller, 2019; Nielsen et al., 2017) make filamentous fungi a favorable host for many applications (Wösten, 2019).

Filamentous fungi are usually cultivated under submerged conditions in which their macromorphology varies from loose disperse mycelia to dense hyphal networks called pellets (Papagianni, 2004; Veiter et al., 2018). The evolution of these macromorphologies from spores, germlings, and hyphae (collectively, structures of micro-morphologies) is a multifactorial process and difficult to predict. A recent review highlighted all known genetic, physiologic, medium,

and process parameters that impact the development of micro- and macromorphologies of filamentous fungi, and it also discussed all relevant advantages and disadvantages of macromorphologies with regard to the production of fungal-based bioprocesses (Cairns et al., 2019). In brief, cultivations with disperse mycelia allow better homogenous distribution of nutrients and oxygen but behave as non-Newtonian fluids, whereas cultivations with pellets behave as Newtonian fluids but suffer from nutrient and oxygen limitation in the pellet cores. For *Aspergillus niger* and *Penicillium chrysogenum* pellets, it was shown that oxygen was often only available in the outer 200 μm (Hille et al., 2005; Wittier et al., 1986), whereas pellet size could range from a millimeter to a centimeter in size. The areas beyond this limit are likely hypoxic and do not sustain growth and/or product formation.

Two factors determine the concentration of nutrients and products inside pellets (Celler et al., 2012; Cui et al., 1998; Lejeune & Baron, 1997; Meyerhoff et al., 1995): the fungal metabolic rate and the transport through the filamentous network. The transport is mainly driven by diffusion, which is hindered by the dense hyphal network (Hille et al., 2005). This transport limitation results in heterogeneity and substrate limitation inside pellets (Hille et al., 2009; Veiter et al., 2020; Wittier et al., 1986; Zacchetti et al., 2018). The following three prerequisites are necessary to compute the concentration profile of any nutrient or product within a pellet (Celler et al., 2012; Cui et al., 1998; Lejeune & Baron, 1997; Meyerhoff et al., 1995): (1) the micro- and macromorphologies of a pellet are known, (2) the correlation between the morphology and the effective diffusivity of the nutrient or product is known, and (3) the metabolic rate, which is also dependent on (1), can be calculated. Notably, the metabolic rate could be estimated if the first two prerequisites and the concentration profile are known. We, therefore, recently harnessed X-ray microcomputed tomography (μCT) and three-dimensional (3D) image analysis to determine the location and number of tips, branches, and hyphal material within whole fungal pellets to meet the first two requirements (Schmieder, Barthel, Friedrich, et al., 2019; Schmieder, Barthel, Müller, et al., 2019). Mathematically, the concentration profile of any molecule *i* within the voids of a pellet could be described by a diffusion reaction equation (Celler et al., 2012; Meyerhoff et al., 1995), where the reaction term describes the consumption or the production of the molecule. We focused on the diffusion term, where the effective diffusion coefficient $D_{i,eff}$ of component *i* determines the diffusivity and can be expressed as (Becker et al., 2011):

$$D_{i,eff} = D_{i,bulk} \, k_{eff}(\vec{m}) \tag{1}$$

where $\vec{m}$ is the vector for morphological properties, and $k_{eff}(\vec{m})$ is the geometrical diffusion hindrance. The diffusion coefficient in the bulk medium $D_{i,bulk}$ can be estimated from medium conditions (Yaws, 2009). Thus, $k_{eff}(\vec{m})$, which is independent of the diffusing component (Becker et al., 2011), is the only unknown variable to determine $D_{i,eff}$. It has to be mentioned that k_{eff}^{-1} is similar to the formation factor, which is often applied to describe the diffusivity, conductivity, or

permeability through porous media (Tomadakis & Robertson, 2005). In our recent study (Schmieder, Barthel, Müller, et al., 2019), we proposed the preliminary correlation $k_{eff} = (1 - c_h)^2$ for one of the main fungal cell factories, *A. niger*, where c_h is the hyphal fraction (equal to solid fraction).

In the current study, we investigated the correlation between the effective diffusivity and the morphology of more than 60 μCT measured pellets from four fungal cell factories (*A. niger*, *P. chrysogenum*, *Rhizopus oryzae*, and *R. stolonifer*) and more than 3000 Monte Carlo simulated pellets. We considered the diffusion through filamentous networks with different resolutions because image resolution can influence computed material properties (Schmieder, Barthel, Müller, et al., 2019; Velichko et al., 2009). Based on the measurements and simulations, we propose here a generalized law for the diffusion of nutrients, oxygen, and fungal metabolites through hyphal networks. This law enables, for the first time, the estimation of metabolic rates at any point within a pellet and forms the mathematical foundation for future targeted genetic and process engineering strategies.

2 | MATERIALS AND METHODS

2.1 | Preparation of pellets

To obtain pellet structures of morphologically different strains of industrially relevant fungal species, we cultivated the hyperbranching *A. niger* MF22.4 (Δ*racA*) and its parental strain MF19.5 (Fiedler et al., 2018; Kwon et al., 2011), *P. chrysogenum* MUM17.85 (indoor paint, Micoteca da Universidade do Minho), *R. stolonifer* (isolated organisms), and *R. oryzae* CBS 607.68 (unknown source). Sporangiospores (*Rhizopus* spp.) and conidospores (*A. niger* and *P. chrysogenum*) of all strains were obtained from agar plate cultures using standard procedures for filamentous fungi (Bennet & Lasure, 1991). Erlenmeyer flasks were inoculated with the spores and cultivated for 24–48 h until pellets became visible. Pellets were carefully removed by pipetting, washed with sterile tap water, frozen while they were floating in water, and subsequently freeze dried to preserve their structure (Schmieder, Barthel, Friedrich, et al., 2019). For detailed description of pellet preparation, we refer to Supplementary Protocol 1.

2.2 | X-ray microcomputed tomography

To obtain the 3D fibrous network of freeze dried pellets, μCT measurements were performed based on the method reported previously (Schmieder, Barthel, Friedrich, et al., 2019). Pellets were fixed on top of a sample holder for image acquisition. Then, at least 2.000 two-dimensional projections from different angles were acquired using a μCT system (XCT-1600HR; Matrix Technologies) and subsequently reconstructed to 3D images with custom-designed software (Matrix Technologies) that is based on CERA (Siemens). Images

were taken with a voxel size of 1, 2, 3, and 4 µm, respectively. For further information, we refer to Supplementary Protocol 2.

2.3 | Image processing

Image processing was applied on the 3D µCT-images of the pellets, based on the methods described previously (Schmieder, Barthel, Friedrich, et al., 2019; Schmieder, Barthel, Müller, et al., 2019), to differentiate between hyphal material and background. The background consisted of the material used for pellet fixation, air between the hyphae, and small impurities.

First, the fixation material was cropped manually with the commercial software VGSTUDIO MAX (version 3.2; Volume Graphics GmbH) or automatically using MATLAB (version 2019b; MathWorks). In the automatic segmentation, the gray level image was first binarised by setting a gray value threshold, which was calculated with Otsu's method (Otsu, 1979). After the binarisation, small connected objects were removed, so that only the sample holder remained as a foreground object in the binarised image. The complement of the binarized image was calculated and multiplied with the original gray level image, resulting in a gray level image without sample holder. Second, the pellets were segmented from each other manually by drawing a region of interest around each pellet with VGSTUDIO MAX or automatically using MATLAB. Therefore, the gray level image without sample holder was binarised by setting a gray value threshold, which was calculated with Otsu's method (Otsu, 1979). The result was a binarised image with the pellets as the foreground object. Furthermore, the binarised pellets were dilated and a watershed segmentation (Meyer, 1994) was performed. The segmented, labeled, and dilated pellet objects were read out successively from the original gray level image with multiple pellets. Finally, the resulting gray level images with only one single pellet were cropped according to the pellet size.

To differentiate between the hyphae and the voids between the hyphae on the cropped gray level images with single pellets, further image processing steps were carried out automatically using MATLAB (version 2019a). *A. niger*, *R. stolonifer*, and *R. oryzae* pellets were binarised by setting a gray value threshold, which was calculated with Otsu's method (Otsu, 1979). However, for *P. chrysogenum* pellets, this method was not sufficient. Therefore, the gray level values were clustered using Gaussian mixture modeling (Bishop, 2009; McLachlan & Peel, 2000) with three classes. To reduce the computational effort, a random sample subset of 10% of the total voxel count was drawn from the image and used for model creation. For the sake of stability, the model was built seven times and the one with the biggest log likelihood was chosen as the final model. Afterwards, all voxels were classified against this model by calculating the largest posterior probability (Bishop, 2009). The three classes represent the gray level values of the background, the noise, and the hyphal material. All gray level values in the class of the hyphal material were set to one, representing the foreground, whereas the gray level values of the other two classes were set to zero, representing the background in the binarised image.

After binarisation, connected objects smaller than or equal to 5000 µm³ for *R. oryzae* and *R. stolonifer* and 1000 µm³ for *P. chrysogenum*, *A. niger* MF19.5, and *A. niger* MF22.4 were deleted, to eliminate small impurities between the hyphae.

Further diffusion computations were conducted with these final processed 3D images of pellets.

2.4 | Diameter of hyphae

We used MATLAB (version 2019a) to determine the diameter of the hyphae based on the maximum ball method (Silin & Patzek, 2006). Therefore, we applied euclidean distance transform on the complemented binarised 3D image with hyphae as foreground (MATLAB function "bwdist"). As a result, the closest Euclidean distance of each hyphal voxel to a nonhyphal voxel was stored in the 3D matrix D (same dimension as the whole 3D image). Nonhyphal voxels were assigned to zero. In addition, we applied ultimate erosion (MATLAB function "bwulterode") on the binarised 3D image, which resulted in the 3D matrix E (same dimension as the whole 3D image), which consisted of the regional maxima of the Euclidean distance transform of the complement of the binarised image. To obtain the regional hyphal diameters within whole pellets, the corresponding elements of D and E were multiplied. The regional hyphal diameters were used to calculate the arithmetic mean of the hyphal diameter.

2.5 | Morphological simulations

Our morphological simulations were based on stochastic growth models for filamentous microorganisms (Celler et al., 2012; Yang et al., 1992) and resulted in 3D images thereof. We implemented the simulations in MATLAB (version 2019a). Video S1 visualizes the growth process of an exemplary noncoagulative pellet from a single spore. In our model, the following fundamental changes were made compared with the model of Celler et al. (2012):

- New in our study: Spore aggregates can be used as initial condition; voxel-based 3D image generation of morphological output that makes the data comparable with µCT images.
- Neglected in our study: Cross wall-formation; oxygen as a limiting component for growth.

Our model can be divided into three sections: (1) spore aggregation, (2) growth, and (3) generation of 3D structure (Figure 1). In the following, the basics of the three sections are described.

We simulated spore aggregation based on the diffusion-limited aggregation (DLA) method (Witten & Sander, 1983; Figure 1, top). DLA was initialized with a seed spore at the origin of a lattice. The second spore started random walk from far away. The coordinate was fixed if the second spore got in contact with the seed spore. If the distance to the seed spore became too large, later contact would be unlikely and the spore was rejected. The next spore started
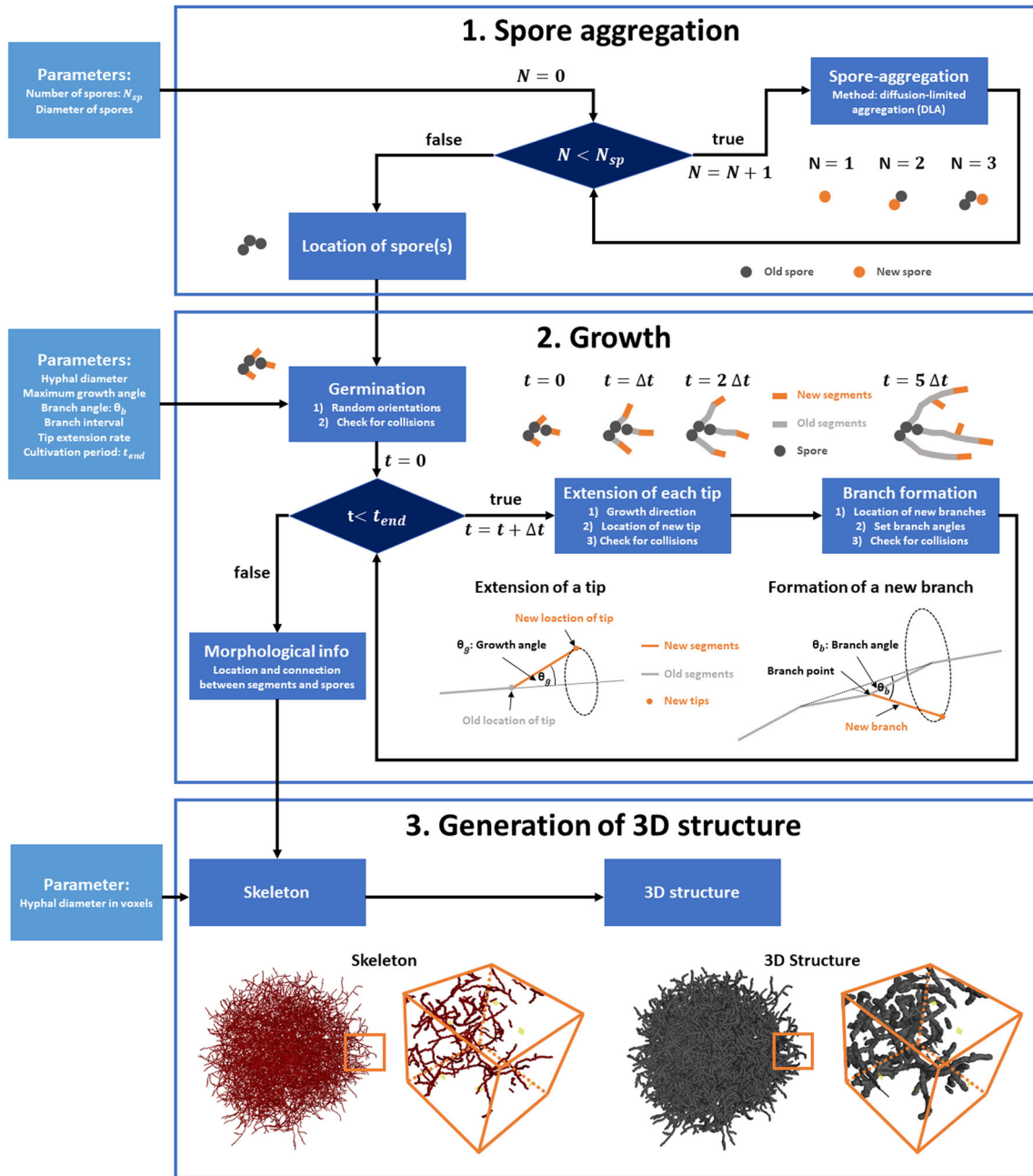
FIGURE 1 Overview of the algorithm of morphological simulations [Color figure can be viewed at wileyonlinelibrary.com]

random walk until it had contact or was too far from the spore aggregate. This procedure was repeated until the desired number of spores N_{sp} (Table S1) was reached.

Growth was based on the germination of spores, the extension of tips, and the formation of branches (Figure 1, middle). The location of spores served as input for the growth section, where they germinated simultaneously in random orientations forming segments with the length l_{germ}. Thereby, collisions of germlings with other germlings or spores were prevented. After germination, the extension of tips and the formation of branches started. These two phenomena repeated until the end of the cultivation. Exemplarily, a cultivation period of $t_{end} = 48h$ and a time step for calculations $\Delta t = 0.1h$ would

result in 480 time steps. In each time step, the extension of each tip is determined. Therefore, a growth angle θ_g between 0° and the maximum growth angle is chosen randomly. The length of the new segment $l_{segment}$ is the product of Δt and the tip extension rate α_t. The growth angle and the length of the segment form a circle, whereon the location of the new tip is calculated randomly (Figure 1). The new segment is defined as the connection between the old and the new tip. To prevent overlapping hyphae, possible collisions between the new segment and other segments or spores are detected with closest-point computations (Ericson, 2010). If a collision is detected, the new segment is rejected. However, the same tip is checked for extension in the next calculation step. Similar to Celler et al. (2012),

new branches could be formed in the subapical region of hyphae. The subapical region had a length of $l_{subapical}$ and started beginning from the tip (Table S1). In each time step, one possible new branch point (node between two segments, Figure 1) per subapical region was chosen randomly. Before the new branch was generated at this branch point, four conditions had to be fulfilled: (1) location in subapical region, (2) no branches in the neighboring four nodes, (3) current number of branches of the hyphae was lower than the possible number of branches, and (4) no collision of new segment with other segments or spores. The possible number of branches per hyphae was calculated by dividing the length of the hyphae by the minimum mean distance between two branches $d_{b,min}$ (Table S1). If conditions one through three were fulfilled, a possible new branch was calculated. The branch angle θ_b and the length of the segment $l_{segment}$ formed a circle, whereon the location of the tip of the new branch was calculated randomly (Figure 1). Similar to the extension of tips, the new segment was checked for collisions with other segments or spores (Ericson, 2010) and rejected if a collision was detected. Finally, the growth section resulted in morphological information, that is, the location and connection of nodes, hyphal segments, and spores.

The morphological information of the growth section served as input to generate voxel-based 3D structures (Figure 1, bottom). To scale the 3D images, the location of nodes (points between segments or center of spores) was multiplied with the scaling factor $f_{scale} = \frac{d_{h,vx}}{d_h}$, where $d_{h,vx}$ and d_h are the hyphal diameters in voxels and μm, respectively. Varying $d_{h,vx}$ for the same morphological information generated 3D images of pellets only differing in resolution. To obtain skeletons of pellets, the connections between nodes were discretised based on Bresenham's line algorithm (Bresenham, 1965). Finally, the skeletonized images were dilated using a spherical structuring element to obtain 3D images of pellets with the desired hyphal diameter and resolution.

2.6 | Diffusion computations

We computed the continuum diffusion through the voxel-based structures of filamentous pellets gained from both simulations and processed μCT measurements. Similar to our previous study (Schmieder, Barthel, Müller, et al., 2019), we calculated the diffusive mass transport using the commercial software GeoDict (Becker et al., 2011; Velichko et al., 2009; Math2Market Gmbh) that uses the explicit jump finite volume solver by Wiegmann and Zemitis (2006) for diffusion computations. Depending on the size of the pellets, approximately 50–150 representative cubic sub-volumes per pellet were extracted using MATLAB (version 2019a) and further used for diffusion computations (Video S2). An edge length sixfold the hyphal diameter proved to be sufficient as representative elementary volume (REV) of the extracted cubes to fit the parameter a in $k_{eff} = (1 - c_h)^a$ (Figure S1) and to investigate the porosity and diffusivity (Figures S2 and S3). The cubes were selected along the three main axes originating from the calculated mass center of the pellets.

We applied a diffusion computation in the radial direction of each extracted cube, resulting in an effective diffusivity (k_{eff}) in radial direction, that is, the direction pointing to the mass centre of the pellet. In addition, the hyphal fraction (c_h) of the cubes, that is, the ratio of volume of hyphae to the total volume, was analyzed. Similar to our previous study (Schmieder, Barthel, Müller, et al., 2019), the diffusion computations were conducted in the liquid between the hyphae, the porous medium. Pure bulk diffusion was assumed, because it is the predominant diffusion regime in liquids (Becker et al., 2011; Panerai et al., 2017). In our study we neglected surface effects on the solid-liquid interface that could influence diffusion (Schmieder, Barthel, Müller, et al., 2019). The diffusion was modeled by the Laplace equation, with Neumann boundary conditions on the pores-to-solids boundaries, and a concentration drop of the diffusing component in the diffusion direction (Becker et al., 2011). In addition, we applied Dirichlet boundary conditions on the in- and outlet and symmetric boundary conditions on the other four faces.

3 | RESULTS AND DISCUSSION

3.1 | Correlation of morphology and diffusive mass transport in μCT-measured pellets

Because pellet morphology is, inter alia, strain dependent, we investigated five different strains from four fungal cell factories: *P. chrysogenum* (penicillin producer); *A. niger* (citric acid and enzyme producer, with one isolate displaying wildtype morphology; strain MF19.5), and one hyperbranching isolate (strain MF22.4; Fiedler et al., 2018)); *R. stolonifer* (fumaric acid); and *R. oryzae* (enzymes, tempeh). At least three pellets per strain were analyzed by μCT, which allows nondestructive 3D investigations of intact pellets (Schmieder, Barthel, Friedrich, et al., 2019). The 3D morphology and an exemplary diffusion computation through a *R. stolonifer* pellet are shown in Video S2.

Remarkably, pellet morphologies were highly diverse among the strains (Figure 2). Equatorial slices of pellets showed that the distribution of hyphal material ranged from nearly spherically symmetric (*R. oryzae*, *R. stolonifer*, and *A. niger*) to a distribution far from spherical symmetry (*P. chrysogenum*). The porosity within the pellets also differed significantly. For example, *R. stolonifer* pellets had a loose structure whereas *A. niger* pellets were much denser. In addition, the porosity varied from nearly homogeneous (*A. niger* MF22.4 and *R. stolonifer*) to strongly heterogeneous (*R. oryzae* and *P. chrysogenum*). The mean hyphal diameter of *P. chrysogenum*, *A. niger* MF19.5, *A. niger* MF22.4, *R. stolonifer*, and *R. oryzae* was 4.3, 4.0, 4.3, 8.3, and 4.5 μm, respectively. Although the morphology of the investigated strains varied strongly, the results of the diffusion computations were surprisingly very similar (Figure 2, bottom row). The correlation

$$k_{eff} = (1 - c_h)^a \qquad (2)$$

between the effective diffusion factor (k_{eff}) and the hyphal fraction (c_h, ratio of hyphal material inside the cubes) fitted well for all strains.
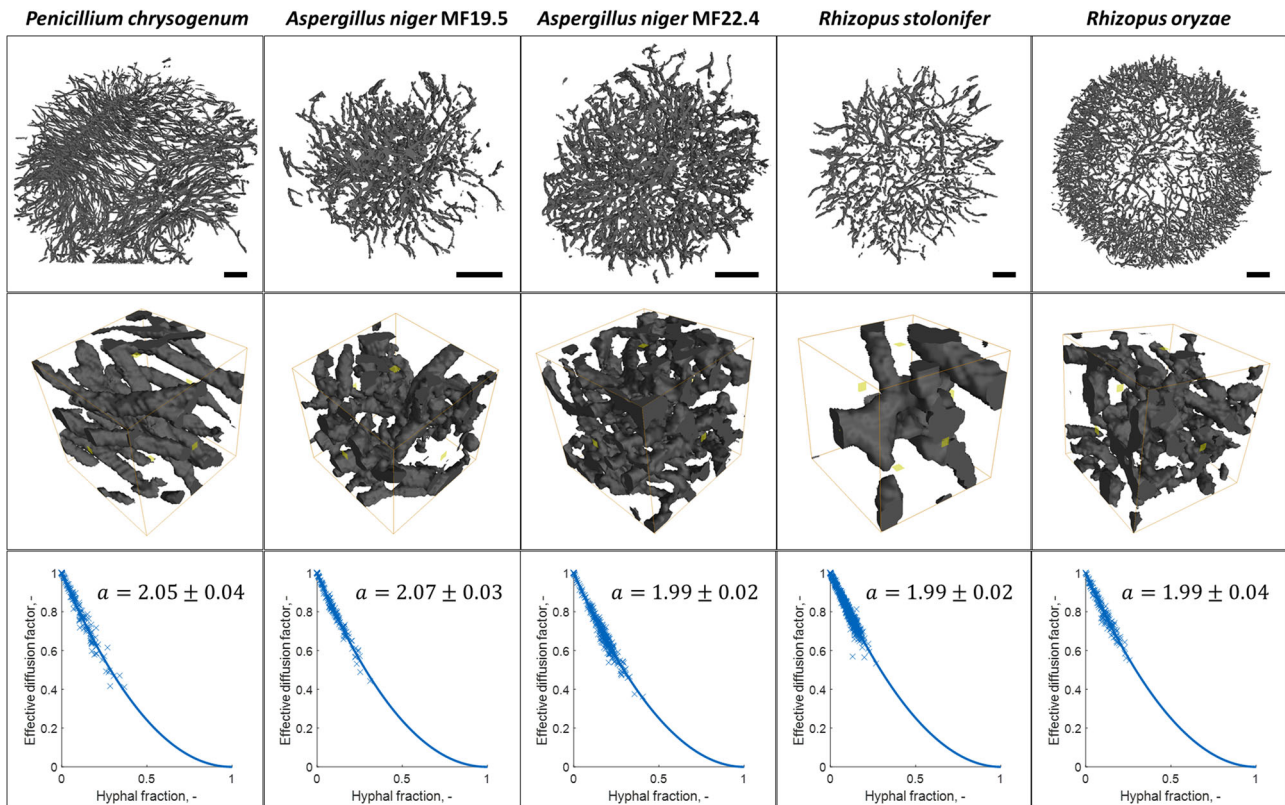
FIGURE 2 Morphology and diffusivity of experimentally investigated pellets. Upper two rows: Exemplary projections of processed three-dimensional microcomputed tomography (µCT) images. Slices are from equatorial regions with a depth of 30 µm. Cubes are 50 × 50 × 50 µm. Bottom row: correlation between hyphal fraction (c_h) and effective diffusion factor (k_{eff}). Each blue data point corresponds to one cube applied for diffusion computations. The solid blue line is the correlation between the hyphal fraction and the effective diffusion factor, resulting in the fitted exponent a in (Schmieder, Barthel, Müller, et al., 2019): $k_{eff} = (1 - c_h)^a$. ± specifies the 95% confidence interval. µCT measurements were conducted with a voxel size of 1 µm (three *Penicillium chrysogenum*, three *Aspergillus niger* MF19.5, five *A. niger* MF22.4, and three *Rhizopus oryzae* pellets) and 2 µm (11 *R. stolonifer* pellets). For each strain, at least 149 cubes were investigated. Scale bar: 100 µm [Color figure can be viewed at wileyonlinelibrary.com]

The correlation is known as Archie's law with a cementation parameter equal to a (Archie, 1942) and was already applied for one *A. niger* strain in our previous study (Schmieder, Barthel, Müller, et al., 2019). Including the 95% confidence interval, the exponent a was 2.05 ± 0.04, 2.07 ± 0.03, 1.99 ± 0.02, 1.99 ± 0.02, and 1.99 ± 0.04 for *P. chrysogenum*, *A. niger* MF19.5, *A. niger* MF22.4, *R. stolonifer*, and *R. oryzae*, respectively.

The similarity of the diffusion laws raises the issue of a generalized law for filamentous fungi. However, as there are an estimated six million fungal species on earth (Taylor et al., 2014), many of them filamentous and capable of forming numerous different morphologies (Cairns et al., 2019), our µCT-based experimental approach is not target orientated to investigate a generalized law.

3.2 | Correlation of morphology and diffusive mass transport in simulated pellets

To determine a generalized law for the diffusivity through fungal pellets that would be applicable to any filamentous fungus of interest,

we decided to follow an unbiased modeling approach. Using a Monte Carlo growth model (Celler et al., 2012; see Section 2), we thus simulated a huge variety of pellet morphologies and then exposed the simulated pellets to diffusion computations (see Section 2 and Video S2).

In the morphological simulations, both the coagulative and noncoagulative fungal spore aggregation phenomena (Metz & Kossen, 1977; Zhang & Zhang, 2016) were taken into account. In brief, a coagulative pellet forms by aggregation of hundreds to thousands of spores before they start to germinate, and a non-coagulative pellet could form from the germination of a single spore (Cairns et al., 2019). For the former case, we decided to model the aggregation of spores by diffusion-limited aggregation (Witten & Sander, 1983; see Section 2). Figure 3 highlights that the unbiased morphological simulations indeed enabled the development of both coagulative and noncoagulative pellet types, which reasonably matched the experimental data for the coagulative *A. niger* MF19.5 and the noncoagulative *R. stolonifer*, respectively. The growth process of a non-coagulative pellet is shown in Video S1.
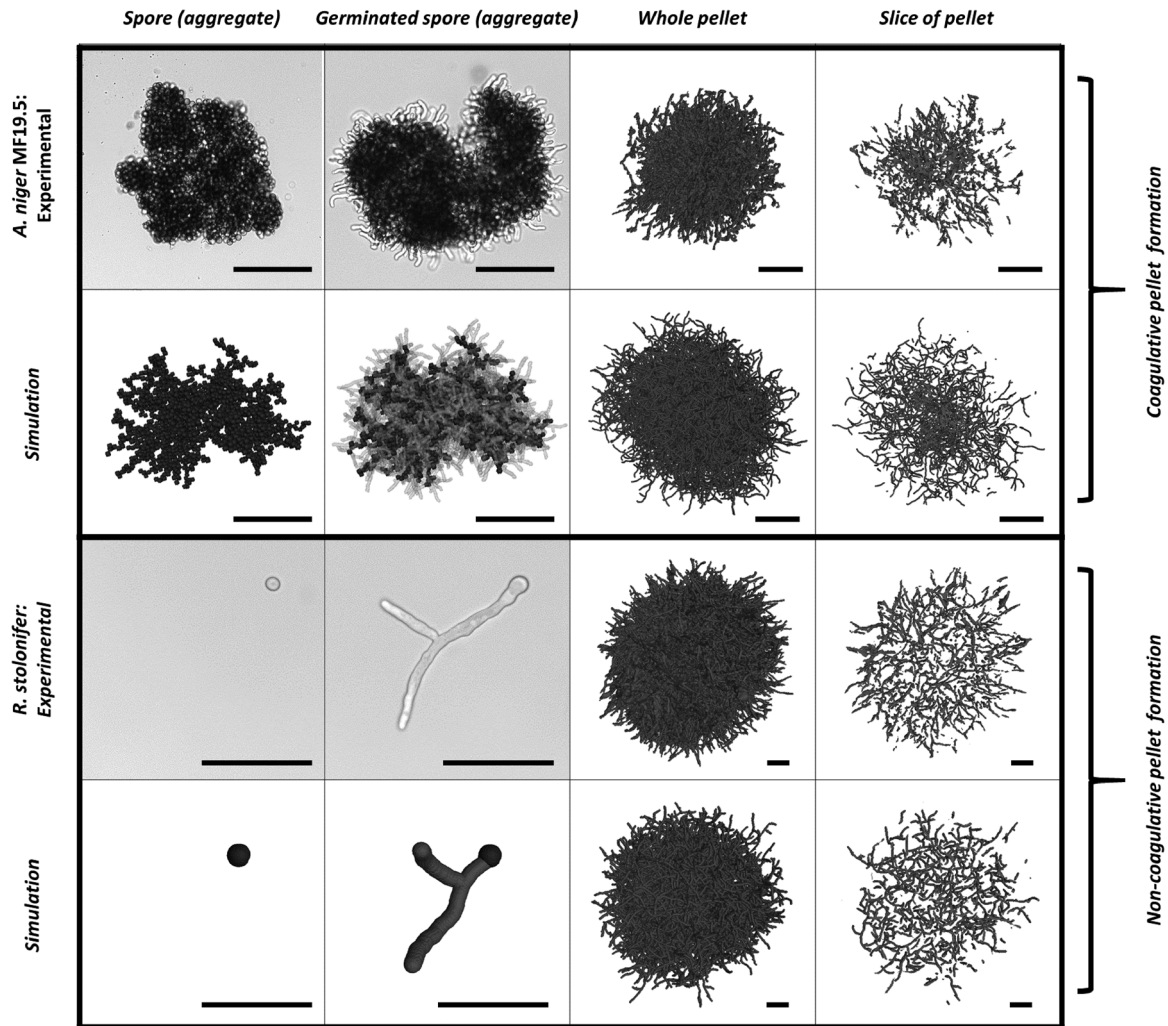
FIGURE 3 Experimental and simulated coagulative and noncoagulative pellet formation. First and third rows show experimental data of coagulative pellet forming *Aspergillus niger* MF19.5 (Fiedler et al., 2018) and noncoagulative pellet forming *Rhizopus stolonifer*, respectively. Second and fourth rows illustrate simulations of coagulative and noncoagulative pellet formation, respectively. First column shows spore (aggregates), second column germinated spore (aggregates), third column two-dimensional (2D) projections of three-dimensional (3D) pellets, and fourth column slices of pellets with a depth of 30 μm. Images of experimental spore aggregates were captured with light microscopy, whereas experimental pellets were measured with microcomputed tomography (μCT) to determine 3D images. Spore aggregation of coagulative pellet formation was simulated with the diffusion-limited aggregation method (Witten & Sander, 1983) and 2048 spores. Pellet growth was simulated with the Monte Carlo model described in Section 2. Scale bar: 100 μm

Pellet formation is not only dependent on coagulative and non-coagulative spore aggregation type but also on the genetic make-up of the species and process-relevant parameters (Cairns et al., 2019). To simulate a broad range of morphologically different pellets, our simulation therefore considered high variation of five morphological parameters (Figure 4): maximum growth angle, branch angle, hyphal diameter, branch interval, and number of initial spores. For each of these parameters, five values were estimated, resulting in $5^5 = 3125$ morphologically different structures in total. In a recent study (Lehmann et al., 2019), the investigation of 31 filamentous fungal species resulted in mean branching angles between 26° and 86°, mean internodal lengths (distance between two branches) between 40 and 453 μm, and mean hyphal diameters between 2.7 and 6.5 μm. However, the diameter of fungal hyphae has been reported to range from 2

to 10 μm (Meyer et al., 2020; Zacchetti et al., 2018). We decided to also consider in the simulations the hyphal diameter of filamentous bacteria (about 0.5–1 μm), as filamentous bacteria are morphologically similar to filamentous fungi (Nielsen, 1996; Zacchetti et al., 2018), with *Streptomycetes* as important cell factories for antibiotic production (Nepal & Wang, 2019). In our simulations, the parameter branch angle was set to 20°, 55°, 90°, 125°, or 160°, whereby angles larger than 90° orient the branch towards the opposite direction of the leading hyphae. The morphological parameter branch interval was defined as the ratio between the internodal length and the hyphal diameter, scaled with the hyphal diameter because large internodal lengths are linked with large hyphal diameters (Lehmann et al., 2019). As expected, simulations with large branch intervals produced disperse mycelia instead of pellets. Thus, we set the maximum branch interval
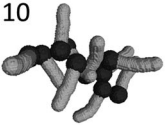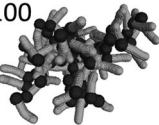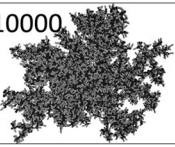
FIGURE 4 Applied morphological parameters for simulations of filamentous structures. Five morphological parameters were applied: maximum growth angle, branch angle, hyphal diameter, branch interval (ratio between the distance between two branches and the hyphal diameter), and number of initial spores. Each of these parameters was varied to five values resulting in a total of $5^5 = 3125$ simulations performed with the Monte Carlo method described in Section 2

to 35. The maximum number of initial spores was set to 10,000 because coagulative pellets can result from hundreds or thousands of agglomerated spores (Fontaine et al., 2010; Metz & Kossen, 1977). Due to the lack of literature describing the growth angle of hyphae, we varied the maximum growth angle within a range to consider straight growing (0°) and strongly curved (48°) hyphae.

Our Monte Carlo simulations covered a broad morphological range of filamentous fungal pellets, which we believe also includes pellets reflecting macromorphologies from smaller filamentous bacteria.

Because image resolution could influence computed properties (Schmieder, Barthel, Müller, et al., 2019; Velichko et al., 2009), we further investigated the influence of pellet resolution on their diffusivity. In Figure 5a, an exemplary cube of a simulated pellet is shown that differs only in resolution, that is, the number of voxels that span a given hyphal diameter. In this figure, the image resolution increases from top to bottom, and the hyphae appear more cylindrical. Notably, the a value in $k_{eff} = (1 - c_h)^a$ decreases with increasing resolution of three exemplary simulated pellets and converges to $1.6 < a < 1.8$, suggesting that the a value converges with increasing resolution.

To investigate the influence of the image resolution of experimentally determined pellets on their diffusivity, we thus conducted µCT measurements with different resolutions. In particular, *R. stolonifer* pellets were measured with a voxel size of 1, 2, 3, and 4 µm and

R. oryzae pellets with a voxel size of 1 and 2 µm. The decrease in the voxel size led to an increased resolution. Similar to simulated pellets, a in $k_{eff} = (1 - c_h)^a$ decreased with increasing resolution (Figure 5b). Note that (i) measurements with a voxel size of 1 µm in the case of *R. stolonifer*, the organism with the highest hyphal diameter in this study, result in hollow hyphae (Figure S4), which cannot be used for diffusion computations and (ii) that low resolutions result in coarse surfaces of the hyphae that do not reflect their smooth nature. Thus, 3D images of filamentous pellets are limited to a minimum and maximum resolution for each organism, which strongly depends on their hyphal diameters. We therefore propose the application of an image resolution that represents hyphae with about four to six voxels in diameter.

Tomadakis and Robertson (2005) summarized and extended correlations between the morphology and the diffusivity, conductivity, and permeability through fiber structures with different orientations. The study was based on previous studies by Tomadakis & Sotirchos, (1991, 1993, 1993, 1993). To validate our diffusion computations and to identify an appropriate resolution for simulated pellets, we compared the solution for randomly orientated overlapping straight fibers by Tomadakis and Sotirchos (1991) with our computed diffusivity through such a morphology. We set up a simulation with 1000 spores, a growth angle of 0°, and allowed collisions (Figure 6a) to obtain randomly orientated overlapping straight fibers. As shown in Figure 6b,c, our simulated structure was
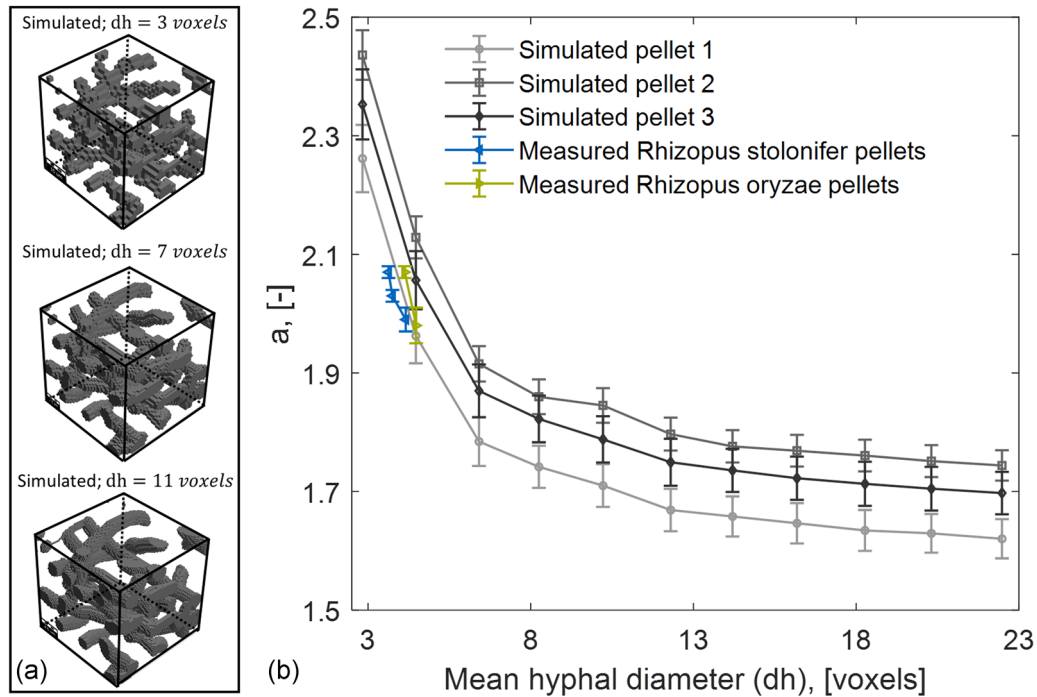
FIGURE 5 Relationship between image resolution and effective diffusivity. Image resolution is represented by the number of voxels that span a given hyphal diameter. Left: Identical exemplary cube of a simulated pellet that differs only in image resolution. Exemplarily, hyphae are represented with 3, 7, and 11 voxels in diameter. Right: a value of experimentally determined pellets and three exemplary simulated pellets fitted on a base of at least 37 cubes per pellet with $k_{eff} = (1 - c_h)^a$, where k_{eff} is the effective diffusion factor, c_h the hyphal fraction, and a the fitted correlation factor (Schmieder, Barthel, Müller, et al., 2019). Morphological simulations of pellets were performed with the Monte Carlo method described in the Section 2. *Rhizopus pellets* were measured with microcomputed tomography (μCT) with a voxel size of 1 μm (three *R. oryzae* pellets), 2 μm (21 *R. oryzae* and 11 *R. stolonifer* pellets), 3 μm (13 *R. stolonifer* pellets), and 4 μm (seven *R. stolonifer* pellets). Each data point of measured pellets was fitted on the base of cubes of the mentioned number of pellets. Error bars specify the 95% confidence interval [Color figure can be viewed at wileyonlinelibrary.com]

comparable to the structure used for the correlation $k_{eff} = \varepsilon\left(\frac{\varepsilon - 0.037}{1 - 0.037}\right)^{0.661}$ (Tomadakis & Sotirchos, 1991). With increasing resolution, that is, with increasing voxels representing the hyphal diameter, the computed diffusivities of the simulated structure approached the correlation of Tomadakis and Sotirchos (1991; Figure 6d). Especially in the hyphal fraction range 0–0.4, our computed diffusivities fit well with their correlation, suggesting that the diffusion computations were accurate for high resolutions in the hyphal fraction range 0–0.4. The range reflects the hyphal fraction of both simulated and experimentally determined pellets (Figures 2 and 7, see next Section 3.3).

3.3 | Merging diffusive mass transport data from simulated and μCT measured pellets

We investigated the diffusive mass transport in filamentous fungal mycelia through the correlation between the diffusivity and morphology of 3125 simulated and 66 μCT analyzed pellets. We applied an image resolution that represented simulated hyphae five voxels in diameter to make the results of simulations and experiments comparable (Figure 7a). Because this resolution could underestimate the

diffusivity (Figure 6 and our previous study; Schmieder, Barthel, Müller, et al., 2019), we also applied a resolution that represented hyphae with 13 voxels in diameter (Figure 7b). We considered this resolution as a compromise between accuracy and computational effort of diffusion computations. Similar to experimentally determined pellets, we used several cubes of each simulated structure for diffusion computations.

Interestingly, pellet formation did not occur for all parameter combinations. The combination of low spore numbers and rare branches resulted in dispersed mycelia instead of pellets. Thus, we marked loose structures with a mean hyphal fraction of the respective cubes less than 0.05. As a result, the initial 3125 simulated structures were reduced to 1280 and 1791 pelletised structures for hyphae represented with 5 and 13 voxels, respectively (Figure 7). The mean correlation factor $a \pm \sigma(a)$ of all 3125 structures was $a = 2.059 \pm 0.182$ and $a = 1.757 \pm 0.150$ for hyphae represented with 5 and 13 voxels, respectively (Figure 7, top and bottom). For pelletized structures, the mean was altered to $a = 2.063 \pm 0.044$ and $a = 1.753 \pm 0.035$, respectively. In Figure 7, pellets with unlikely morphological parameters were marked, namely all pellets with straight hyphae (maximum growth angle = 0°) or extreme branch angles (branch angle = 20° and branch angle = 160°). Thus, the
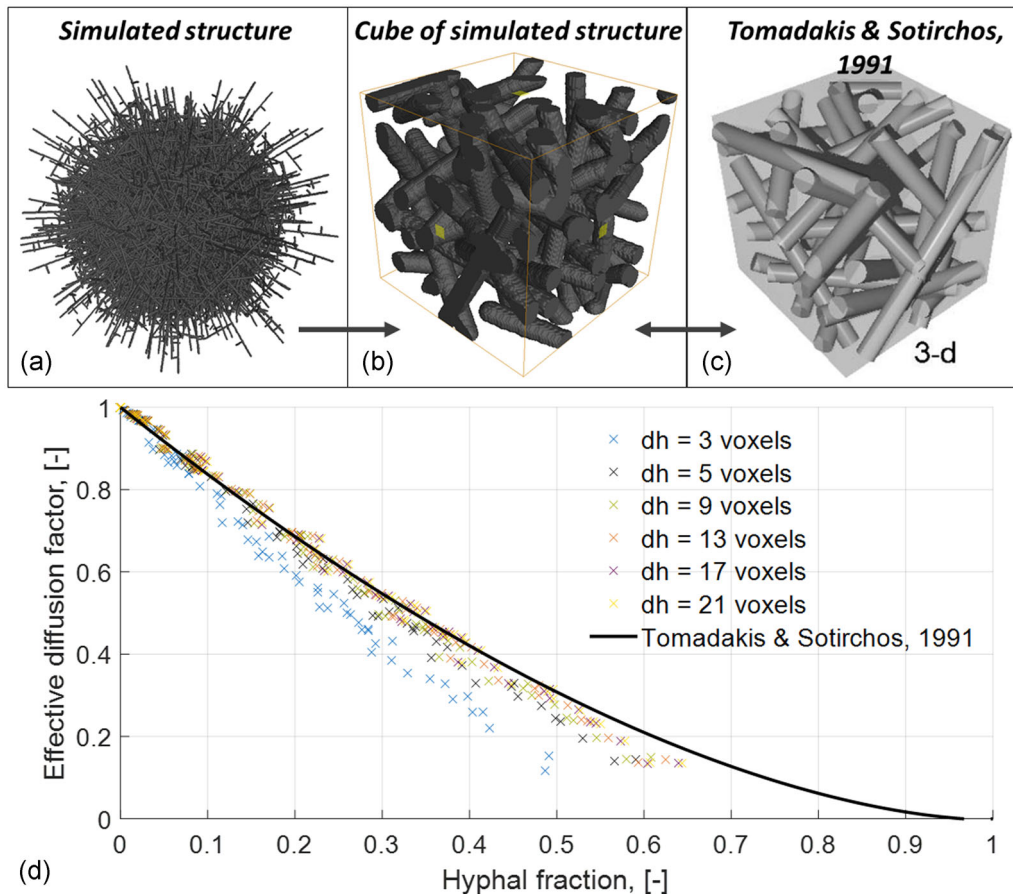
FIGURE 6 Validation of diffusion computations. The solution for the effective diffusion factor k_{eff} through randomly orientated overlapping straight fibers $k_{eff} = \varepsilon \left(\frac{\varepsilon - 0.037}{1 - 0.037} \right)^{0.661}$ by Tomadakis and Sotirchos (1991) was compared with the computed k_{eff} through similar simulated structures. The porosity was $\varepsilon = 1 -$ hyphalfraction. We performed the morphological simulations with the Monte Carlo method described in the Methods section. (a) Whole simulated structure. (b) Exemplary cube of simulated structure. For diffusion computations, 76 cubes were investigated for each resolution. Resolution is represented by the number of voxels that spanned the given hyphal diameter. (c) Model structure applied for solution by Tomadakis and Sotirchos (1991). (d) Solution by Tomadakis and Sotirchos (1991) (black line) and computed diffusivities through simulated structure. Each data point corresponds to the diffusivity through one cube [Color figure can be viewed at wileyonlinelibrary.com]

number of pellets was reduced to 898 and 712, with a narrow distribution of the correlation factor $a = 2.072 \pm 0.025$ and $a = 1.760 \pm 0.023$ for hyphae represented with 5 and 13 voxels in diameter, respectively. Pellets with unlikely morphological parameters explain the outliers for the correlation factor a. For the experimentally determined pellets of *P. chrysogenum*, *A. niger* MF19.5, *A. niger* MF22.4, *R. stolonifer*, and *R. oryzae*, a was 2.05, 2.07, 1.99, 1.99, and 1.99 (Figure 2), respectively, and thus in the range of the simulated pellets where the hyphae are represented with 5 voxels in diameter (Figure 7, top). Applying the maximum ball method (Section 2), this is a mean hyphal diameter of 4.5 voxels that lies in the range of our experimental pellets (4.3, 4.0, 4.3, 4.2, and 4.5 voxels for the different strains).

The results strongly indicate that the diffusion law $k_{eff} = (1 - c_h)^a$ is applicable to fungal pellets with arbitrary morphology. In addition, the only fitting parameter a lies in a narrow range while the resolution of the images does not change. This implies that there is a generalizable law for the diffusivity through fungal pellets with the hyphal fraction c_h as the only independent variable. Contrary to our expectations, detailed morphological parameters such as growth angles, branch angles, hyphal diameters, number of initial spores, and branching frequency did not affect the diffusive hindrance. For all 3125 simulated pellets we applied image resolutions to represent the hyphal diameter with 5 and 13 voxels, respectively. We were able to show that low resolutions (Figure 7a) lead to an underestimation of the diffusivity (Figure 6 and our previous study; Schmieder, Barthel, Müller, et al., 2019). In addition, the results of three simulated pellets with different image resolutions (Figure 5b) show that the a parameter converges with increasing resolution for each pellet. Thus, we suggest to use the law for high resolutions (the hyphal diameter is represented with 13 voxels in diameter; Figure 7b) to calculate the diffusivity through fungal pellets:

$$k_{eff} = (1 - c_h)^{1.76} \tag{3}$$

(a) Hyphae represented with 5 voxels in diameter

(b) Hyphae represented with 13 voxels in diameter
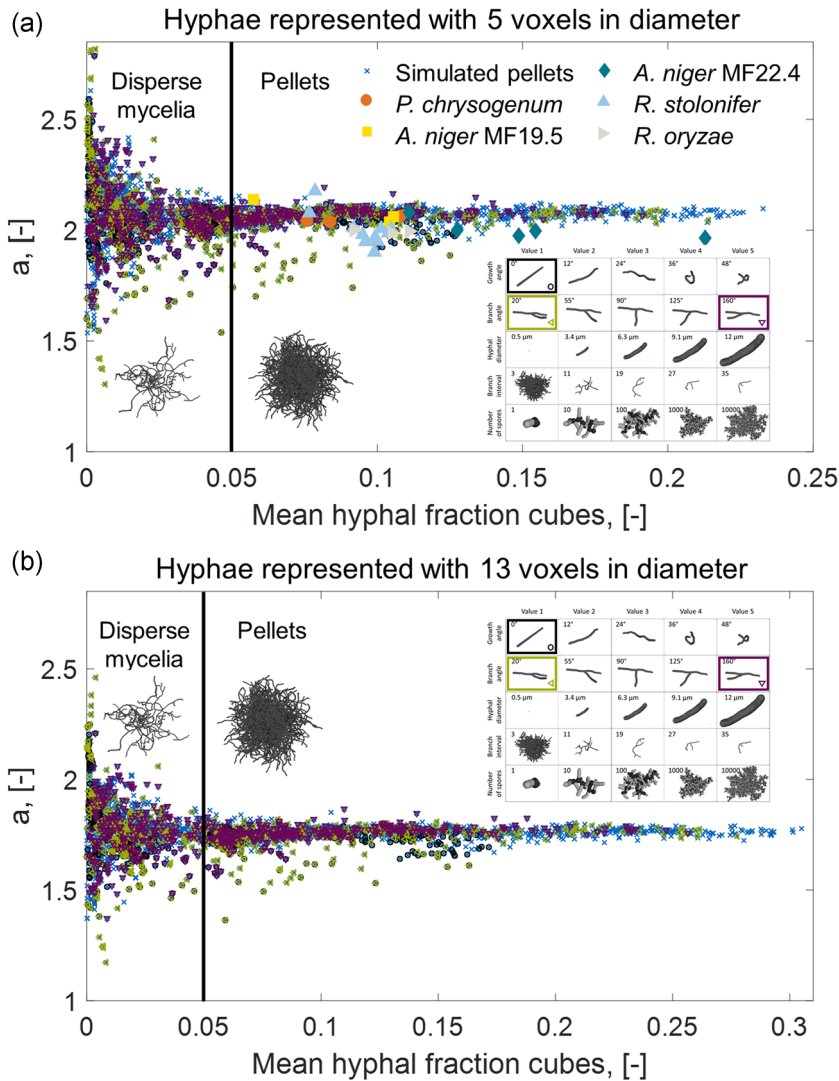
FIGURE 7 Correlation factor a for simulated and experimentally determined pellets. Each data point corresponds to the correlation between the hyphal fraction c_h and the effective diffusion factor k_{eff} of one pellet, resulting in the fitted exponent a. For each pellet, the fit is based on diffusion computations through several cubes and the correlation $k_{eff} = (1 - c_h)^a$. Hyphae of simulated pellets are represented with a "resolution" of five (top) and 13 (bottom) voxels in diameter. The increasing resolution decreases the correlation factor a, and thus the diffusivity decreases as well. Morphological simulations for diffusion computations of simulated pellets were performed with the Monte Carlo method described in the Section 2. Microcomputed tomography (μCT) measurements for diffusion computations of experimentally determined pellets were conducted with a voxel size of 1 μm (three *Penicillium chrysogenum*, three *Aspergillus niger* MF19.5, five *A. niger* MF22.4, three *Rhizopus oryzae* pellets), and 2 μm (11 *R. stolonifer* pellets) [Color figure can be viewed at wileyonlinelibrary.com]

where k_{eff} is the effective diffusion factor (k_{eff}^{-1} is similar to the formation factor) describing the geometrical diffusion hindrance through a 3D structure, and c_h is the hyphal fraction (similar to solid fraction). As shown in Figure S5, our law is not very distinct from the law of random orientated overlapping fibers by Tomadakis and Sotirchos (1991). However, our correlation differs very strongly from the correlation for random orientated overlapping fibers proposed by He et al. (2017). For low porosities, the correlation of He et al. (2017) proposes effective diffusion factors larger than 1, which is physically unreasonable. It has to be mentioned that our law might slightly underestimate the diffusivity through filamentous fungal networks, because Figure 5 implies that the convergence might not be fully developed for a resolution of 13 voxels. However, doubling the resolution increases the volume of pellets and cubes for diffusion computations eightfold. The increase of the cube-volumes would result in excessive computational times (With a resolution of 13 voxels, the diffusion computations of all 3125 pellets last about 3 weeks with an Intel Xeon E5-1660 CPU (3.7 GHz)). In addition, some pellets could not be reconstructed with very high resolutions because

they would result in working memories larger than our available 128 GB. Thus, the resolution of 13 voxels was a compromise between accuracy and computational effort/feasibility.

4 | CONCLUSIONS

This study showed that a universal law (see Equation 3) holds for the diffusive transport of nutrients, oxygen, and secreted metabolites through any filamentous fungal pellet. As mentioned above, the correlation is also known as Archie's law (Archie, 1942) with a cementation parameter equal to 1.76, which is in the range of porous rocks (Glover et al., 1997, e.g., determined that the cementation parameter of sandstone is between 1.5 and 2.5). Strictly speaking, our law is valid for hyphal fractions less than 0.4 because the maximum hyphal fraction of simulated and measured pellets was 0.4. However, to the best of our knowledge, there are no studies about filamentous fungi where the measured hyphal fraction is more than 0.4. For example, Cui et al. (1997, 1998) reported average hyphal

fractions between 0.07 and 0.30 for whole *A. awamori* pellets. If future studies are confronted with hyphal fractions more than 0.4, we propose to fall back on the correlation for randomly orientated overlapping fibers proposed by Tomadakis and Sotirchos (1991), which is (as already stated) not very distinct from our correlation. They were able to show that their correlation was valid for solid fractions less than 0.6, whereas higher solid fractions resulted in another correlation. Our law predicts that only one independent variable, the hyphal fraction (c_h), affects pellet diffusivity. Knowing the profile of the hyphal fraction in pellets, the law $k_{eff} = (1 - c_h)^{1.76}$ determines the mass transport of molecules inside pellets. Molecule concentrations inside pellets are affected by metabolic rates and the transport through filamentous mycelia (Celler et al., 2012; Cui et al., 1998). As the transport can now be calculated, the estimation of metabolic rates within pellets becomes, for the first time, feasible. Future experiments should provide information about the morphology and metabolic activity or nutrient profiles of pellets, which can be, for example, measured through flow cytometry or confocal laser scanning microscopy (Schrinner et al., 2020; Tegelaar et al., 2020; Veiter & Herwig, 2019). One possibility to determine the distribution of oxygen and hyphal material inside pellets would be the application of microelectrodes inside pellets (Hille et al., 2005; Wittier et al., 1986) followed by μCT measurements (Schmideder, Barthel, Friedrich, et al., 2019).

This generalized law was deduced from experimental and simulation data. On the one hand, it proved the usefulness and power of laboratory μCT systems to investigate the natural 3D morphology of different filamentous fungi in utmost detail. However, as this method is time and cost intensive and only applicable to a small number of pellets, the use of Monte Carlo simulations proved to be powerful for the massive generation of data covering a broad range of morphological characteristics. This computational approach allowed us to generate a database of 3125 morphologically different pellets, which will also open up new avenues of research. Such a database, which can be accessed by the community, could also open new paths towards parameter estimation of measured pellets of fungal or bacterial origin. Conclusions about the evolution of measured pellets could be deduced because growth and morphological parameters of simulated pellets are known.

We furthermore anticipate that this contribution will inspire more sophisticated correlation measurements between morphology and mass transport in any complex material, for example, in biofilms, fiber materials, porous media, and fuel cells. In fact, correlations between the morphology and transport properties (Archie, 1942; Carman, 1937; Epstein, 1989; Kozeny, 1927) are crucial to compute transport phenomena in several fields. Exemplarily, correlation laws for fibrous materials (He et al., 2017; Tamayol et al., 2012; Tomadakis & Robertson, 2005) are already applied to design nano- and microporous membranes (Yuan et al., 2008), heat insulations (Panerai et al., 2017) and dissipations (Jung et al., 2016), acoustic insulations (Tang & Yan, 2017), electrodes (Kim et al., 2019), and batteries (Ke et al., 2018). Concerning fibrous materials, a direct link to our study was shown (Figure 6). For nonfibrous materials, a combination of 3D

image acquisition, morphological simulations, and mass transport computations could significantly enhance the understanding of morphology-dependent transport phenomena. Hence, we foresee that the biological and computational approach followed in this study may be synergistically adopted to other research questions in bio(techno)logy and beyond.

CONFLICTS OF INTEREST

The authors have no conflicts of interest to declare.

AUTHOR CONTRIBUTIONS

Stefan Schmideder did the conception and design of the study. Stefan Schmideder, Henri Müller, and Lars Barthel wrote the manuscript, which was edited and approved by all authors. Heiko Briesen and Vera Meyer supervised the study. Lars Barthel and Ludwig Niessen cultivated filamentous fungi and prepared pellets for microcomputed tomography (μCT) measurements. Henri Müller and Stefan Schmideder performed μCT measurements of pellets. Stefan Schmideder, Henri Müller, and Tiaan Friedrich performed image analysis. Stefan Schmideder and Tiaan Friedrich set up the code for morphological Monte Carlo simulations. Stefan Schmideder performed the diffusion computations and analyzed the results.

DATA AVAILABILITY STATEMENT

The data that support the findings of this study are available from the corresponding author upon reasonable request.

ORCID

Stefan Schmideder http://orcid.org/0000-0003-4328-9724
Henri Müller https://orcid.org/0000-0002-4831-0003
Lars Barthel https://orcid.org/0000-0001-8951-5614
Tiaan Friedrich https://orcid.org/0000-0001-8346-4908
Ludwig Niessen https://orcid.org/0000-0003-4083-2779
Vera Meyer https://orcid.org/0000-0002-2298-2258
Heiko Briesen https://orcid.org/0000-0001-7725-5907

REFERENCES

Archie, G. E. (1942). The electrical resistivity log as an aid in determining some reservoir characteristics. *Transactions of the AIME*, *146*(01), 54–62. https://doi.org/10.2118/942054-G

Becker, J., Wieser, C., Fell, S., & Steiner, K. (2011). A multi-scale approach to material modeling of fuel cell diffusion media. *International Journal of Heat and Mass Transfer*, *54*(7-8), 1360–1368. https://doi.org/10.1016/j.ijheatmasstransfer.2010.12.003

Bennet, J. W., & Lasure, L. L. (1991). *More Gene Manipulations in Fungi*. Academic Press.

Bishop, C. M. (2009). Pattern Recognition and Machine Learning *(Corrected at 8th printing 2009)*. Information science and statistics. Springer.

Brakhage, A. A. (2013). Regulation of fungal secondary metabolism. *Nature Reviews Microbiology*, *11*(1), 21–32. https://doi.org/10.1038/nrmicro2916

Bresenham, J. E. (1965). Algorithm for computer control of a digital plotter. *IBM Systems Journal*, *4*(1), 25–30. https://doi.org/10.1147/sj.41.0025

Cairns, T. C., Zheng, X., Zheng, P., Sun, J., & Meyer, V. (2019). Moulding the mould: Understanding and reprogramming filamentous fungal growth and morphogenesis for next generation cell factories. *Biotechnology for Biofuels*, *12*(1), 77. https://doi.org/10.1186/s13068-019-1400-4

Carman, P. C. (1937). Fluid flow through granular beds. *Transactions of the Institution of Chemical Engineers*, *15*, 150–166.

Celler, K., Picioreanu, C., van Loosdrecht, Mark, C. M., & van Wezel, G. P. (2012). Structured morphological modeling as a framework for rational strain design of Streptomyces species. *Antonie Van Leeuwenhoek*, *102*(3), 409–423. https://doi.org/10.1007/s10482-012-9760-9

Cui, Y. Q., van der Lans, R., & Luyben, K. (1997). Effect of agitation intensities on fungal morphology of submerged fermentation. *Biotechnology and Bioengineering*, *55*(5), 715–726. https://doi.org/10.1002/(SICI)1097-0290(19970905)55:5<715::AID-BIT>3.0.CO;2-E

Cui, Y. Q., van der Lans, R., & Luyben, K. (1998). Effects of dissolved oxygen tension and mechanical forces on fungal morphology in submerged fermentation. *Biotechnology and Bioengineering*, *57*(4), 409–419. https://doi.org/10.1002/(SICI)1097-0290(19980220)57:4<409::AID-BIT>3.0.CO;2-Q

Epstein, N. (1989). On tortuosity and the tortuosity factor in flow and diffusion through porous media. *Chemical Engineering Science*, *44*(3), 777–779. https://doi.org/10.1016/0009-2509(89)85053-5

Ericson, C. (2010). *Morgan Kaufmann series in interactive 3D technology. Real-time collision detection* (pp. 125–233). Elsevier.

Fiedler, M. R. M., Barthel, L., Kubisch, C., Nai, C., & Meyer, V. (2018). Construction of an improved *Aspergillus niger* platform for enhanced glucoamylase secretion. *Microbial Cell Factories*, *17*(1), 1–12. https://doi.org/10.1186/s12934-018-0941-8

Fontaine, T., Beauvais, A., Loussert, C., Thevenard, B., Fulgsang, C. C., Ohno, N., Clavaud, C., Prevost, M. C., & Latgé, J. P. (2010). Cell wall alpha1-3glucans induce the aggregation of germinating conidia of Aspergillus fumigatus. *Fungal Genetics and Biology*, *47*(8), 707–712. https://doi.org/10.1016/j.fgb.2010.04.006

Glover, P. W. J., Gómez, J. B., Meredith, P. G., Hayashi, K., Sammonds, P. R., & Murrell, S. A. F. (1997). Damage of saturated rocks undergoing triaxial deformation using complex electrical conductivity measurements: Experimental results. *Physics and Chemistry of the Earth*, *22*(1-2), 57–61. https://doi.org/10.1016/S0079-1946(97)00078-5

He, X., Guo, Y., Li, M., Pan, N., & Wang, M. (2017). Effective gas diffusion coefficient in fibrous materials by mesoscopic modeling. *International Journal of Heat and Mass Transfer*, *107*, 736–746. https://doi.org/10.1016/j.ijheatmasstransfer.2016.11.097

Hille, A., Neu, T. R., Hempel, D. C., & Horn, H. (2005). Oxygen profiles and biomass distribution in biopellets of *Aspergillus niger*. *Biotechnology and Bioengineering*, *92*(5), 614–623. https://doi.org/10.1002/bit.20628

Hille, A., Neu, T. R., Hempel, D. C., & Horn, H. (2009). Effective diffusivities and mass fluxes in fungal biopellets. *Biotechnology and Bioengineering*, *103*(6), 1202–1213. https://doi.org/10.1002/bit.22351

Jung, S. M., Preston, D. J., Jung, H. Y., Deng, Z., Wang, E. N., & Kong, J. (2016). Porous Cu nanowire aerosponges from one-step assembly and their applications in heat dissipation. *Advanced Materials*, *28*(7), 1413–1419. https://doi.org/10.1002/adma.201504774

Ke, X., Prahl, J. M., Alexander, J. I. D., Wainright, J. S., Zawodzinski, T. A., & Savinell, R. F. (2018). Rechargeable redox flow batteries: Flow fields, stacks and design considerations. *Chemical Society Reviews*, *47*(23), 8721–8743. https://doi.org/10.1039/c8cs00072g

Keller, N. P. (2019). Fungal secondary metabolism: Regulation, function and drug discovery. *Nature Reviews Microbiology*, *17*(3), 167–180. https://doi.org/10.1038/s41579-018-0121-1

Kim, M. J., Seo, Y., Cruz, M. A., & Wiley, B. J. (2019). Metal nanowire felt as a flow-through electrode for high-productivity electrochemistry. *ACS Nano*, *13*(6), 6998–7009. https://doi.org/10.1021/acsnano.9b02058

Kozeny, J. (1927). Über kapillare Leitung des Wassers im Boden. *Royal Academy of Science, Vienna*, *136*, 271–306.

Kwon, M. J., Arentshorst, M., Roos, E. D., van den Hondel, C. A. M. J. J., Meyer, V., & Ram, A. F. J. (2011). Functional characterization of Rho GTPases in *Aspergillus niger* uncovers conserved and diverged roles of Rho proteins within filamentous fungi. *Molecular Microbiology*, *79*(5), 1151–1167. https://doi.org/10.1111/j.1365-2958.2010.07524.x

Lehmann, A., Zheng, W., Soutschek, K., Roy, J., Yurkov, A. M., & Rillig, M. C. (2019). Tradeoffs in hyphal traits determine mycelium architecture in saprobic fungi. *Scientific Reports*, *9*(1), 14152. https://doi.org/10.1038/s41598-019-50565-7

Lejeune, R., & Baron, G. V. (1997). Simulation of growth of a filamentous fungus in 3 dimensions. *Biotechnology and Bioengineering*, *53*(2), 139–150. https://doi.org/10.1002/(SICI)1097-0290(19970120)53:2<139::AID-BIT3>3.0.CO;2-P

McLachlan, G. J., & Peel, D. (2000). Finite mixture models. Wiley series in probability and statistics Applied probability and statistics section. Wiley.

Metz, B., & Kossen, N.W.F. (1977). The growth of molds in the form of pellets–a literature review. *Biotechnology and Bioengineering*, *19*(6), 781–799. https://doi.org/10.1002/bit.260190602

Meyer, F. (1994). Topographic distance and watershed lines. *Signal Processing*, *38*(1), 113–125. https://doi.org/10.1016/0165-1684(94)90060-4

Meyer, V., Basenko, E. Y., Benz, J. P., Braus, G. H., Caddick, M. X., Csukai, M., de Vries, R. P., Endy, D., Frisvad, J. C., Gunde-Cimerman, N., Haarmann, T., Hadar, Y., Hansen, K., Johnson, R. I., Keller, N. P., Kraševec, N., Mortensen, U. H., Perez, R., Ram, A. F. J., ... Wösten, H. A. B. (2020). Growing a circular economy with fungal biotechnology: A white paper. *Fungal Biology and Biotechnology*, *7*(1), 5. https://doi.org/10.1186/s40694-020-00095-z

Meyerhoff, J., Tiller, V., & Bellgardt, K.-H. (1995). Two mathematical models for the development of a single microbial pellet. *Bioprocess Engineering*, *12*(6), 305–313. https://doi.org/10.1007/BF00369507

Nepal, K. K., & Wang, G. (2019). *Streptomycetes*: Surrogate hosts for the genetic manipulation of biosynthetic gene clusters and production of natural products. *Biotechnology Advances*, *37*(1), 1–20. https://doi.org/10.1016/j.biotechadv.2018.10.003

Nielsen, J. (1996). Modelling the morphology of filamentous microorganisms. *Trends in Biotechnology*, *14*(11), 438–443. https://doi.org/10.1016/0167-7799(96)10055-X

Nielsen, J. C., Grijseels, S., Prigent, S., Ji, B., Dainat, J., Nielsen, K. F., Frisvad, J. C., Workman, M., & Nielsen, J. (2017). Global analysis of biosynthetic gene clusters reveals vast potential of secondary metabolite production in *Penicillium* species. *Nature Microbiology*, *2*, 17044. https://doi.org/10.1038/nmicrobiol.2017.44

Otsu, N. (1979). A threshold selection method from gray-level histograms. *Systems, Man and Cybernetics, IEEE Transactions on*, *9*(1), 62–66. https://doi.org/10.1109/TSMC.1979.4310076

Panerai, F., Ferguson, J. C., Lachaud, J., Martin, A., Gasch, M. J., & Mansour, N. N. (2017). Micro-tomography based analysis of thermal conductivity, diffusivity and oxidation behavior of rigid and flexible fibrous insulators. *International Journal of Heat and Mass Transfer*, *108*, 801–811. https://doi.org/10.1016/j.ijheatmasstransfer.2016.12.048

Papagianni, M. (2004). Fungal morphology and metabolite production in submerged mycelial processes. *Biotechnology Advances*, *22*(3), 189–259. https://doi.org/10.1016/j.biotechadv.2003.09.005

Schmieder, S., Barthel, L., Friedrich, T., Thalhammer, M., Kovačević, T., Niessen, L., Meyer, V., & Briesen, H. (2019). An X-ray microtomography-based method for detailed analysis of the three-dimensional morphology of fungal pellets. *Biotechnology and Bioengineering*, *116*(6), 1355–1365. https://doi.org/10.1002/bit.26956

Schmieder, S., Barthel, L., Müller, H., Meyer, V., & Briesen, H. (2019). From three-dimensional morphology to effective diffusivity in filamentous fungal pellets. *Biotechnology and Bioengineering*, *116*(12), 3360–3371. https://doi.org/10.1002/bit.27166

Schrinner, K., Veiter, L., Schmieder, S., Doppler, P., Schrader, M., Münch, N., Althof, K., Kwade, A., Briesen, H., Herwig, C., & Krull, R. (2020). Morphological and physiological characterization of filamentous Lentzea aerocolonigenes: Comparison of biopellets by microscopy and flow cytometry. *PLoS One*, *15*(6), e0234125. https://doi.org/10.1371/journal.pone.0234125

Silin, D., & Patzek, T. (2006). Pore space morphology analysis using maximal inscribed spheres. *Physica A: Statistical Mechanics and Its Applications*, *371*(2), 336–360. https://doi.org/10.1016/j.physa.2006.04.048

Tamayol, A., McGregor, F., & Bahrami, M. (2012). Single phase through-plane permeability of carbon paper gas diffusion layers. *Journal of Power Sources*, *204*, 94–99. https://doi.org/10.1016/j.jpowsour.2011.11.084

Tang, X., & Yan, X. (2017). Acoustic energy absorption properties of fibrous materials: A review. *Composites, Part A: Applied Science and Manufacturing*, *101*, 360–380. https://doi.org/10.1016/j.compositesa.2017.07.002

Taylor, D. L., Hollingsworth, T. N., McFarland, J. W., Lennon, N. J., Nusbaum, C., & Ruess, R. W. (2014). A first comprehensive census of fungi in soil reveals both hyperdiversity and fine-scale niche partitioning. *Ecological Monographs*, *84*(1), 3–20. https://doi.org/10.1890/12-1693.1

Tegelaar, M., Aerts, D., Teertstra, W. R., & Wösten, H. A. B. (2020). Spatial induction of genes encoding secreted proteins in micro-colonies of *Aspergillus niger*. *Scientific Reports*, *10*(1), 1536. https://doi.org/10.1038/s41598-020-58535-0

Tomadakis, M. M., & Robertson, T. J. (2005). Viscous permeability of random fiber structures: Comparison of electrical and diffusional estimates with experimental and analytical results. *Journal of Composite Materials*, *39*(2), 163–188. https://doi.org/10.1177/0021998305046438

Tomadakis, M. M., & Sotirchos, S. V. (1991). Effects of fiber orientation and overlapping on knudsen, transition, and ordinary regime diffusion in fibrous substrates. *MRS Proceedings*, *250*, 221. https://doi.org/10.1557/PROC-250-221

Tomadakis, M. M., & Sotirchos, S. V. (1993). Effective diffusivities and conductivities of random dispersions of nonoverlapping and partially overlapping unidirectional fibers. *The Journal of Chemical Physics*, *99*(12), 9820–9827. https://doi.org/10.1063/1.465464

Tomadakis, M. M., & Sotirchos, S. V. (1993). Ordinary and transition regime diffusion in random fiber structures. *AIChE Journal*, *39*(3), 397–412. https://doi.org/10.1002/aic.690390304

Tomadakis, M. M., & Sotirchos, S. V. (1993). Transport properties of random arrays of freely overlapping cylinders with various orientation distributions. *The Journal of Chemical Physics*, *98*(1), 616–626. https://doi.org/10.1063/1.464604

Veiter, L., & Herwig, C. (2019). The filamentous fungus *Penicillium chrysogenum* analysed via flow cytometry-a fast and statistically sound insight into morphology and viability. *Applied Microbiology and Biotechnology*, *103*(16), 6725–6735. https://doi.org/10.1007/s00253-019-09943-4

Veiter, L., Kubicek, M., Hutter, H., Pittenauer, E., Herwig, C., & Slouka, C. (2020). Study of metabolism and identification of productive regions in filamentous fungi via spatially resolved time-of-flight secondary ion mass spectrometry. *Analytical and Bioanalytical Chemistry*, *412*(9), 2081–2088. https://doi.org/10.1007/s00216-019-01980-2

Veiter, L., Rajamanickam, V., & Herwig, C. (2018). The filamentous fungal pellet-relationship between morphology and productivity. *Applied Microbiology and Biotechnology*, *102*(7), 2997–3006. https://doi.org/10.1007/s00253-018-8818-7

Velichko, A., Wiegmann, A., & Mücklich, F. (2009). Estimation of the effective conductivities of complex cast iron microstructures using FIB-tomographic analysis. *Acta Materialia*, *57*(17), 5023–5035. https://doi.org/10.1016/j.actamat.2009.07.004

Wang, Q., Zhong, C., & Xiao, H. (2020). Genetic engineering of filamentous fungi for efficient protein expression and secretion. *Frontiers in Bioengineering and Biotechnology*, *8*, 293. https://doi.org/10.3389/fbioe.2020.00293

Ward, O.P. (2012). Production of recombinant proteins by filamentous fungi. *Biotechnology Advances*, *30*(5), 1119–1139. https://doi.org/10.1016/j.biotechadv.2011.09.012

Wiegmann, A., & Zemitis, A. (2006). *EJ-HEAT: A fast explicit jump harmonic averaging solver for the effective heat conductivity of composite materials* (Fraunhofer ITWM Report, 94).

Witten, T. A., & Sander, L. M. (1983). Diffusion-limited aggregation. *Physical Review B*, *27*(9), 5686–5697. https://doi.org/10.1103/PhysRevB.27.5686

Wittier, R., Baumgartl, H., Lübbers, D. W., & Schügerl, K. (1986). Investigations of oxygen transfer into *Penicillium chrysogenum* pellets by microprobe measurements. *Biotechnology and Bioengineering*, *28*(7), 1024–1036. https://doi.org/10.1002/bit.260280713

Wösten, H. A. B. (2019). Filamentous fungi for the production of enzymes, chemicals and materials. *Current Opinion in Biotechnology*, *59*, 65–70. https://doi.org/10.1016/j.copbio.2019.02.010

Yang, H., Reichl, U., King, R., & Gilles, E. D. (1992). Measurement and simulation of the morphological development of filamentous microorganisms. *Biotechnology and Bioengineering*, *39*(1), 44–48. https://doi.org/10.1002/bit.260390108

Yaws, C. L. (2009). *Transport properties of chemicals and hydrocarbons* (pp. 502–596). Andrew.

Yuan, J., Liu, X., Akbulut, O., Hu, J., Suib, S. L., Kong, J., & Stellacci, F. (2008). Superwetting nanowire membranes for selective absorption. *Nature Nanotechnology*, *3*(6), 332–336. https://doi.org/10.1038/nnano.2008.136

Zacchetti, B., Wösten, H. A. B., & Claessen, D. (2018). Multiscale heterogeneity in filamentous microbes. *Biotechnology Advances*, *36*(8), 2138–2149. https://doi.org/10.1016/j.biotechadv.2018.10.002

Zhang, J., & Zhang, J. (2016). The filamentous fungal pellet and forces driving its formation. *Critical Reviews in Biotechnology*, *36*(6), 1066–1077. https://doi.org/10.3109/07388551.2015.1084262

SUPPORTING INFORMATION

Additional supporting information may be found online in the Supporting Information section.

Supplementary Materials for Paper III: Universal law for diffusive mass transport through mycelial networks
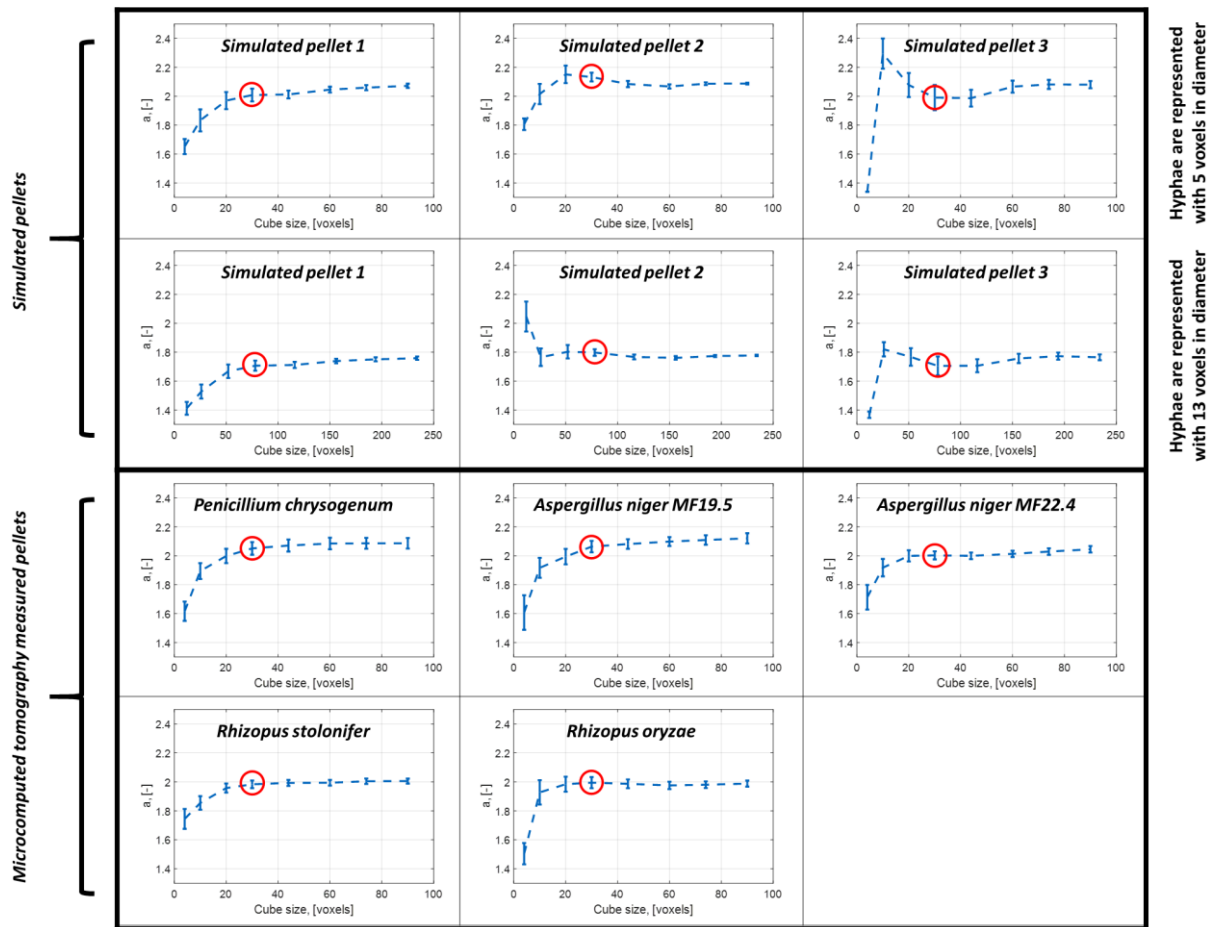
Fig. S1: Influence of cube size on diffusion computations

Diffusion computations were conducted with different cube sizes of experimentally determined pellets and three exemplary simulated pellets. a value was fitted on base of $k_{eff} = (1 - c_h)^a$, where k_{eff} is the effective diffusion factor, c_h the hyphal fraction, and a the fitted correlation factor (Schmideder et al., 2019). Error bars specify the 95% confidence interval. Morphological simulations of pellets were performed with the Monte Carlo method described in the Methods section. Microcomputed tomography measurements were conducted with a voxel size of 1 µm (three *Penicillium chrysogenum*, three *Aspergillus niger* MF19.5, five *Aspergillus niger* MF22.4, three *Rhizopus oryzae* pellets) and 2 µm (11 *Rhizopus stolonifer* pellets). Red circles mark the cube size used for diffusion computations in the Results section of this study.
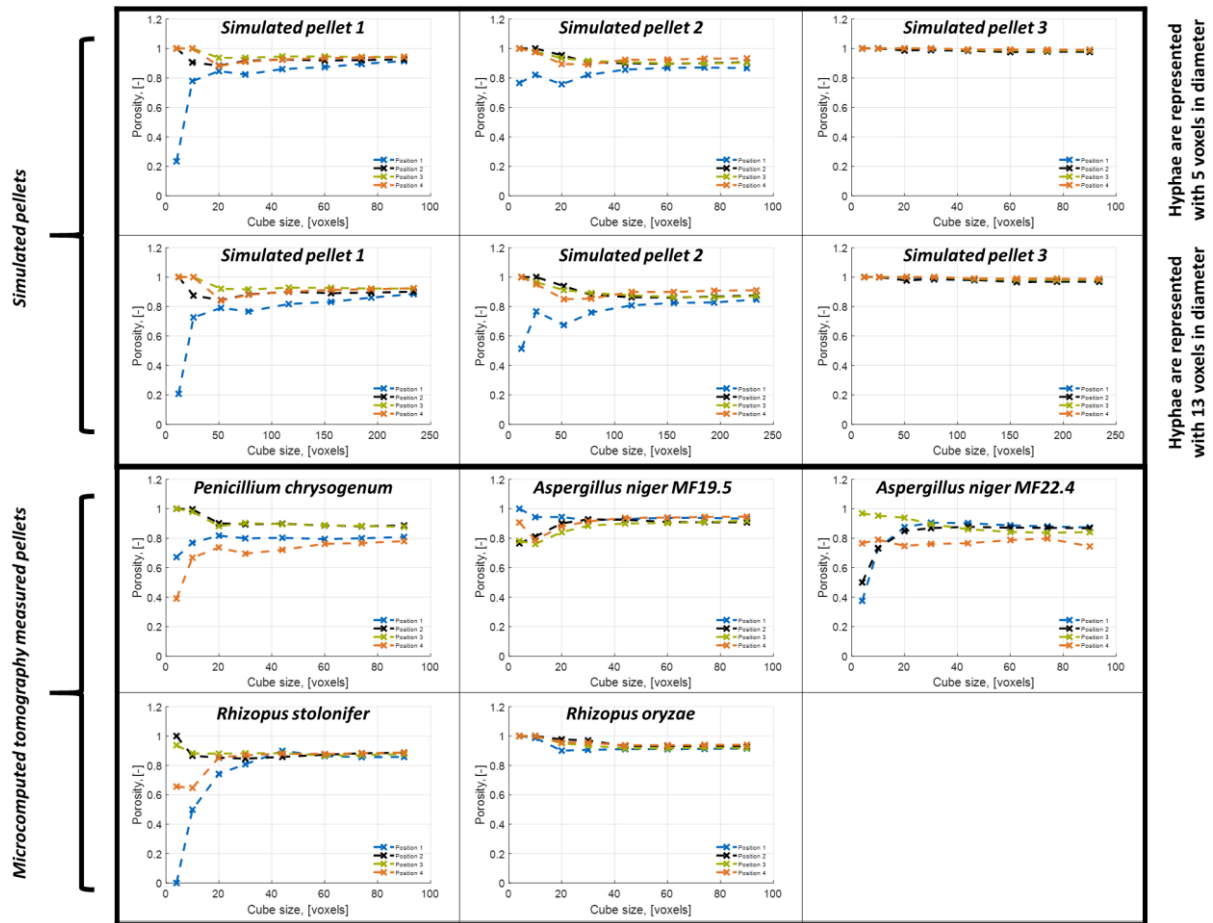
Fig. S2: Influence of cube size on porosity to determine size of representative elementary volume (REV)

We investigated the porosity at four positions per pellet. At these positions we altered the cube size and analyzed the porosity. Analyses were conducted with one pellet per experimentally determined strain and three exemplary simulated pellets. Morphological simulations of pellets were performed with the Monte Carlo method described in the Methods section. Microcomputed tomography measurements were conducted with a voxel size of 1 μm (three *Penicillium chrysogenum*, three *Aspergillus niger* MF19.5, five *Aspergillus niger* MF22.4, three *Rhizopus oryzae* pellets) and 2 μm (11 *Rhizopus stolonifer* pellets).

65
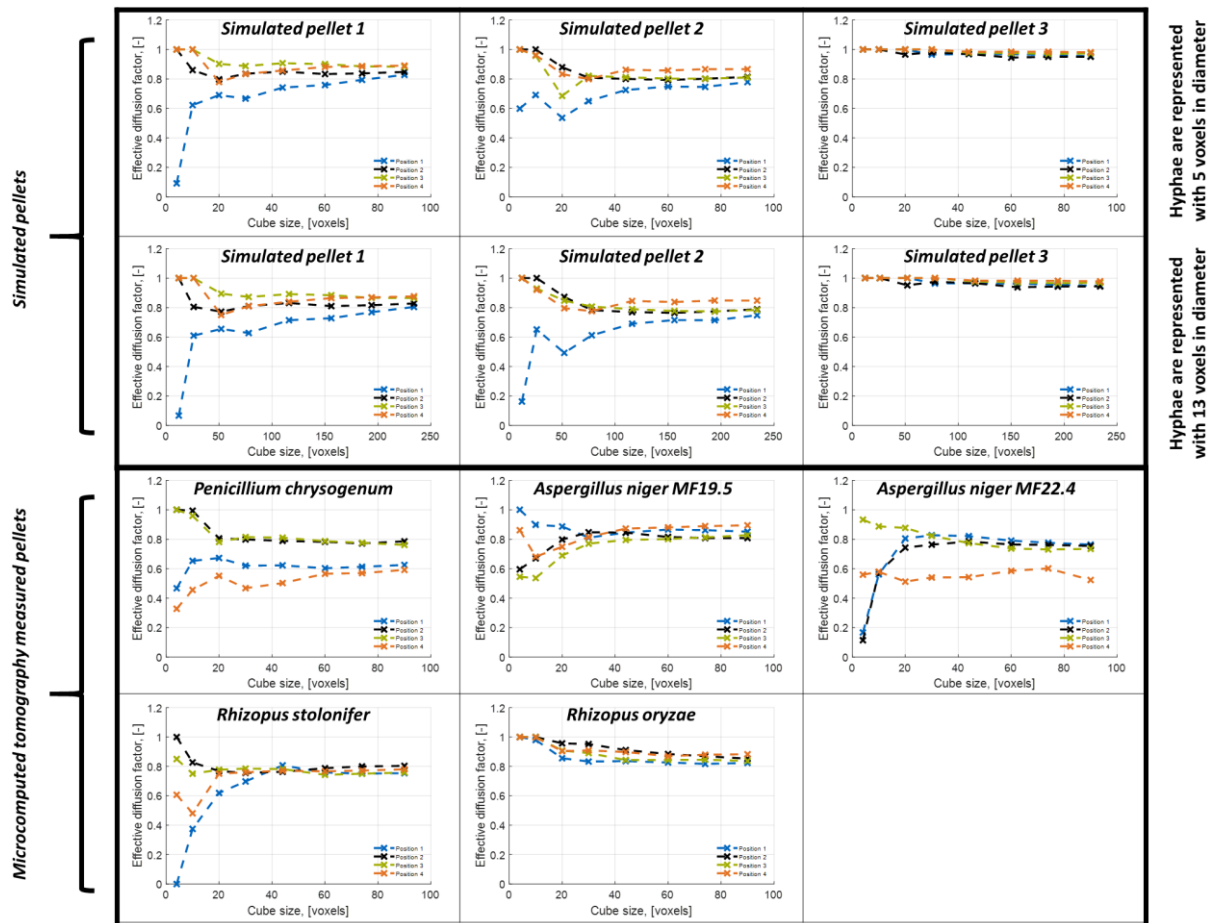
Fig. S3: Influence of cube size on effective diffusion factor to determine size of representative elementary volume (REV)

We investigated the effective diffusion factor at four positions per pellet. At these positions we altered the cube size and analyzed the effective diffusion factor. Analyses were conducted with one pellet per experimentally determined strain and three exemplary simulated pellets. Morphological simulations of pellets were performed with the Monte Carlo method described in the Methods section. Microcomputed tomography measurements were conducted with a voxel size of 1 µm (three *Penicillium chrysogenum*, three *Aspergillus niger* MF19.5, five *Aspergillus niger* MF22.4, three *Rhizopus oryzae* pellets) and 2 µm (11 *Rhizopus stolonifer* pellets).
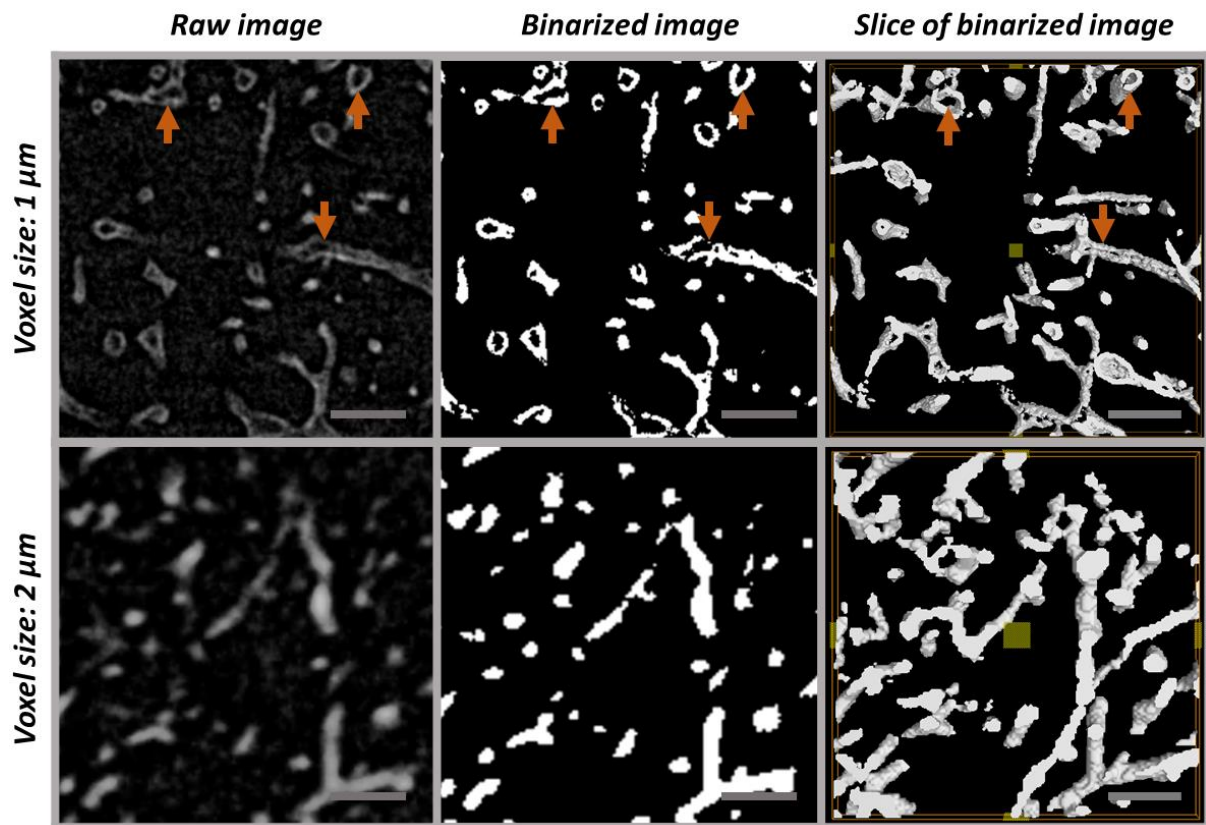
Fig. S4: Comparison of microcomputed tomography (µCT) images of *R. stolonifer* with a voxel size of 1 and 2 µm.

Raw and binarised images are exemplary $250 \times 250\,\mu m$ plane cut outs of pellets. The slices of binarised images are $250 \times 250 \times 10\,\mu m$ of the same region as the raw and binarised images. Arrows indicate exemplary hollow hyphae. Scale bar: $50\,\mu m$.
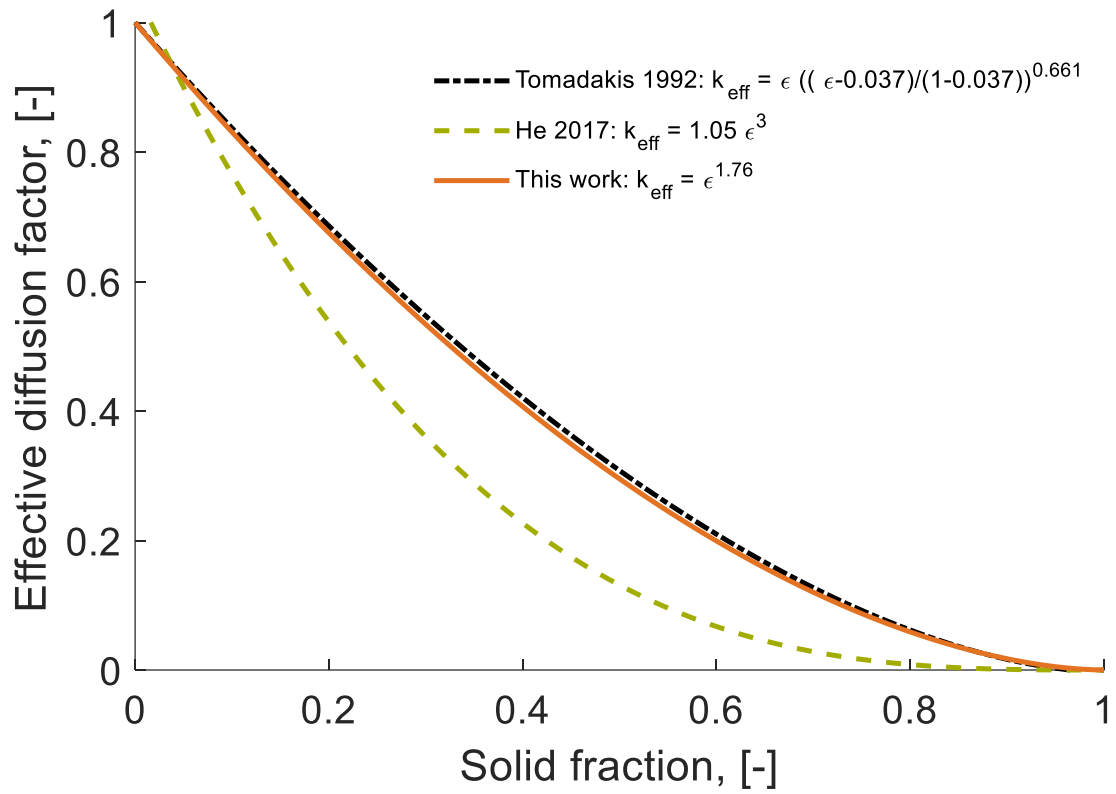
Fig. S5: Comparison of correlations between diffusivity and solid fraction.

The correlation proposed by He et al. (2017) and Tomadakis and Sotirchos (1992) were both proposed for random orientated overlapping fibers. The effective diffusion factors k_{eff} are shown as functions of the porosity ε, which is defined by the solid/hyphal fraction Φ: $\varepsilon = 1 - \Phi$.

Table S1: Parameters for morphological simulations. Parameters with the value 'user defined' could be varied by the user and define all further parameters.

Parameter	Symbol	Value	Unit
Number of spores	N_{sp}	User defined	$-$
Hyphal diameter	d_h	User defined	μm
Maximum growth angle	$\theta_{g,max}$	User defined	$^\circ$
Branch angle	θ_b	User defined	$^\circ$
Branch interval	b	User defined	$-$
Tip extension rate	α_t	User defined	$\mu m\,h^{-1}$
Cultivation period	t_{end}	User defined	h
Diameter of spores	d_{sp}	$1.5 \cdot d_h$	μm
Length of germlings	l_{germ}	$0.5 \cdot d_{sp} + d_h$	μm
Time step for calculation	Δt	$\dfrac{d_h}{2\,\alpha_t}$	h
Length of a segment	$l_{segment}$	$\dfrac{d_h}{2}$	μm
Length of apical region	l_{apical}	$\dfrac{b\,d_h}{4}$	μm
Length of subapical region	$l_{subapical}$	$\dfrac{b\,d_h}{4}$	μm
Minimum mean distance between two branches	$d_{b,min}$	$b\,d_h$	μm
Hyphal diameter in voxels	$d_{h,vx}$	User defined	vox
Scaling factor for nodes	f_{scale}	$\dfrac{d_{h,vx}}{d_h}$	$vox\,\mu m^{-1}$

1

Supplementary Protocol 1: Preparation of pellets

	Aspergillus niger	*Rhizopus stolonifer*
Initial cultivation	Complete medium (CM) agar	Potato extract glucose agar
Spore harvest	Add 10 mL physiological salt (PS) solution, scrape spores off with sterile cotton stick and transfer to sterile 15 mL tube. Vortex for 30 s, filter through miracloth filter paper into fresh tube.	Add 10 mL physiological salt (PS) solution, scrape spores off with sterile cotton stick and transfer to sterile 15 mL tube. Vortex for 30 s, filter through miracloth filter paper into fresh tube.
Serial dilution	10^{-1} in sterile PS solution	10^{-1} in sterile PS solution
Spore count	From 10^{-1} dilution, Thoma type counting chamber, 0.1 mm chamber depth.	From 10^{-1} dilution, Thoma type counting chamber, 0.1 mm chamber depth.
Storage of spores	4 °C	4 °C
Pellet production	50 mL CM medium in 250 mL shake flask	100 mL Potato extract glucose medium in 500 mL shake flask
Inoculation	$5*10^6$ spores per mL medium	$8*10^2$ spores per mL medium
Incubation conditions	250 rpm, 30 °C, 48 h	250 rpm, 23 °C, 48 h

PS solution
Sodium chloride   8.9g
Add aqua demin. to 1 L
Autoclave at 121 °C for 20 min

Preparation of CM medium
ASP+N (50x), pH 5,5   20 mL
Glucose solution (50% (w/v))   20 mL
Magnesium sulfate solution (1 M)   2 mL
Trace element solution (1000x)   1 mL
Casamino acid solution (10% (w/v))   10 mL
Yeast extract solution (10% (w/v)   50 mL
Add aqua demin. to 1 L
Autoclave at 121 °C for 20 min

Preparation of ASP+N (50x)
Potassium chloride   26.1 g
Potassium dihydrogen phosphate   74.85 g
Sodium nitrate   297.47 g
Add aqua demin. to 1 L, pH 5.5
Autoclave at 121 °C for 20 min

Preparation of trace element solution (1000x)

Zinc sulfate heptahydrate	12.27 g
Boric acid	11 g
Manganese (II) chloride tetrahydrate	3.15 g
Iron (II) sulfate heptahydrate	2.73 g
Cobalt (II) chloride hexahydrate	0.92 g
Copper (II) sulfate pentahydrate	1.02 g
Sodium molybdate dihydrate	1.28 g
EDTA	50.85 g

Add aqua demin. to 1 L
Autoclave at 121 °C for 20 min

Preparation of potato extract glucose

Potato Extract Glucose Broth (Carl Roth)	26.5g

Add aqua demin. to 1 L
Autoclave at 121 °C for 20 min

	Penicillium chrysogenum	*Rhizopus oryzae*
Initial cultivation	3 % malt extract agar (MEA)	3 % MEA
Spore harvest	5 mL sterile tap water, 2 min. homogenization with sterile spatula. Fill to 15 mL sterile Falcon tube and centrifuge 5 min at 5,000 x g. Wash 2x with 5 mL sterile tap water and discard supernatant. Suspend washed conidiospores in 1 mL sterile tap water.	5 mL sterile tap water, 2 min. homogenization with sterile spatula. Fill to 15 mL sterile Falcon tube and centrifuge 5 min at 5,000 x g. Wash 2x with 5 mL sterile tap water and discard supernatant. Suspend washed sporangiospores in 1 mL sterile tap water.
Serial dilution	10^{-1}-10^{-6} in sterile tap water	10^{-1}-10^{-6} in sterile tap water
Spore count	From 10^{-2} dilution, Thoma type counting chamber, 0.1 mm chamber depth.	From 10^{-2} dilution, Thoma type counting chamber, 0.1 mm chamber depth.
Storage of spores	4 °C	4 °C
Pellet production	100 mL pellet production medium for *P. chrysogenum*	100 mL pellet production medium for *Rh. oryzae*
Inoculation	10^4 spores per mL medium	10^5 spores per mL medium
Incubation conditions	250 rpm, 23 °C, 48 h	250 rpm, 23 °C, 16 h

Preparation of MEA

Malt extract	30 g
Peptone from soy	3 g
Agar	15 g

Add aqua demin. to 1 L, pH 5.2
Autoclave at 121 °C for 15 min

Preparation of pellet production medium for *P. chrysogenum*
Component 1: Ammoniumsulfat 0.55 % (w/v)
autoclave at 121 °C for 15 min
Component 2: Difco Yeast Carbon Base 11.7 % (w/v)
            Glucose 5,5 % (w/v)
Filter sterilize though 0.2 µm membrane
Mix Component 1: Component 2   9:1 prior to inoculation

Preparation of pellet production medium for *R. oryzae*

Glucose	5g
Peptone from soy	1.5g
Yeast extract	1.4g
NaCl	2g
K_2HPO_4	1g

Add aqua demin. to 1 L, pH 5.0
Autoclave at 121 °C for 15 min

Supplementary Protocol 2:
X-ray microcomputed tomography (µCT) measurements of filamentous fungal pellets

Equipment

- Freeze-dried samples of filamentous fungal pellets (*P. chrysogenum*, *A. niger*, *R. stolonifer*, and *R. oryzae*)
- X-ray microcomputed tomography system (XCT-1600HR; Matrix Technologies, Feldkirchen, Germany)
- Sample rod for µCT measurements with a voxel size of 1 µm
- Sample rod for µCT measurements with a voxel size of 2 µm, 3 µm, and 4 µm
- Self-constructed sample holder A made of polyoxymethylene (POM), in the shape of a platform
- Self-constructed sample holder B made of polyoxymethylene (POM), in the shape of a ton
- Self-constructed sample holder C made of polyoxymethylene (POM) and polyimide (PI), in the shape of a platform (POM) with an attached tube (PI)
- Two-component epoxy adhesive(UHU$^©$ PLUS sofortfest, Bühl, Germany)
- Double-sided tape (Tesa, Norderstedt, Germany)

Procedure

Preparation of *P. chrysogenum* pellets for µCT measurements with a voxel size of 1 µm:

Double sided tape:

- Place a piece of the double-sided tape directly on the sample rod for µCT measurements with a voxel size of 1 µm.
- Place a single *P. chrysogenum* pellet directly on top of the double-sided tape in a centered position.

Epoxy adhesive:

- Mix the two components of the epoxy adhesive.
- Place a drop of the epoxy adhesive on top of the sample rod for µCT measurements with a voxel size of 1 µm.
- Led the adhesive dry for 5 minutes until a solid, but still sticky surface remains.
- Place a single *P. chrysogenum* pellet directly on top of the adhesive in a centered position.

Preparation of *A. niger* pellets for µCT measurements with a voxel size of 1 µm:

- Place the sample holder A on the sample rod for µCT measurements with a voxel size of 1 µm.
- Mix the two components of the epoxy adhesive.
- Cover the whole top of the sample holder A with a thin layer of the adhesive.
- Led the adhesive dry for 5 minutes until a solid, but still sticky surface remains.
- Place single or multiple *A. niger* pellets on top of the adhesive layer in a centered position. The diameter of all placed pellets together may not be bigger than 2 mm for µCT measurements with a voxel size of 1 µm

Preparation of *R. oryzae* pellets for µCT measurements with a voxel size of 1 µm:

- Place the sample holder B on the sample rod for µCT measurements with a voxel size of 1 µm.
- Place single or multiple *R. oryzae* pellets in the ton (sample holder B) until the ton is filled. The ton has the size of the field of view of the µCT measurement.

Preparation of *R. oryzae* and *R. stolonifer* pellets for µCT measurements with a voxel size of 2, 3, and 4 µm:

- Place the sample holder C on the sample rod for µCT measurements with a voxel size of 2, 3, and 4 µm.
- Place single or multiple pellets of *R. oryzae or R. stolonifer* in the tube (sample holder C) until the tube is filled. The tube has the size of the field of view of the µCT measurement.

Table 1: Strain, sample holder, and fixation method, used for the pellet preparation for the µCT measurements.

Strain	Sample holder	Fixation
P. chrysogenum	Directly on the sample rod	Double-sided tape or epoxy adhesive
A. niger	A	Epoxy adhesive
R. oryzae; 1 µm voxel size	B	-
R. oryzae; 2, 3, 4 µm voxel size	C	-
R. stolonifer	C	-

µCT measurements:

- Perform a dark field and flat field correction of the µCT system for the chosen parameters before each measurement.
- Place the sample rod with the prepared pellets in the manipulator of the µCT system.
- Perform a sample rod correction.
- Start the µCT measurement with the following parameters:
  - For µCT measurements with 1 µm voxel size:
    - Number of projections: at least 2000
    - Acceleration voltage: 60 kV
    - Current: 20 mA
  - For µCT measurements with 2, 3, 4 µm voxel size:
    - Number of projections: 2000
    - Acceleration voltage: 60 kV
    - Current: 60 mA

6 Discussion

The embedded papers describe developed methods to analyze the detailed three-dimensional morphology and diffusivity within filamentous fungal pellets. Further, a universal law for the diffusivity through mycelial networks is proposed based on diffusion computations through numerous simulated and measured pellets. These methods and findings as well as possible new paths towards morphological engineering are discussed in the following.

6.1 Morphological analysis of pellets

In the last decades, there has been much progress in macromorphological analysis of pellets (Table 1 and Sections 2.1.2 and 2.1.3). However, methods to determine the hyphal network, i.e., the micromorphology, of whole pellets were lacking. Because three-dimensional methods are required for this purpose, focused beam reflectance measurement, flow cytometry, laser diffraction, and two-dimensional microscopy are not sufficient (Section 2.1.3). So far, only confocal laser scanning microscopy (CLSM) was used to visualize three-dimensional hyphal networks. However, CLSM is limited to a penetration depth of approximately 50 - 150 μm, and thus, only the periphery (Tegelaar et al., 2020; Villena et al., 2010) or slices of pellets (Hille et al., 2005, 2009) can be visualized. In addition, these studies missed to analyze the micromorphology of the visualized 3D hyphal network.

Paper I describes an X-ray microcomputed tomography (μCT) based method to visualize the micromorphology of whole intact filamentous fungal pellets. This method bridged the length scale between macroscopic samples, i.e., pellets with a few hundred micrometers in size, and microscopic inner structures consisting of dense mycelial networks with hyphal diameters down to 3 μm. Three-dimensional image analysis of the μCT measurements revealed the micromorphology of whole pellets including the location of tips and branches as well as the total hyphal length. Until today, this was only described for germinating spores and young dispersed hyphae with the help of two-dimensional image analysis (Figure 2) (Barry et al., 2015; Cardini et al., 2020; Schmideder et al., 2018). Additionally, the spatial distributions of the hyphal fraction, tip and branch density, and HGU were determined within whole intact pellets (Paper I). The spatial distribution of the hyphal fraction provided new insights into the symmetry of fungal pellets. Further, hypotheses with respect to their development can be deduced. Analyzed *A. niger* pellets (Paper I, II, and III) showed almost spherical symmetry and a dense center, which are strong indicators for the pellet formation being of coagulative type (Veiter et al., 2018; Zhang and Zhang, 2016). *P. chrysogenum* pellets (Paper I and III) showed no spherical symmetry and a couple of dense regions which could be caused by their hyphal element agglomeration pellet formation type (Veiter et al., 2018). Contrary, *R. stolonifer* pel-

lets (Paper III) showed a homogeneous spatial distribution of the hyphal fraction, which is an indicator for non-coagulative pellet formation (Cairns et al., 2019b; Žnidaršič et al., 1998).

The developed method to analyze pellets based on μCT measurements has significant advantages compared to established methods. Most importantly, it is the only approach to analyze the micromorphology of whole intact pellets. Contrary to pellet slicing (Hille et al., 2005; Priegnitz et al., 2012), μCT measurements offer a nondestructive technique to visualize microscopic structures (Salvo et al., 2003; Stock, 2009), which was proven for filamentous fungi in Paper I. With freeze-drying, sample preparation is rather simple, especially compared to fluorescent staining for CLSM measurements (Hille et al., 2009; Veiter and Herwig, 2019) and/or pellet slicing (Hille et al., 2005; Priegnitz et al., 2012). However, every method has its limitations. Due to restricted measurement volumes and long measurement times, the number of investigated pellets in the presented studies was low. Depending on the size of the pellets and the required settings of the applied laboratory μCT system (XCT1600HR; Matrix Technologies, Feldkirchen, Germany), the measurement of 1 - 10 pellets took 1.5 - 4 hours. Additionally, the resolution of μCT systems can be restricting. While hyphal diameters of filamentous fungi range between 2 - 10 μm (Lehmann et al., 2019; Meyer et al., 2020), hyphae of filamentous bacteria often have diameters smaller than 1 μm (Zacchetti et al., 2018). Because the minimum voxel size with a sufficient signal to noise ratio of the applied laboratory μCT system is 1 μm, the hyphal network of the filamentous bacterium *Lentzea aerocolonigenes* (Schrinner et al., 2020) could not be visualized. However, pellets of two common filamentous fungal cell factories, *Aspergillus niger* and *Penicillium chrysogenum*, have been analyzed in Paper I. Paper III showed that *Rhizopus stolonifer* and *Rhizopus oryzae* pellets can also be visualized with the applied μCT system.

It is conceivable to adapt the developed image analysis pipeline in Paper I to CLSM measurements of dispersed hyphae and the periphery or slices of pellets. Because CLSM is often available in laboratories working with filamentous fungi, this could strongly contribute to three-dimensional morphological analyses. To overcome the limitation of the small number of analyzed pellets, synchrotron measurements can be applied in the future. As proposed in a conference contribution (Müller et al., 2020), synchrotron measurements were recently applied to visualize thousands of pellets to track the development and heterogeneity of *A. niger* pellets during a shake flask cultivation. However, the results of these measurements are not part of this thesis. Measurements with synchrotron or high-end laboratory μCT systems will also shift restrictions concerning image resolution. Thus, pellets of filamentous bacteria with hyphae thinner than 1 μm might be measured and analyzed in future studies.

The ability to determine the three-dimensional microscopic structure of pellets enabled the computation of the effective diffusion through filamentous fungal networks (Section 6.2). Further, this method will open new paths towards morphological engineering to increase the productivity of pellets (Section 6.3).

6.2 Diffusive transport through mycelial networks

The transport of nutrients and oxygen into pellets is mainly driven by diffusion and limited by the dense hyphal network (Cairns et al., 2019b; Hille et al., 2005; Veiter et al., 2018). As a result, the concentrations of oxygen and nutrients decrease towards the center of pellets (Cronenberg et al., 1994; Hille et al., 2005), which can reduce growth and metabolic activity (Cairns et al., 2019b; Veiter et al., 2018). While correlation laws between transport properties and three-dimensional structures of fibrous materials are already used to design membranes (Yuan et al., 2008), heat insulations (Panerai et al., 2017), acoustic insulations (Tang and Yan, 2017), electrodes (Kim et al., 2019), and batteries (Ke et al., 2018), such laws do not exist for filamentous microorganisms. A correlation between the diffusivity and the micromorphology of hyphal networks can be harnessed to compute the diffusion of nutrients, oxygen, and secreted metabolites through filamentous pellets, and thus, contribute to the rational design of pellet morphologies.

Paper II describes the only method to date to correlate the microscopic structure and the effective diffusivity of filamentous fungi. This method is based on diffusion computations through three-dimensional hyphal networks. To reveal a universal law for filamentous fungi, diffusion computations were conducted through structures gained from three-dimensional µCT measurements of 66 fungal pellets and 3125 Monte Carlo simulated pellets that considered the broad morphological range of filamentous microorganisms (Paper III). Depending on the size of the pellets, approximately $50 - 150$ representative cubic sub-volumes per pellet were extracted and further used to compute the geometrical diffusion hindrance k_{eff}. Correlating k_{eff} with the hyphal fraction c_h (similar to solid fraction), the data showed an excellent fit to the following equation:

$$k_{eff} = (1 - c_h)^{1.76}. \tag{6.1}$$

Because k_{eff} is independent from the diffusing component i (Becker et al., 2011) and the diffusion coefficient of the bulk medium $D_{i,bulk}$ can be estimated from medium conditions (Yaws, 2014), k_{eff} determines the effective diffusion coefficient $D_{i,eff}$ (Equation 2.3), and thus, the diffusive mass transport of molecules through pellets. Equation 6.1 unveils that only one independent variable, the hyphal fraction (c_h), affects the diffusivity through hyphal networks. Contrary, micromorphological parameters such as growth angles, branch angles, hyphal diameters, branching frequency, and number of initial spores do not influence the diffusion hindrance (Paper III).

The presented correlation (Equation 6.1) is not very distinct from the law of randomly orientated overlapping fibers by Tomadakis and Sotirchos (1991) and similar to Archie's law (Archie, 1942) with a cementation parameter equal to 1.76. Contrary, the suggested correlation uncovered discrepancies with assumptions made in morphological modeling of pellets (Buschulte, 1992; Celler et al., 2012; Cui et al., 1998; Lejeune and Baron, 1997; Meyerhoff et al., 1995). However, these studies lacked reasonable mechanistic or empirical derivations of the effective diffusivity. Until today, Cronenberg et al. (1994) and Hille et al. (2009) conducted probably the most extensive experiments to determine the effective diffusivity through

inactivated pellets by stimulus response measurements of the oxygen concentration. While they obtained comparable effective diffusion factors as in Paper II and III, they did not quantify the corresponding micromorphology reasonably.

To validate the accuracy of the diffusion computations, the solutions for parallel nonoverlapping fibers (Perrins et al., 1979; Tomadakis and Sotirchos, 1991) and for randomly orientated overlapping straight fibers (Tomadakis and Sotirchos, 1991) were compared with the computed diffusivities through such structures (Paper II and III). Because image resolution can influence computed properties (Velichko et al., 2009), simulated structures were varied in resolution, i.e., the diameter of the fibers were represented with a different number of voxels. The diffusion computations with high resolutions (fibers represented with more than 10 voxels in diameter) showed a high accuracy, whereas computations through images with low resolutions resulted in a slight underestimation of the diffusivity (Paper II and III). As the image resolution of μCT measurements was restricted, hyphae were represented with approximately 4 - 5 voxels in diameter. Thus, computed diffusivities might be slightly underestimated (Paper II and III). The cementation parameters of measured *P. chrysogenum*, *A. niger*, *R. stolonifer*, and *R. oryzae* pellets were comparable to the mean cementation parameter of 3125 simulated pellets with a resolution to represent hyphae with 5 voxels in diameter. To achieve a high accuracy, the diffusion computations were also conducted through the 3125 simulated pellets with a resolution of 13 voxels. As a result, the universal law (Equation 6.1) was obtained.

The diffusion computations through numerous measured and simulated pellets spanning the broad morphological range of filamentous fungi suggest that the determined correlation (Equation 6.1) is universal for filamentous fungi. Because the micromorphology of filamentous bacteria was also considered in the simulations, this correlation might also be applicable to them.

To determine the universal law, the radial diffusivity was investigated (Paper III), i.e., the direction of the diffusion pointed to the center of pellets. However, possible anisotropic behaviors of filamentous pellets could alter the diffusivity. Contrary to simulated pellets, measured pellets showed a slight anisotropy, which has been discussed for one *A. niger* strain (MF22.4) in Paper II. For this strain, diffusivity in tangential direction was slightly lower compared to the radial direction. While the universal diffusion law of Paper III can be applied to isotropic pellets, diffusion computations (Paper II) should be conducted to determine the diffusion behavior of strongly anisotropic pellets.

The combination of three-dimensional image acquisition, morphological simulations, and diffusion computations significantly enhanced the understanding of morphology-dependent transport phenomena. Because the determined effective diffusion factor k_{eff} (Paper II and III) is the inverse of the formation factor, it can be also used to describe the conductivity or permeability of porous media (Tomadakis and Robertson, 2005). Hence, the described methodology for filamentous fungi is transferable to other research questions in bio(techno)logy and beyond.

The described methods and findings enable the correlation between microscopic structures and diffusivities of filamentous fungal networks. This knowledge will contribute to engineer the morphology of pellets to reach a desired nutrient supply resulting in an increased product formation.

6.3 New paths towards morphological engineering

The morphology of filamentous fungi has a strong influence on their productivity. Thus, morphological engineering is a key in filamentous fungal biotechnology (Cairns et al., 2019b; Krull et al., 2013). To understand and control the morphogenesis of filamentous pellets, it is essential to analyze their hyphal networks and to know the diffusive barrier for nutrients, oxygen, and secreted metabolites. Because the embedded Paper I - III enable the micromorphological analysis of whole pellets and propose a universal diffusion law, new paths towards morphological engineering of filamentous pellets will be opened. The following paragraphs present a few examples of prospects concerning experimental and modeling approaches.

Experimental approaches suggest numerous opportunities for morphological engineering. For example, genetic approaches aim to alter morphological properties (Cairns et al., 2019b) such as the branching frequency (Fiedler et al., 2018; He et al., 2016). Process engineering approaches often have the goal to alter the spatial distribution of the hyphal fraction within pellets (Lin et al., 2010). So far, analyzing the outcome of these engineering approaches with respect to the inner morphology of pellets was limited to qualitative statements about the spatial distribution of the hyphal fraction (Hille et al., 2005, 2009; Lin et al., 2010; Priegnitz et al., 2012). Now, μCT measurements and subsequent image analysis enable the characterization of the micromorphology within whole pellets. Thus, the outcome of experimental approaches can be investigated in unprecedented detail.

Modeling approaches deepen a mechanistic understanding of the morphogenesis of pellets. Although several useful models to simulate the development of the morphology and nutrient supply in pellets exist, most of them lack suitable experimental input about the inner structure and diffusivity of pellets. The microscopic and continuum pellet models described in Section 2.3.2 consider spatial distributions of morphological properties. For these approaches, the developed μCT based method (Paper I) can provide morphological data to an unprecedented extent. Additionally, many morphological modeling approaches include the diffusive mass transport of nutrients and oxygen through the hyphal network (Buschulte, 1992; Celler et al., 2012; Lejeune and Baron, 1997; Meyerhoff et al., 1995). Based on the suggested universal law for the diffusivity of filamentous fungal networks (Paper III), the required effective diffusion coefficient can be calculated. Hence, the validation and improvement of existing models through the use of micromorphological data and laws for the diffusivity through hyphal networks can be achieved.

The concentration of molecules such as nutrients, oxygen, and secreted metabolites within pellets are affected by metabolic rates and the transport through the hyphal network (Celler et al., 2012; Cui et al., 1998). Because the transport can now be calculated (Paper II and III),

the estimation of metabolic rates within pellets will become feasible. To estimate metabolic rates, experiments should provide information about the spatial distribution of molecules and morphological properties within pellets. For example, the application of microelectrodes within pellets (Cronenberg et al., 1994; Hille et al., 2009) followed by µCT measurements (Paper I) would provide the spatial distribution of oxygen and (micro)morphological properties within pellets. Based on partial differential diffusion-reaction equations that are already proposed in several modeling approaches (Buschulte.1992, King.1998, Celler.2012), the estimation of oxygen consumption rates might then be conducted. The described procedure might also be used to determine metabolic rates of other substances including nutrients and secreted metabolites.

The product of interest determines whether a saturation or a limitation of nutrients inside fungal pellets is pursued (Veiter et al., 2018). Thus, optimal pellet morphologies cannot be generalized in bioprocesses (Krull et al., 2010). In Figure 5, an idealized workflow for the construction of pellets as optimized production hosts is proposed, which is based on a sketch in Paper II. The first step of this workflow is the generation of a database consisting of numerous pellet structures. The database might consist of both µCT measured and simulated pellets. Further, partial differential diffusion-reaction equations (Buschulte, 1992; Celler et al., 2012; King, 1998) should be applied to compute substrate-limited and substrate-saturated regions of each pellet of the database. For the reaction term, substrate consumption rates have to be acquired from literature or experiments. The spatial distribution of the hyphal fraction (from database) and the universal diffusion law described in Paper III determine the diffusion term. Depending on whether substrate limitation or saturation is desired, a suitable pellet structure can be selected from the database. Based on process and/or genetic engineering approaches, the chosen pellet structure should then be realized in bioreactors. Although there have been many advances in morphological engineering, the realization of suitable pellets is most likely going to be an iterative process. For this, a detailed verification of the pellet morphology can be conducted based on µCT measurements and 3D image analysis. Obviously, some of the proposed steps of the idealized workflow have to be investigated and elaborated in much more detail. However, this workflow shows that the developed methods and findings embedded in this thesis are important steps towards the construction of filamentous fungal pellets as optimized production hosts.

So far, this dissertation mainly addressed individual pellets. However, submerged cultures of filamentous microorganisms can result in broad pellet size distributions (Kurt et al., 2018; Schrinner et al., 2020) influencing the further growth and production behavior (King, 1998; Wösten et al., 2013) as well as the rheology and mass transfer in the bioprocess (Bliatsiou et al., 2020). Contrary to the microscopic and continuum models elaborated in Section 2.3.2, population balance equations (PBEs) allow the modeling of the development of the morphological heterogeneity (King, 1998). On the one hand, recent advances in measuring the macromorphology of numerous pellets (Sections 2.1.2 and 2.1.3) might contribute to PBEs that describe the development of the size distribution (Edelstein and Hadar, 1983; Tough et al., 1995). On the other hand, micromorphological data lacks as input of future PBEs with
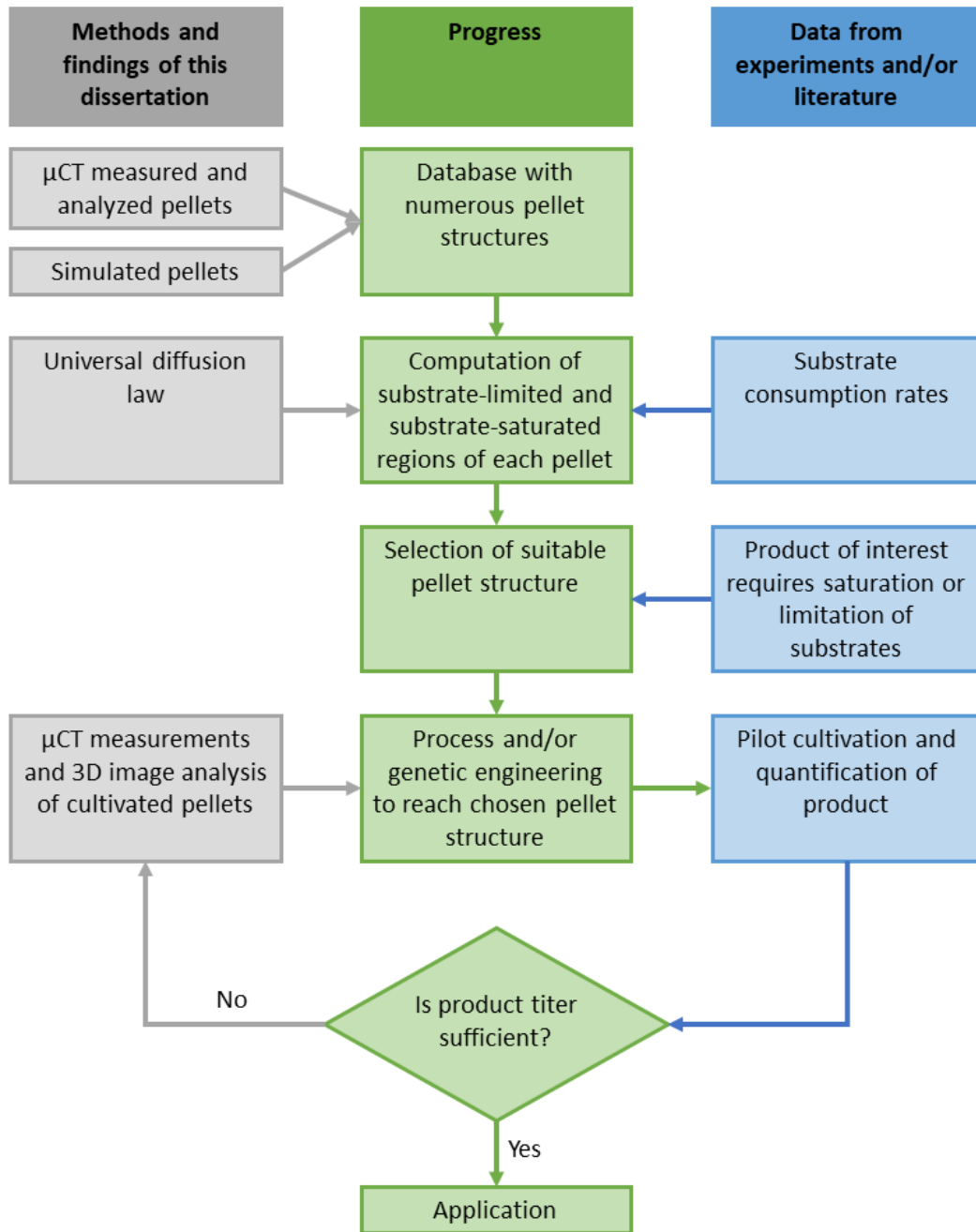
Figure 5: Idealized workflow for the construction of filamentous fungal pellets as optimized production hosts.

a high structuredness. As proposed in Schmideder et al. (2018), population balance models with a high structuredness can consider several morphological properties including the size of pellets, the diameter of the shell layer supplied with oxygen, the total length of active and inactive hyphae, and the total number of growing tips. The location of tips and hyphal material can be determined based on µCT measurements and subsequent image analysis (Paper I). While laboratory µCT systems enable the visualization of a few pellets with one measurement, hundreds of pellets can be visualized based on synchrotron radiation within a few minutes (Section 6.1). Further, active and inactive regions of pellets can be estimated based on experimental approaches (Section 2.2.2) or diffusion-reaction equations (Celler et al., 2012; King, 1998). Thus, PBEs with a high morphological structuredness can be developed through the use of micromorphological data (Paper I) and the proposed universal diffusion law (Paper III). Such modeling approaches will deepen the mechanistic understanding of the development of (pellet) heterogeneities including growth, breakage, and aggregation processes.

To conclude, the developed methods to determine the micromorphology (Paper I) and effective diffusivity (Paper II) of pellets and the universal diffusion law through hyphal networks (Paper III) will open new paths towards morphological engineering to enhance productivities in filamentous fungal biotechnology.

7 References

Antecka, A., Bizukojc, M., and Ledakowicz, S. (2016). Modern morphological engineering techniques for improving productivity of filamentous fungi in submerged cultures. *World Journal of Microbiology and Biotechnology*, 32:193.

Archie, G. E. (1942). The electrical resistivity log as an aid in determining some reservoir characteristics. *Transactions of the AIME*, 146(01):54–62.

Barry, D. J., Williams, G. A., and Chan, C. (2015). Automated analysis of filamentous microbial morphology with AnaMorf. *Biotechnology Progress*, 31(3):849–852.

Becker, J., Wieser, C., Fell, S., and Steiner, K. (2011). A multi-scale approach to material modeling of fuel cell diffusion media. *International Journal of Heat and Mass Transfer*, 54(7-8):1360–1368.

Biesebeke, R., Record, E., van Biezen, N., Heerikhuisen, M., Franken, A., Punt, P. J., and van den Hondel, C. A. M. J. J. (2005). Branching mutants of Aspergillus oryzae with improved amylase and protease production on solid substrates. *Applied Microbiology and Biotechnology*, 69(1):44–50.

Bizukojc, M. and Ledakowicz, S. (2006). A kinetic model to predict biomass content for Aspergillus niger germinating spores in the submerged culture. *Process Biochemistry*, 41(5):1063–1071.

Bizukojc, M. and Ledakowicz, S. (2010). The morphological and physiological evolution of Aspergillus terreus mycelium in the submerged culture and its relation to the formation of secondary metabolites. *World Journal of Microbiology and Biotechnology*, 26:41.

Bliatsiou, C., Schrinner, K., Waldherr, P., Tesche, S., Böhm, L., Kraume, M., and Krull, R. (2020). Rheological characteristics of filamentous cultivation broths and suitable model fluids. *Biochemical Engineering Journal*, 163:107746.

Bocking, S. P., Wiebe, M. G., Robson, G. D., Hansen, K., Christiansen, L. H., and Trinci, A. P. J. (1999). Effect of branch frequency in Aspergillus oryzae on protein secretion and culture viscosity. *Biotechnology and Bioengineering*, 65(6):638–648.

Böl, M., Schrinner, K., Tesche, S., and Krull, R. (2021). Challenges of influencing cellular morphology by morphology engineering techniques and mechanical induced stress on filamentous pellet systems - A critical review. *Engineering in Life Sciences*, 21(3-4):51–67.

Brakhage, A. A. (2013). Regulation of fungal secondary metabolism. *Nature Reviews Microbiology*, 11(1):21–32.

Brunk, M., Sputh, S., Doose, S., van de Linde, S., and Terpitz, U. (2018). HyphaTracker: An ImageJ toolbox for time-resolved analysis of spore germination in filamentous fungi. *Scientific Reports*, 8(1):605.

Buschulte, T. C. (1992). *Mathematische Modellbildung und Simulation von Zellwachstum, Stofftransport und Stoffwechsel in Pellets aus Streptomyceten*. PhD thesis, Fakultät Verfahrenstechnik der Universität Stuttgart.

Cairns, T. C., Feurstein, C., Zheng, X., Zheng, P., Sun, J., and Meyer, V. (2019a). A quantitative image analysis pipeline for the characterization of filamentous fungal morphologies as a tool to uncover targets for morphology engineering: a case study using aplD in Aspergillus niger. *Biotechnology for Biofuels*, 12:149.

Cairns, T. C., Nai, C., and Meyer, V. (2018). How a fungus shapes biotechnology: 100 years of Aspergillus niger research. *Fungal Biology and Biotechnology*, 5:13.

Cairns, T. C., Zheng, X., Zheng, P., Sun, J., and Meyer, V. (2019b). Moulding the mould: understanding and reprogramming filamentous fungal growth and morphogenesis for next generation cell factories. *Biotechnology for Biofuels*, 12(1):77.

Cardini, A., Pellegrino, E., Del Dottore, E., Gamper, H. A., Mazzolai, B., and Ercoli, L. (2020). HyLength: a semi-automated digital image analysis tool for measuring the length of roots and fungal hyphae of dense mycelia. *Mycorrhiza*, 30(2-3):229–242.

Celler, K., Picioreanu, C., van Loosdrecht, Mark C. M., and van Wezel, G. P. (2012). Structured morphological modeling as a framework for rational strain design of Streptomyces species. *Antonie van Leeuwenhoek*, 102(3):409–423.

Choy, V., Patel, N., and Thibault, J. (2011). Application of image analysis in the fungal fermentation of Trichoderma reesei RUT-C30. *Biotechnology Progress*, 27(6):1544–1553.

Colin, V. L., Baigori, M. D., and Pera, L. M. (2013). Tailoring fungal morphology of Aspergillus niger MYA 135 by altering the hyphal morphology and the conidia adhesion capacity: biotechnological applications. *AMB Express*, 3:27.

Cronenberg, C. C. H., Ottengraf, S. P. P., Heuvel, J. C., Pottel, F., Sziele, D., Schgerl, K., and Bellgardt, K. H. (1994). Influence of age and structure of Pencillium chrysogenum pellets on the internal concentration profiles. *Bioprocess Engineering*, 10(5-6):209–216.

Cui, Y. Q., van der Lans, R., and Luyben, K. (1998). Effects of dissolved oxygen tension and mechanical forces on fungal morphology in submerged fermentation. *Biotechnology and Bioengineering*, 57(4):409–419.

Cui, Y. Q., vanderLans, R., and Luyben, K. (1997). Effect of agitation intensities on fungal morphology of submerged fermentation. *Biotechnology and Bioengineering*, 55(5):715–726.

Demain, A. L. (2014). Importance of microbial natural products and the need to revitalize their discovery. *Journal of Industrial Microbiology and Biotechnology*, 41(2):185–201.

Driouch, H., Haensch, R., Wucherpfennig, T., Krull, R., and Wittmann, C. (2012). Improved enzyme production by bio-pellets of Aspergillus niger: Targeted morphology engineering using titanate microparticles. *Biotechnology and Bioengineering*, 109(2):462–471.

Driouch, H., Sommer, B., and Wittmann, C. (2010). Morphology Engineering of Aspergillus niger for Improved Enzyme Production. *Biotechnology and Bioengineering*, 105(6):1058–1068.

Du, H., Lv, P., Ayouz, M., Besserer, A., and Perré, P. (2016). Morphological characterization and quantification of the mycelial growth of the brown-rot fungus Postia placenta for modeling purposes. *PloS ONE*, 11(9):e0162469.

Dynesen, J. and Nielsen, J. (2003). Surface hydrophobicity of Aspergillus nidulans conidiospores and its role in pellet formation. *Biotechnology Progress*, 19(3):1049–1052.

Edelstein, L. and Hadar, Y. (1983). A model for pellet size distributions in submerged mycelial cultures. *Journal of Theoretical Biology*, 105(3):427–452.

Ehgartner, D., Herwig, C., and Fricke, J. (2017). Morphological analysis of the filamentous fungus Penicillium chrysogenum using flow cytometry-the fast alternative to microscopic image analysis. *Applied Microbiology and Biotechnology*, 101(20):7675–7688.

El-Enshasy, H., Kleine, J., and Rinas, U. (2006). Agitation effects on morphology and protein productive fractions of filamentous and pelleted growth forms of recombinant Aspergillus niger. *Process Biochemistry*, 41(10):2103–2112.

Emerson, S. (1950). The growth phase in Neurospora corresponding to the logarithmic phase in unicellular organisms. *Journal of Bacteriology*, 60(3):221–223.

Fiedler, M. R. M., Barthel, L., Kubisch, C., Nai, C., and Meyer, V. (2018). Construction of an improved Aspergillus niger platform for enhanced glucoamylase secretion. *Microbial Cell Factories*, 17:95.

Fleming, A. (1929). On the antibacterial action of cultures of a penicillium, with special reference to their use in the isolation of B. influenzae. *British Journal of Experimental Pathology*, 10(3):226–236.

Fontaine, T., Beauvais, A., Loussert, C., Thevenard, B., Fulgsang, C. C., Ohno, N., Clavaud, C., Prevost, M.-C., and Latgé, J.-P. (2010). Cell wall alpha1-3glucans induce the aggregation of germinating conidia of Aspergillus fumigatus. *Fungal Genetics and Biology*, 47(8):707–712.

Gibbs, P. A., Seviour, R. J., and Schmid, F. (2000). Growth of filamentous fungi in submerged culture: Problems and possible solutions. *Critical Reviews in Biotechnology*, 20(1):17–48.

Grimm, L. H., Kelly, S., Hengstler, J., Gobel, A., Krull, R., and Hempel, D. C. (2004). Kinetic studies on the aggregation of Aspergillus niger conidia. *Biotechnology and Bioengineering*, 87(2):213–218.

Grimm, L. H., Kelly, S., Krull, R., and Hempel, D. C. (2005). Morphology and productivity of filamentous fungi. *Applied Microbiology and Biotechnology*, 69(4):375–384.

He, R., Li, C., Ma, L., Zhang, D., and Chen, S. (2016). Effect of highly branched hyphal morphology on the enhanced production of cellulase in Trichoderma reesei DES-15. *3 Biotech*, 6:214.

Hille, A., Neu, T. R., Hempel, D. C., and Horn, H. (2005). Oxygen profiles and biomass distribution in biopellets of Aspergillus niger. *Biotechnology and Bioengineering*, 92(5):614–623.

Hille, A., Neu, T. R., Hempel, D. C., and Horn, H. (2009). Effective diffusivities and mass fluxes in fungal biopellets. *Biotechnology and Bioengineering*, 103(6):1202–1213.

Hoffmeister, D. and Keller, N. P. (2007). Natural products of filamentous fungi: enzymes, genes, and their regulation. *Natural Product Reports*, 24(2):393–416.

Karahalil, E., Coban, H. B., and Turhan, I. (2019). A current approach to the control of filamentous fungal growth in media: microparticle enhanced cultivation technique. *Critical Reviews in Biotechnology*, 39(2):192–201.

Ke, X., Prahl, J. M., Alexander, J. I. D., Wainright, J. S., Zawodzinski, T. A., and Savinell, R. F. (2018). Rechargeable redox flow batteries: flow fields, stacks and design considerations. *Chemical Society Reviews*, 47(23):8721–8743.

Keller, N. P. (2019). Fungal secondary metabolism: regulation, function and drug discovery. *Nature Reviews Microbiology*, 17(3):167–180.

Kelly, S., Grimm, L. H., Jonas, R., Hempel, D. C., and Krull, R. (2006). Investigations of the morphogenesis of filamentous microorganisms. *Engineering in Life Sciences*, 6(5):475–480.

Kim, M. J., Seo, Y., Cruz, M. A., and Wiley, B. J. (2019). Metal nanowire felt as a flow-through electrode for high-productivity electrochemistry. *ACS Nano*, 13(6):6998–7009.

King, R. (1998). Mathematical modelling of the morphology of streptomyces species. In *Relation between morphology and process performances*, pages 95–124. Springer, Berlin, Heidelberg.

King, R. (2015). A framework for an organelle-based mathematical modeling of hyphae. *Fungal Biology and Biotechnology*, 2:5.

Krull, R., Cordes, C., Horn, H., Kampen, I., Kwade, A., Neu, T. R., and Nörtemann, B. (2010). Morphology of filamentous fungi: linking cellular biology to process engineering using Aspergillus niger. In *Biosystems Engineering II: Linking Cellular Networks and Bioprocesses*, pages 1–21. Springer, Berlin, Heidelberg.

Krull, R., Wucherpfennig, T., Esfandabadi, M. E., Walisko, R., Melzer, G., Hempel, D. C., Kampen, I., Kwade, A., and Wittmann, C. (2013). Characterization and control of fungal morphology for improved production performance in biotechnology. *Journal of Biotechnology*, 163(2):112–123.

Kunz, P. J., Barthel, L., Meyer, V., and King, R. (2020). Vesicle transport and growth dynamics in Aspergillus niger: Microscale modeling of secretory vesicle flow and centerline extraction from confocal fluorescent data. *Biotechnology and Bioengineering*, 117(9):2875–2886.

Kurt, T., Marbà-Ardébol, A.-M., Turan, Z., Neubauer, P., Junne, S., and Meyer, V. (2018). Rocking Aspergillus: morphology-controlled cultivation of Aspergillus niger in a wave-mixed bioreactor for the production of secondary metabolites. *Microbial Cell Factories*, 17:128.

Kwon, M. J., Nitsche, B. M., Arentshorst, M., Jørgensen, T. R., Ram, A. F. J., and Meyer, V. (2013). The transcriptomic signature of RacA activation and inactivation provides new insights into the morphogenetic network of Aspergillus niger. *PloS ONE*, 8(7):e68946.

Lecault, V., Patel, N., and Thibault, J. (2007). Morphological characterization and viability assessment of Trichoderma reesei by image analysis. *Biotechnology Progress*, 23(3):734–740.

Lehmann, A., Zheng, W., Soutschek, K., Roy, J., Yurkov, A. M., and Rillig, M. C. (2019). Tradeoffs in hyphal traits determine mycelium architecture in saprobic fungi. *Scientific Reports*, 9:14152.

Lejeune, R. and Baron, G. V. (1997). Simulation of growth of a filamentous fungus in 3 dimensions. *Biotechnology and Bioengineering*, 53(2):139–150.

Lin, P.-J., Grimm, L. H., Wulkow, M., Hempel, D. C., and Krull, R. (2008). Population balance modeling of the conidial aggregation of Aspergillus niger. *Biotechnology and Bioengineering*, 99(2):341–350.

Lin, P.-J., Scholz, A., and Krull, R. (2010). Effect of volumetric power input by aeration and agitation on pellet morphology and product formation of Aspergillus niger. *Biochemical Engineering Journal*, 49(2):213–220.

Metz, B. and Kossen, N. W. F. (1977). The growth of molds in the form of pellets–a literature review. *Biotechnology and Bioengineering*, 19(6):781–799.

Meyer, V. (2008). Genetic engineering of filamentous fungi - Progress, obstacles and future trends. *Biotechnology Advances*, 26(2):177–185.

Meyer, V., Andersen, M. R., Brakhage, A. A., Braus, G. H., Caddick, M. X., Cairns, T. C., de Vries, R. P., Haarmann, T., Hansen, K., Hertz-Fowler, C., Krappmann, S., Mortensen, U. H., Peñalva, M. A., Ram, A. F. J., and Head, R. M. (2016). Current challenges of research on filamentous fungi in relation to human welfare and a sustainable bio-economy: a white paper. *Fungal Biology and Biotechnology*, 3:6.

Meyer, V., Basenko, E., Benz, P., Braus, G., Caddick, M., Csukai, M., Vries, R., Endy, D., Frisvad, J., Gunde-Cimerman, N., Haarmann, T., Hadar, Y., Hansen, K., Johnson, R., Keller, N., Kraševec, N., Mortensen, U., Perez, R., Ram, A., Record, E., Ross, P., Shapaval, V., Steiniger, C., van den Brink, H., van Munster, J., Yarden, O., and Wösten, H. (2020). Growing a circular economy with fungal biotechnology: a white paper. *Fungal Biology and Biotechnology*, 7:5.

Meyerhoff, J., Tiller, V., and Bellgardt, K.-H. (1995). Two mathematical models for the development of a single microbial pellet. *Bioprocess and Biosystems Engineering*, 12(6):305–313.

Müller, H., Schmideder, S., Barthel, L., Niessen, L., Meyer, V., and Briesen, H. (2020). Optimized X–ray microcomputed tomography and 3D volumetric image processing of filamentous fungal pellets. *ProcessNet Jahrestagung und DECHEMA Jahrestagung der Biotechnologen 2020, Web-Konferenz.*

Nielsen, J., Johansen, C. L., Jacobsen, M., Krabben, P., and Villadsen, J. (1995). Pellet formation and fragmentation in submerged cultures of Penicillium chrysogenum and its relation to penicillin production. *Biotechnology Progress*, 11(1):93–98.

Nielsen, J. C., Grijseels, S., Prigent, S., Ji, B., Dainat, J., Nielsen, K. F., Frisvad, J. C., Workman, M., and Nielsen, J. (2017). Global analysis of biosynthetic gene clusters reveals vast potential of secondary metabolite production in Penicillium species. *Nature Microbiology*, 2:17044.

Nieminen, L., Webb, S., Smith, M. C. M., and Hoskisson, P. A. (2013). A flexible mathematical model platform for studying branching networks: Experimentally validated using the model actinomycete, Streptomyces coelicolor. *PloS ONE*, 8(2):e54316.

Olmos, E., Mehmood, N., Haj Husein, L., Goergen, J.-L., Fick, M., and Delaunay, S. (2013). Effects of bioreactor hydrodynamics on the physiology of Streptomyces. *Bioprocess and Biosystems Engineering*, 36(3):259–272.

Panerai, F., Ferguson, J. C., Lachaud, J., Martin, A., Gasch, M. J., and Mansour, N. N. (2017). Micro-tomography based analysis of thermal conductivity, diffusivity and oxidation behavior of rigid and flexible fibrous insulators. *International Journal of Heat and Mass Transfer*, 108:801–811.

Papagianni, M. (2004). Fungal morphology and metabolite production in submerged mycelial processes. *Biotechnology Advances*, 22(3):189–259.

Papagianni, M. (2014). Characterization of fungal morphology using digital image analysis techniques. *Journal of Microbial and Biochemical Technology*, 6(4):189–194.

Papagianni, M. and Mattey, M. (2006). Morphological development of Aspergillus niger in submerged citric acid fermentation as a function of the spore inoculum level. Application of neural network and cluster analysis for characterization of mycelial morphology. *Microbial Cell Factories*, 5:3.

Papagianni, M., Mattey, M., and Kristiansen, B. (1999). The influence of glucose concentration on citric acid production and morphology of Aspergillus niger in batch and culture. *Enzyme and Microbial Technology*, 25(8-9):710–717.

Paul, G. C., Kent, C. A., and Thomas, C. R. (1993). Viability testing and characterization of germination of fungal spores by automatic image analysis. *Biotechnology and Bioengineering*, 42(1):11–23.

Pearson, A. P., Glennon, B., and Kieran, P. M. (2003). Comparison of morphological characteristics of Streptomyces natalensis by image analysis and focused beam reflectance measurement. *Biotechnology Progress*, 19(4):1342–1347.

Pearson, A. P., Glennon, B., and Kieran, P. M. (2004). Monitoring of cell growth using the focused beam reflectance method. *Journal of Chemical Technology and Biotechnology*, 79(10):1142–1147.

Perrins, W. T., McKenzie, D. R., and Mc Phedran, R. C. (1979). Transport properties of regular arrays of cylinders. *Proceedings of the Royal Society A*, 369(1737):207–225.

Petersen, N., Stocks, S., and Gernaey, K. V. (2008). Multivariate models for prediction of rheological characteristics of filamentous fermentation broth from the size distribution. *Biotechnology and Bioengineering*, 100(1):61–71.

Pirt, S. J. (1966). A theory of the mode of growth of fungi in the form of pellets in submerged culture. *Proceedings of the Royal Society B*, 166(1004):369–373.

Posch, A. E., Herwig, C., and Spadiut, O. (2013). Science-based bioprocess design for filamentous fungi. *Trends in Biotechnology*, 31(1):37–44.

Priegnitz, B.-E., Wargenau, A., Brandt, U., Rohde, M., Dietrich, S., Kwade, A., Krull, R., and Fleissner, A. (2012). The role of initial spore adhesion in pellet and biofilm formation in Aspergillus niger. *Fungal Genetics and Biology*, 49(1):30–38.

Prosser, J. I. and Tough, A. J. (1991). Growth mechanisms and growth kinetics of filamentous microorganisms. *Critical Reviews in Biotechnology*, 10(4):253–274.

Punt, P. J., van Biezen, N., Conesa, A., Albers, A., Mangnus, J., and van den Hondel, C. (2002). Filamentous fungi as cell factories for heterologous protein production. *Trends in Biotechnology*, 20(5):200–206.

Quintanilla, D., Chelius, C., Iambamrung, S., Nelson, S., Thomas, D., Gernaey, K. V., and Marten, M. R. (2018). A fast and simple method to estimate relative, hyphal tensile-strength of filamentous fungi used to assess the effect of autophagy. *Biotechnology and Bioengineering*, 115(3):597–605.

Riquelme, M., Aguirre, J., Bartnicki-García, S., Braus, G. H., Feldbrügge, M., Fleig, U., Hansberg, W., Herrera-Estrella, A., Kämper, J., Kück, U., Mouriño-Pérez, R. R., Takeshita, N., and Fischer, R. (2018). Fungal morphogenesis, from the polarized growth of hyphae to complex reproduction and infection structures. *Microbiology and Molecular Biology Reviews*, 82(2):e00068–17.

Rønnest, N. P., Stocks, S. M., Lantz, A. E., and Gernaey, K. V. (2012). Comparison of laser diffraction and image analysis for measurement of Streptomyces coelicolor cell clumps and pellets. *Biotechnology Letters*, 34(8):1465–1473.

Sachs, C. C., Koepff, J., Wiechert, W., Grünberger, A., and Nöh, K. (2019). mycelyso - high-throughput analysis of Streptomyces mycelium live cell imaging data. *BMC Bioinformatics*, 20:452.

Salvo, L., Cloetens, P., Maire, E., Zabler, S., Blandin, J., Buffière, J., Ludwig, W., Boller, E., Bellet, D., and Josserond, C. (2003). X-ray micro-tomography an attractive characterisation technique in materials science. *Nuclear Instruments and Methods in Physics Research Section B: Beam Interactions with Materials and Atoms*, 200:273–286.

Schmideder, S., Barthel, L., Friedrich, T., Thalhammer, M., Kovačević, T., Niessen, L., Meyer, V., and Briesen, H. (2019a). An X-ray microtomography-based method for detailed analysis of the three-dimensional morphology of fungal pellets. *Biotechnology and Bioengineering*, 116(6):1355–1365.

Schmideder, S., Barthel, L., Müller, H., Meyer, V., and Briesen, H. (2019b). From three-dimensional morphology to effective diffusivity in filamentous fungal pellets. *Biotechnology and Bioengineering*, 116(12):3360–3371.

Schmideder, S., Friedrich, T., Kovačević, T., Barthel, L., Kunz, P., Meyer, V., King, R., and Briesen, H. (2018). Growth of filamentous microorganisms: PBM and experimental determination of rate equations. *Conference Procceedings: 6th Population Balance Modelling Conference (PBM 2018), Ghent, Belgium*.

Schmideder, S., Müller, H., Barthel, L., Friedrich, T., Niessen, L., Meyer, V., and Briesen, H. (2021). Universal law for diffusive mass transport through mycelial networks. *Biotechnology and Bioengineering*, 118(2):930–943.

Schrinner, K., Veiter, L., Schmideder, S., Doppler, P., Schrader, M., Münch, N., Althof, K., Kwade, A., Briesen, H., Herwig, C., and Krull, R. (2020). Morphological and physiological characterization of filamentous Lentzea aerocolonigenes: Comparison of biopellets by microscopy and flow cytometry. *PLoS ONE*, 15(6):e0234125.

Silva, E. M. E., Gutierrez, G. F., Dendooven, L., Hugo, J. I., and Ochoa-Tapia, J. A. (2001). A method to evaluate the isothermal effectiveness factor for dynamic oxygen into mycelial pellets in submerged cultures. *Biotechnology Progress*, 17(1):95–103.

Stock, S. R. (2009). *Microcomputed tomography: Methodology and applications*. CRC Press.

Tang, X. and Yan, X. (2017). Acoustic energy absorption properties of fibrous materials: A review. *Composites Part A: Applied Science and Manufacturing*, 101:360–380.

Tegelaar, M., Aerts, D., Teertstra, W. R., and Wösten, H. A. B. (2020). Spatial induction of genes encoding secreted proteins in micro-colonies of Aspergillus niger. *Scientific Reports*, 10:1536.

Tomadakis, M. M. and Robertson, T. J. (2005). Viscous permeability of random fiber structures: comparison of electrical and diffusional estimates with experimental and analytical results. *Journal of Composite Materials*, 39(2):163–188.

Tomadakis, M. M. and Sotirchos, S. V. (1991). Effects of Fiber Orientation and Overlapping on Knudsen, Transition, and Ordinary Regime Diffusion in Fibrous Substrates. *MRS Proceedings*, 250:221–226.

Tough, A. J., Pulham, J., and Prosser, J. I. (1995). A mathematical model for the growth of mycelial pellet populations. *Biotechnology and Bioengineering*, 46(6):561–572.

Veiter, L. and Herwig, C. (2019). The filamentous fungus Penicillium chrysogenum analysed via flow cytometry-a fast and statistically sound insight into morphology and viability. *Applied Microbiology and Biotechnology*, 103(16):6725–6735.

Veiter, L., Rajamanickam, V., and Herwig, C. (2018). The filamentous fungal pellet-relationship between morphology and productivity. *Applied Microbiology and Biotechnology*, 102(7):2997–3006.

Velichko, A., Wiegmann, A., and Mücklich, F. (2009). Estimation of the effective conductivities of complex cast iron microstructures using FIB-tomographic analysis. *Acta Materialia*, 57(17):5023–5035.

Vidal-Diez de Ulzurrun, G., Huang, T.-Y., Chang, C.-W., Lin, H.-C., and Hsueh, Y.-P. (2019). Fungal feature tracker (FFT): A tool for quantitatively characterizing the morphology and growth of filamentous fungi. *PLoS Computational Biology*, 15(10):e1007428.

Vignoles, G. L., Coindreau, O., Ahmadi, A., and Bernard, D. (2007). Assessment of geometrical and transport properties of a fibrous C/C composite preform as digitized by x-ray computerized microtomography: Part II. Heat and gas transport properties. *Journal of Materials Research*, 22(6):1537–1550.

Villena, G. K., Fujikawa, T., Tsuyumu, S., and Gutierrez-Correa, M. (2010). Structural analysis of biofilms and pellets of Aspergillus niger by confocal laser scanning microscopy and cryo scanning electron microscopy. *Bioresource Technology*, 101(6):1920–1926.

Walisko, J., Vernen, F., Pommerehne, K., Richter, G., Terfehr, J., Kaden, D., Dähne, L., Holtmann, D., and Krull, R. (2017). Particle-based production of antibiotic rebeccamycin with Lechevalieria aerocolonigenes. *Process Biochemistry*, 53:1–9.

Wang, B., Chen, J., Li, H., Sun, F., Li, Y., and Shi, G. (2017). Pellet-dispersion strategy to simplify the seed cultivation of Aspergillus niger and optimize citric acid production. *Bioprocess and Biosystems Engineering*, 40(1):45–53.

Wang, Q., Zhong, C., and Xiao, H. (2020). Genetic engineering of filamentous fungi for efficient protein expression and secretion. *Frontiers in Bioengineering and Biotechnology*, 8:293.

Ward, O. P. (2012). Production of recombinant proteins by filamentous fungi. *Biotechnology Advances*, 30(5):1119–1139.

Whelan, J., Murphy, E., Pearson, A., Jeffers, P., Kieran, P., McDonnell, S., Raposo, S., Lima-Costa, M. E., and Glennon, B. (2012). Use of focussed beam reflectance measurement (FBRM) for monitoring changes in biomass concentration. *Bioprocess and Biosystems Engineering*, 35(6):963–975.

Willemse, J., Büke, F., van Dissel, D., Grevink, S., Claessen, D., and van Wezel, G. P. (2018). SParticle, an algorithm for the analysis of filamentous microorganisms in submerged cultures. *Antonie van Leeuwenhoek*, 111(2):171–182.

Wittier, R., Baumgartl, H., Lübbers, D. W., and Schügerl, K. (1986). Investigations of oxygen transfer into Penicillium chrysogenum pellets by microprobe measurements. *Biotechnology and Bioengineering*, 28(7):1024–1036.

Wösten, H. A. B. (2019). Filamentous fungi for the production of enzymes, chemicals and materials. *Current Opinion in Biotechnology*, 59:65–70.

Wösten, H. A. B., van Veluw, G. J., de Bekker, C., and Krijgsheld, P. (2013). Heterogeneity in the mycelium: implications for the use of fungi as cell factories. *Biotechnology Letters*, 35(8):1155–1164.

Wucherpfennig, T., Hestler, T., and Krull, R. (2011). Morphology engineering - osmolality and its effect on Aspergillus niger morphology and productivity. *Microbial Cell Factories*, 10:58.

Xin, B., Xia, Y., Zhang, Y., Aslam, H., Liu, C., and Chen, S. (2012). A feasible method for growing fungal pellets in a column reactor inoculated with mycelium fragments and their application for dye bioaccumulation from aqueous solution. *Bioresource Technology*, 105:100–105.

Yang, H., King, R., Reichl, U., and Gilles, E. D. (1992a). Mathematical model for apical growth, septation, and branching of mycelial microorganisms. *Biotechnology and Bioengineering*, 39(1):49–58.

Yang, H., Reichl, U., King, R., and Gilles, E. D. (1992b). Measurement and simulation of the morphological development of filamentous microorganisms. *Biotechnology and Bioengineering*, 39(1):44–48.

Yaws, C. L. (2014). Diffusion coefficient at infinite dilution in Water - inorganic compounds. *In transport properties of chemicals and hydrocarbons*, pages 704–705. William Andrew.

Yuan, J., Liu, X., Akbulut, O., Hu, J., Suib, S. L., Kong, J., and Stellacci, F. (2008). Superwetting nanowire membranes for selective absorption. *Nature Nanotechnology*, 3(6):332–336.

Zacchetti, B., Wösten, H. A. B., and Claessen, D. (2018). Multiscale heterogeneity in filamentous microbes. *Biotechnology Advances*, 36(8):2138–2149.

Zhang, J. and Zhang, J. (2016). The filamentous fungal pellet and forces driving its formation. *Critical Reviews in Biotechnology*, 36(6):1066–1077.

Žnidaršič, P., Komel, R., and Pavko, A. (1998). Studies of a pelleted growth form of Rhizopus nigricans as a biocatalyst for progesterone 11alpha-hydroxylation. *Journal of Biotechnology*, 60(3):207–216.

Žnidaršič, P., Komel, R., and Pavko, A. (2000). Influence of some environmental factors on Rhizopus nigricans submerged growth in the form of pellets. *World Journal of Microbiology and Biotechnology*, 16(7):589–593.

8 Appendix: List of Publications

Peer-Reviewed Publications

Stefan Schmideder, Christoph Kirse, Julia Hofinger, Sascha Rollié, and Heiko Briesen, 2018, Modeling the separation of microorganisms in bioprocesses by flotation. Processes, 6(10): 184.

Stefan Schmideder, Lars Barthel, Tiaan Friedrich, Michaela Thalhammer, Tijana Kovačević, Ludwig Niessen, Vera Meyer, and Heiko Briesen, 2019, An X-ray microtomography-based method for detailed analysis of the three-dimensional morphology of fungal pellets. Biotechnology and Bioengineering, 116(6): 1355–1365.

Stefan Schmideder, Lars Barthel, Henri Müller, Vera Meyer, and Heiko Briesen, 2019, From three-dimensional morphology to effective diffusivity in filamentous fungal pellets. Biotechnology and Bioengineering, 116(12): 3360–3371.

Kathrin Schrinner, Lukas Veiter, **Stefan Schmideder**, Philipp Doppler, Marcel Schrader, Nadine Münch, Kristin Althof, Arno Kwade, Heiko Briesen, Christoph Herwig, and Rainer Krull, 2020, Morphological and physiological characterization of filamentous *Lentzea aerocolonigenes*: Comparison of biopellets by microscopy and flow cytometry. PLOS ONE, 15(6): e0234125.

Stefan Schmideder, Henri Müller, Lars Barthel, Tiaan Friedrich, Ludwig Niessen, Vera Meyer, and Heiko Briesen, 2021, Universal law for diffusive mass transport through mycelial networks. Biotechnology and Bioengineering, 118(2):930–943.

Oral Presentations

Stefan Schmideder, Christoph Kirse, Julia Hofinger, Sascha Rollié, and Heiko Briesen, 2018, Modeling the separation of microorganisms in bioprocesses by flotation. 6th Population Balance Modelling Conference (PBM 2018), Gent, Belgium.

Kathrin Pommerehne, Marcel Schrader, Chrysoula Bliatsiou, **Stefan Schmideder**, Lutz Böhm, Heiko Briesen, Matthias Kraume, Arno Kwade, and Rainer Krull1, 2018, Experimental and numerical investigations on cultivations of filamentous microorganisms towards a better understanding and process control. ProcessNet Jahrestagung und DECHEMA-Jahrestagung der Biotechnologen 2018, Aachen, Germany.

Heiko Briesen, **Stefan Schmideder**, Henri Müller, 2020, Morphological characterization and modeling of filamentous fungi. 4th Indo-German Workshop on Advances in Materials, Reaction & Separation Processes, Berlin, Germany.

Stefan Schmideder, Lars Barthel, Henri Müller, Vera Meyer, and Heiko Briesen, 2020, On the three-dimensional morphology and substrate-diffusion in filamentous fungal pellets. 15th European Conference on Fungal Genetics (ECFG15), Rome, Italy.

Stefan Schmideder, Lars Barthel, Henri Müller, Vera Meyer, and Heiko Briesen, 2020, From macro- to micro-morphological properties of filamentous fungal pellets. ProcessNet Jahrestagung und DECHEMA-Jahrestagung der Biotechnologen 2020, Web-Konferenz.

Poster Presentations

Stefan Schmideder, Tiaan Friedrich, Tijana Kovačević, Lars Barthel, Philipp Kunz, Vera Meyer, Rudibert King, and Heiko Briesen, 2018, Growth of filamentous microorganisms: PBM and experimental determination of rate equations. 6th Population Balance Modelling Conference (PBM 2018), Gent, Belgium.

Lars Barthel, **Stefan Schmideder**, Heiko Briesen, and Vera Meyer, 2019, An X-ray microtomography-based method for detailed analysis of the three-dimensional morphology of fungal pellets: Aspergillus niger as a case study. Molecular Biology of Fungi (MBF 2019), Göttingen, Germany.

Henri Müller, **Stefan Schmideder**, Lars Barthel, Ludwig Niessen, Vera Meyer, and Heiko Briesen, 2020, Optimized X-ray microcomputed tomography and 3D volumetric image processing of filamentous fungal pellets. ProcessNet Jahrestagung und DECHEMA-Jahrestagung der Biotechnologen 2020, Web-Konferenz.